

**Best Available  
Copy  
for all Pictures**

AD-776 804

VISIBLE AND INFRARED LASER-INDUCED  
DAMAGE TO TRANSPARENT MATERIALS

David W. Fradin, et al

Raytheon Company

Prepared for:

Air Force Cambridge Research Laboratories  
Advanced Research Projects Agency

January 1974

DISTRIBUTED BY:

**NTIS**

National Technical Information Service  
U. S. DEPARTMENT OF COMMERCE  
5285 Port Royal Road, Springfield Va. 22151

Unclassified

SECURITY CLASSIFICATION OF THIS PAGE (When Data Entered)

REPORT DOCUMENTATION PAGE		READ INSTRUCTIONS BEFORE COMPLETING FORM
1. REPORT NUMBER AFCRL-TR-74-0082	2. GOVT ACCESSION NO.	3. RECIPIENT'S CATALOG NUMBER AD 776 804
4. TITLE (and Subtitle) VISIBLE AND INFRARED LASER-INDUCED DAMAGE TO TRANSPARENT MATERIALS		5. TYPE OF REPORT & PERIOD COVERED Final Technical Report 1/1/73 - 12/31/73
		6. PERFORMING ORG. REPORT NUMBER S-1660
7. AUTHOR(s) D.W. Fradin      D.P. Bua M. Bass          L. Holway, Jr.		8. CONTRACT OR GRANT NUMBER(s) F19628-73-C0127
9. PERFORMING ORGANIZATION NAME AND ADDRESS Raytheon Research Division 28 Seyon Street Waltham, Massachusetts 02154		10. PROGRAM ELEMENT, PROJECT, TASK AREA & WORK UNIT NUMBERS DoD Element 61101E Project 1434
11. CONTROLLING OFFICE NAME AND ADDRESS Defense Advanced Research Projects Agency 1400 Wilson Blvd. Arlington, Virginia 22209		12. REPORT DATE January 1974
14. MONITORING AGENCY NAME & ADDRESS (if different from Controlling Office) Air Force Cambridge Research Laboratories (OP) Air Force Systems Command, U.S. Air Force Bedford, Massachusetts 01730		13. NUMBER OF PAGES 156
		15. SECURITY CLASS. (of this report) Unclassified
15a. DECLASSIFICATION/DOWNGRADING SCHEDULE		
16. DISTRIBUTION STATEMENT (of this Report)  Approved for public release - distribution unlimited		
17. DISTRIBUTION STATEMENT (of the abstract entered in Block 20, if different from Report)		
18. SUPPLEMENTARY NOTES  This research was supported by the Defense Advanced Research Projects Agency, ARPA Order No. 1434.		
19. KEY WORDS (Continue on reverse side if necessary and identify by block number) Laser-induced damage Electron avalanche breakdown Inclusions Self-Focusing  Reproduced by NATIONAL TECHNICAL INFORMATION SERVICE U. S. Department of Commerce Springfield VA 22151		
20. ABSTRACT (Continue on reverse side if necessary and identify by block number)  By using Q-switched and mode-locked Nd:YAG lasers, we have meas- ured the dependence of intrinsic damage fields on both lattice disorder and laser pulse duration and have interpreted the results in terms of avalanche breakdown. It was found that severe lattice disorder such as present in fused silica measurably increases the intrinsic damage intensity. The breakdown field was also found to increase when the pulse duration was reduced below about 1 ns.		

DD FORM 1 JAN 73 1473

EDITION OF 1 NOV 65 IS OBSOLETE

Unclassified

SECURITY CLASSIFICATION OF THIS PAGE (When Data Entered)

Unclassified

SECURITY CLASSIFICATION OF THIS PAGE(When Data Entered)

20. Abstract (Cont'd)

Damage from inclusions was observed in various dielectric coatings. It was found that inclusions having diameters  $\sim 3.5 \mu\text{m}$  were responsible for damage from Q-switched pulses and that inclusions with diameters less than  $\sim 0.4 \mu\text{m}$  were responsible for threshold damage from 20 ps mode-locked pulses.

A CO<sub>2</sub> TEA laser was constructed for use as a source in damage measurements. This laser, operating in a TEM<sub>00</sub> mode, was used to induce optical damage in ZnSe. Under the conditions of measurement, damage at  $10.6 \mu\text{m}$  developed from inclusion absorption. The dependence of inclusion damage intensities on the degree of external focusing was used to infer the average density of damaging inclusions. Comparison was made to intrinsic damage levels.

The relationship between self-focusing and optical damage was used as the basis for a new technique for measuring self-focusing parameters. By using previously published data, the self-focusing critical power for sapphire was determined.

Finally, the results of recent measurements of intrinsic laser damage were interpreted in terms of an analytical model of electron avalanche breakdown. The model, based on a classical Fokker-Planck formula, treats both polar and nonpolar lattice interactions by using a relaxation-time approximation.

Unclassified

SECURITY CLASSIFICATION OF THIS PAGE(When Data Entered)

ia

ARPA Order No. 1434

Program Code No. 3D10

Contractor: Raytheon Research  
Division

Effective Date of Contract:  
1 January 1973

Contract No. F19628-73-C-0127

Principal Investigator and Phone No.  
David W. Fradin/617-899-8400

AFCRL Project Scientist and Phone No.  
Dr. David Milam/617-861-3897

Contract Expiration Date:  
31 December 1973

RECESSION for	
NTIS	White Section <input checked="" type="checkbox"/>
DDC	Blue Section <input type="checkbox"/>
UNCLASSIFIED	<input type="checkbox"/>
JUSTIFICATION	
BY	
DISTRIBUTION/AVAILABILITY CODES	
DISC. ANAL. MOD. OR SPECIAL	
A	

Qualified requestors may obtain additional copies from the Defense Documentation Center. All others should apply to the National Technical Information Service.

VISIBLE AND INFRARED LASER-INDUCED  
DAMAGE TO TRANSPARENT MATERIALS

by

David W. Fradin  
Michael Bass  
Domenic P. Bua  
Lowell H. Holway, Jr.

Raytheon Research Division  
Waltham, Massachusetts 02154

Contract No. F19628-73-C-0127  
Project No. 1434

Final Technical Report

January 1974

Contract Monitor: David Milam  
Optical Physics Laboratory



Approved for public release; distribution unlimited

Sponsored by

Defense Advanced Research Projects Agency  
ARPA Order No. 1434

Monitored by

Air Force Cambridge Research Laboratories  
Air Force Systems Command  
United States Air Force  
Bedford, Massachusetts 01730

## TECHNICAL REPORT SUMMARY

Laser-induced damage to initially transparent materials represents a serious limitation to the design and operation of high power lasers. In order to assess these limitations and to provide standards for material performance, it is necessary to obtain reliable measurements of damage intensities. The primary goal of the present program is to measure damage intensities in various transparent solids and to interpret these results in terms of possible damage mechanisms. Using techniques which we developed in earlier work, we have been able to isolate and to study the intrinsic damage process of electron avalanche breakdown. Such work establishes measured upper limits for the propagation of high intensity light in solids and indicates how these intrinsic limits change with laser pulse and material characteristics. We have, in addition, observed damage from small absorbing inclusions and have begun to develop techniques which can be applied to optical materials evaluation. As part of the present effort, a  $\text{CO}_2$  TEA laser was designed and constructed as a  $\text{TEM}_{00}$  mode,  $10.6 \mu\text{m}$  source for optical damage.

A study of intrinsic damage in polycrystalline and disordered materials has been completed and interpreted in terms of electron avalanche breakdown. By comparing the optical bulk damage fields for a polycrystal, various single-crystal alloys, and two glassy solids to the damage fields for the respective pure single crystals, it was found that only severe lattice disorder such as present in completely amorphous fused quartz causes the damage fields to increase. For the polycrystal and the less disordered systems, the damage fields are the same as those of the pure single crystal. It was found, in addition, that high concentrations of certain types of atomic impurities have no measurable effect on intrinsic damage levels.

Measurements have been made of the pulse width independence of intrinsic damage in NaCl at  $1.06 \mu\text{m}$ . It was found that the intrinsic damage field increased by nearly an order of magnitude to over  $10^7$  volts/cm as the laser pulse duration was decreased from 10 ns to 15 ps. These results, interpreted in terms of electron avalanche breakdown, are the first measurements of intrinsic damage induced by mode-locked laser pulses.

Optical damage to dielectric coatings was studied with weakly focused ruby laser pulses having durations between 20 ns and 20 ps. Under these conditions of measurement, damage was found to result from highly absorbing inclusions. Inclusions with diameters  $\gtrsim 3.5 \mu\text{m}$  were most easily damaged with 20 ns pulses while inclusions with diameters  $\lesssim 0.4 \mu\text{m}$  determined damage resistance to 20 ps pulses.

Bulk optical damage from inclusions was observed in measurements at  $10.6 \mu\text{m}$  on chemical vapor deposition grown ZnSe. The inclusion damage intensity was observed to be statistical in nature and, as found recently in studies of thin film damage, varied with the degree of external focusing. A statistical model of inclusion damage was used in the present work to explain these observations and to calculate, from the experimental data, an average inclusion density. The intrinsic damage intensity for ZnSe was also determined.

Finally, a classical model of electron avalanche breakdown was used to interpret recent experimental data on intrinsic laser damage. The model, based on a Fokker-Planck equation formula, was used to show the relationship between dc and laser-induced damage.

The present work on intrinsic damage has extended over knowledge of electron avalanche breakdown. It may now be possible to refine our models of this damage process in order to enable us to accurately predict the effects of material parameters on intrinsic damage fields at red and near infrared frequencies. Damage measurements should be extended to higher optical frequencies in order to determine if damage from electron avalanche breakdown still dominates as material bandgaps are approached.

Our studies of inclusion and self-focusing damage can serve as a model for future materials evaluation. Since inclusions and self-focusing normally limit the intensity of light that materials can withstand, such evaluation is essential for the development of damage-resistant optics and for the design of damage-resistant systems.

## FOREWORD

This scientific report describes work performed under Contract No. F 19628-73-C-0127 between 1 January 1973 and 31 December 1973. The report was assigned a Raytheon internal number S-1660.

Work was carried out at the Raytheon Research Division in Waltham, Massachusetts. The Principal Investigator until June 30, 1973 was Dr. Michael Bass. After that date Dr. David Fradin became Principal Investigator. Additional experiments were performed at the Naval Research Laboratories, Washington, D.C., in collaboration with Dr. J. P. Letellier, and at the Air Force Cambridge Research Laboratories, Bedford, Mass., in collaboration with Dr. David Milam and R. A. Bradbury. This technical report was prepared under the direction of Dr. Fradin in collaboration with D. P. Bua. The authors have benefitted from the many discussions with Keimpe Andringa, Dr. Frank A. Horrigan, Dr. Thomas Deutsch and Dr. Robert Rudko. Miss Carol Christian assisted in the studies of Sec. VII and VIII. Dr. A. Linz generously provided several of the sample used in the damage study of disorder materials and J. VanderSande conducted electron reflection diffraction measurements for that study.

This report was submitted by the authors on 31 January 1974.

## TABLE OF CONTENTS

	<u>Page</u>
ABSTRACT .....	iii
TECHNICAL REPORT SUMMARY .....	v
FOREWORD .....	vii
LIST OF ILLUSTRATIONS .....	xi
LIST OF TABLES .....	xiv
I. GENERAL INTRODUCTION .....	1
II. DESIGN AND CONSTRUCTION OF A CO <sub>2</sub> TEA LASER..	4
A. Introduction .....	4
B. Resonator Design .....	4
C. Conclusion .....	18
III. EFFECTS OF LATTICE DISORDER ON THE INTRINSIC OPTICAL DAMAGE FIELDS OF SOLIDS .....	20
A. Introduction .....	20
B. Effects of Lattice Disorder on the Intrinsic Optical Damage Fields of Solids .....	21
IV. DEPENDENCE OF LASER INDUCED BREAKDOWN FIELD STRENGTH ON PULSE DURATION .....	28
A. Introduction .....	28
B. Dependence of Laser Induced Breakdown Field Strength on Pulse Duration <sup>17</sup> .....	30
V. THE ROLE OF INCLUSIONS AND LINEAR ABSORPTION IN LASER DAMAGE TO DIELECTRIC MIRRORS .....	38
A. Introduction .....	38
B. The Role of Inclusions and Linear Absorption in Laser Damage to Dielectric Mirrors .....	39
1. Introduction .....	40
2. Experimental Conditions .....	41
2.1 Damage Apparatus .....	41
2.2 Damage Specimens .....	41

## TABLE OF CONTENTS (CONT'D)

	<u>Page</u>
3. Inclusion Damage in Coatings .....	41
3.1 Damage at 20 psec .....	41
3.2 Damage at 1.4 nsec .....	42
3.3 Damage at 20 nsec .....	45
3.4 Interpretation of Threshold Damage ..	45
4. Double-pulse damage experiments .....	50
5. Conclusions .....	56
6. Acknowledgments .....	58
 VI. RELATIONSHIP BETWEEN SELF-FOCUSING AND OPTICAL DAMAGE .....	 59
A. Introduction .....	59
B. The Measurement of Self-Focusing Parameters Using Intrinsic Optical Damage .....	 60
 VII. INCLUSION DAMAGE IN ZnSe .....	 69
A. Introduction .....	69
B. Laser Damage From Inclusion Absorption in ZnSe .....	 70
1. Introduction .....	71
2. Theory .....	71
3. Intrinsic damage statistics .....	79
4. Experimental measurements of inclusion damage .....	 80
5. Conclusions .....	83
6. Acknowledgments .....	84
 VIII. EFFECTS OF ATOMIC IMPURITY CONCENTRATION ON INTRINSIC BREAKDOWN FIELDS .....	 85
 IX. THEORY OF ELECTRON AVALANCHE BREAKDOWN ...	 87
A. Introduction .....	87
B. Electron Avalanche Breakdown Generated by Laser Radiation in Insulating Crystal .....	 89
1. Introduction .....	90
2. Experimental studies of optical breakdown..	94

TABLE OF CONTENTS (CONT'D)

	<u>Page</u>
3. The physical model .....	97
4. The kinetic equation .....	101
5. Numerical results .....	112
6. Conclusions .....	127
REFERENCES .....	129
APPENDIX A - Range of Validity of the Fokker-Planck Equation	
APPENDIX B - Publications and Presentations on Visible and Infrared Laser-Induced Damage to Transparent Materials	

## LIST OF ILLUSTRATIONS

<u>Number</u>	<u>Title</u>	<u>Page</u>
1	Rogowski Shaped Graphite Electrodes	6
2	Schematic of Electrical Design of the Laser Discharge (see Ref. 2)	7
3	Pictorial View of CO <sub>2</sub> Laser with Discharge Circuit	9
4	Two Views of the Actual CO <sub>2</sub> Laser Built for this Program	10
5	Complete CO <sub>2</sub> TEA Laser System	11
6	Multimode Resonator Configuration	12
7	Multimode Laser Output (200 ns/cm)	12
8	TEM <sub>00</sub> Resonator Configuration	14
9	TEM <sub>00</sub> Mode Laser Output (200 ns/cm)	14
10	Logarithmic Plot of Intensity Distribution of TEM <sub>00</sub> Mode Laser Output	15
11	Intensity Distribution of the TEM <sub>00</sub> Mode Laser Outputs Vertical Scale Arbitrary Units	15
12	TEM <sub>00</sub> Single Longitudinal Mode Resonator Configuration	16
13	Single-Frequency, TEM <sub>00</sub> Laser Output (40 ns/cm)	16
14	Schematic of Arrangement for Laser Damage Studies with a CO <sub>2</sub> TEA Laser	19
15	Stress Induced Fractures in Crystalline and in Glassy Ba <sub>2</sub> MgGe <sub>2</sub> O <sub>7</sub>	23
16	Intrinsic Breakdown Fields for KBr <sub>x</sub> KCl <sub>1-x</sub> Alloys	25
17	The Functional Relationship Between the Optical Breakdown Field Strength and the Pulse Duration	35
18	Laser Damage in a Dielectric Mirror Produced by a Single 20 psec Duration Pulse Focused to a Spot Size of 190 μm (FWHM) in Intensity Profile	43

# LIST OF ILLUSTRATIONS (CONT'D)

<u>Number</u>	<u>Title</u>	<u>Page</u>
19	Laser Damage in a Dielectric Mirror Produced by a Single 1.4 nsec Duration Pulse Focused to a Spot Size of 130 $\mu\text{m}$ (FWHM in the Intensity profile)	19
20	Near-Threshold Damage in a Dielectric Mirror Produced by 23 nsec Duration Pulse Focused to a Spot Size of 400 $\mu\text{m}$ (FWHM in the intensity profile)	46
21	Damage in a Dielectric Mirror Produced by Single 20 psec Pulses of Successively Higher Energy	49
22	Above-Threshold Damage in a Dielectric Mirror Produced by a 23 nsec Duration Pulse Focused to a Spot Size of 400 $\mu\text{m}$	51
23	Shutter for Generating Single Pulses of 1.4 nsec Duration, or Pairs of 1.4 nsec Pulses Spaced by a Reproducible Interval	53
24	Histogram of a Damage Experiment on a $\text{ZrO}_2/\text{SiO}_2$ Mirror	25
25	Record of Some Double-Pulse Experiments on the Sample for Which Single-Pulse Data is Shown in Fig. 26	55
26	Double-Pulse Damage Experiments on a $\text{ThF}_4/\text{ZnS}$ Mirror	57
27	The Effect of the Index Nonlinearity on the Diameter of the Focal Point	62
28	The Dependence of Damage Power for Sapphire on Beam Focal Diameter	67
29	Approximate Focal Volume for a Gaussian Beam	75
30	Schematic Showing the Relationship Between $P_D$ and $I_0$ for Two Different Values of $\bar{n}$	78
31	Intrinsic Laser Damage at 1.06 $\mu$ in ZnSe	82
32	Ruby Laser Pulses Transmitted Through a NaCl Sample	95

# LIST OF ILLUSTRATIONS (CONT'D)

<u>Number</u>	<u>Title</u>	<u>Page</u>
33	RMS Electric Fields Necessary to Damage Nine Alkali Halides, Normalized to the Damaging Field for NaCl	96
34	Collision Frequency	106
35a	Coefficients in the Fokker-Planck Equation for Collision Frequency (1) with $\lambda = 1.06 \mu\text{m}$	107
35b	Curves Similar to 35a for $\lambda = 1.06 \mu\text{m}$	109
36	Distribution Function which Evolves from an Original Maxwellian at $300^\circ\text{K}$ and a Total Number Density of $10^8$ per Unit Volume when NaCl is Irradiated by and RMS Field of 15 MV/cm with a $1.06 \mu\text{m}$ Wavelength	113
37a	Quantized Contours of a Distribution Function Which Evolving from an Initial Maxwellian at $300^\circ$ , When NaCl is Irradiated by a $1.06 \mu\text{m}$ Laser with $E = 15$ MV/cm	114
37b	Quantized Contours Evolving from a Uniform Distribution Function, $E = 10$ MV/cm, $\lambda = 1.06 \mu\text{m}$	115
38a	Currents in Energy Space Normalized to One Electron for the same conditions as Fig. 37a	117
38b	Currents in Energy Space Normalized for Conditions in Fig. 37b	118
39	Ionization Rate from Theory and Experiments for $1.06$ and $10.6 \mu\text{m}$ Radiation	120
40	Coefficients in the Fokker-Planck Equation for $\lambda = 1.06 \mu\text{m}$ Including the Effects of the Deformation Potential.	122
41a	Quantized Contours of a Distribution Function Calculated Using the Coefficients of Fig. 40 with $E = 8$ MW/cm and $\lambda = 1.06 \mu\text{m}$	124
41b	Currents in Energy Space for the Problem in Fig. 41a	125
42	Ionization Rate From Experiment and Calculated by Including the Deformation Potential	126

## LIST OF TABLES

<u>Number</u>	<u>Title</u>	<u>Page</u>
I	Measured Optical Damage Fields	24
II	Experimental Breakdown Fields and Calculated Self-Focusing Parameters in NaCl	33
III	Damage Power In Sapphire for Different Beam Sizes	66
IV	Absolute Breakdown Strength of NaCl <sup>67</sup>	98

## I. GENERAL INTRODUCTION

The basic objectives of this program was to analyze data obtained from carefully controlled damage measurements at laser wavelengths between 0.69 and 10.6  $\mu\text{m}$  and at various laser pulse durations. Laser damage thresholds of various materials of interest were determined using techniques developed during the past year, and the results studied to ascertain the mechanisms responsible for damage. Theoretical studies of intrinsic laser damage from avalanche breakdown were conducted, and a new technique was developed to measure self-focusing parameters by inducing optical damage.

The effort was divided into six major areas: They were (1) design and assembly of a pulsed  $\text{CO}_2$  TEA laser for use in 10.6  $\mu\text{m}$  damage measurements, (2) a study of the effects of lattice disorder, polycrystallinity, alloying, and atomic impurity doping on intrinsic damage fields, (3) measurements of the dependence of intrinsic breakdown fields on laser pulse duration, (4) bulk and thin film optical damage from inclusion absorption, (5) the relationship between self-focusing and optical damage, and (6) analytical studies of laser-induced electron avalanche breakdown.

A major effort in the present program was the design and construction of a  $\text{CO}_2$  pulsed laser. By using Rogowski shaped electrodes and atmospheric resonator pressures, it was possible to produce a uniform, large volume discharge inside the resonator and to obtain approximately 0.8 joules of multimode laser output with pulse durations of about 140 ns. With intracavity aperturing the laser intensity distribution was restricted to a gaussian mode having peak powers of about 1 MW. This power was more than sufficient for optical damage studies.

Intrinsic optical damage was investigated in a cooperative effort involving both the Raytheon Research Division and the Naval Research Laboratories. The work at Raytheon investigated the possible effects of selected material parameters on intrinsic damage fields. It was found that intrinsic damage is insensitive to atomic impurities and lattice disorder. Only the severe lattice disorder that is found in a truly amorphous solid such as fused quartz can increase intrinsic breakdown limits. Alloyed material have

intrinsic breakdown intensities intermediate between those of the pure constituent. These results are shown to be consistent with an electron avalanche damage mechanism.

Experiments at NRL, in collaboration with personnel from NRL and Harvard University, probed the dependence of intrinsic breakdown fields on laser pulse duration. The laser intensity necessary to induce damage in NaCl was found to increase for pulse durations  $\lesssim 1$  ns. This dependence is shown to be consistent with dc dielectric breakdown measurements on thin samples of NaCl. The agreement between laser and dc results underscores the fundamental similarity between dc and laser-induced electrical breakdown in insulators.

Studies of thin film damage from inclusion absorption were conducted by the Air Force Cambridge Research Laboratories at AFCRL's Optical Physics Laboratory, with Raytheon personnel participating in the analysis and interpretation of results. By using weakly focused ruby laser pulses of varying time duration and by carefully studying the residual damage morphology, it was found that threshold damage resulted from inclusions whose diameters were related in a predictable manner to laser pulse width.

Bulk damage from inclusion absorption was studied by using the CO<sub>2</sub> TEA laser to induce damage inside chemical vapor deposition grown ZnSe polycrystals. Consistent with previously published measurements of thin film damage, it was found that the damage intensity varied with the degree of external focusing. A simple model of inclusion damage was developed to explain this dependence and is used to infer an average inclusion density from the damage data. It is shown that inclusion damage can appear to be statistical in character because of the random placement of inclusions inside the sample.

The known relationship between self-focusing and optical damage at low laser input powers is used as the basis for a new technique to measure self-focusing parameters. As an illustration of the use of the technique, the self-focusing parameters for sapphire are determined.

Finally, classical model of avalanche breakdown is presented in order to provide a semiquantitative framework for interpreting the intrinsic damage studies. This model, based on a Fokker-Planck equation formalism, is an extension of earlier analysis at Raytheon.

## II. DESIGN AND CONSTRUCTION OF A CO<sub>2</sub> TEA LASER

### A. Introduction

A major objective of the present program was the design and construction of a CO<sub>2</sub> transverse-excited-atmospheric (TEA) laser. This work was divided into three phases:

1. selection of a gas discharge design
2. construction of an operating laser resonator
3. application of design refinements of the resonator optics to produce TEM<sub>00</sub> output with sufficient power and spectral purity to perform optical damage measurements.

The three phases have been completed and the laser has been delivered to the Air Force Cambridge Research Laboratories. A double Rogowski electrode configuration<sup>1</sup> was selected for our use. Using a published electrical design<sup>2</sup> with minor modifications, we were able to achieve a stable, uniform discharge, and to produce approximately 0.2 joules of TEM<sub>00</sub> mode output at 10.6  $\mu\text{m}$ . Single-longitudinal mode operation was also achieved by using an intracavity germanium etalon.

### B. Resonator Design

High peak powers can be obtained with CO<sub>2</sub> lasers by use of atmospheric pressure and fast electric discharges.<sup>3</sup> There are two reasons for using transverse excitation at high pressures instead of a longitudinal discharge. First, lower voltages are required to produce gas breakdown since the discharge path is reduced. In addition, the discharge impedance is lower for transverse excitation so that energy can be rapidly injected into the discharge volume. This second advantage is important because it allows the laser to be excited in times short compared to the excited-state lifetime of the CO<sub>2</sub> molecule, a lifetime equal to about 10  $\mu\text{s}$  at atmospheric pressure.<sup>4</sup> As a result of this rapid excitation, the laser can be Q-switched without using such intracavity devices as electro-optic shutters or rotating mirrors.

A number of schemes for transverse excitation have been discussed in the literature.<sup>1-3,5,6</sup> Two of them, pin electrodes and Rogowski electrodes with trigger wires, were compared in our laboratory. The latter design was chosen because it offered the advantages of a large discharge volume, comparative simplicity, and a relatively low level of radiated rf noise.

The laser was constructed with two parallel, graphite electrodes shaped to approximate a Rogowski profile.<sup>7</sup> Two thin (9-mil) tungsten trigger wires running parallel to the electrodes and placed just outside the lasing region (Fig. 1) provided preionization of the discharge volume<sup>1</sup> with the main discharge occurring across the graphite electrodes.

Chang and Wood<sup>2</sup> have published a simple electrical arrangement for this type of laser, and we adopted their design with minor modifications. Figure 2 shows a schematic of this design with the circuit element values that we used in our system. To produce the discharge, capacitors  $C_1$  and  $C_2$  were initially charged to about 30 kV. A short voltage spike from a trigger transformer fired spark gap SG, causing current  $i_1$  to flow. The spark gap was a commercial device (Tachisto) especially modified for our use.<sup>8</sup> Because of the spark gap inductance,  $i_1$  started to oscillate and drive the trigger wires T and cathode K to negative voltages. When the voltage at T began to drop below ground, an arc discharge was produced between T and the resonator anode A. UV light from this arc caused preionization in the gas volume between the laser electrodes K and A and helped to initiate a large-volume uniform main discharge. This discharge rapidly damped out the ringing current and absorbed most of the energy stored in the circuit.<sup>2</sup>

The discharge characteristics were influenced by the gases flowing in the resonator. We used approximately 800 torr of  $N_2:CO_2:He$  mixed in the ratio 3.2:3.2:10.5. This mixture produced both a uniform glow discharge and optimized laser output. No vacuum pump was used in this system.<sup>2</sup> Instead, the gases are passed through an exhaust in the resonator box at a total rate of about 33 liters/minute.

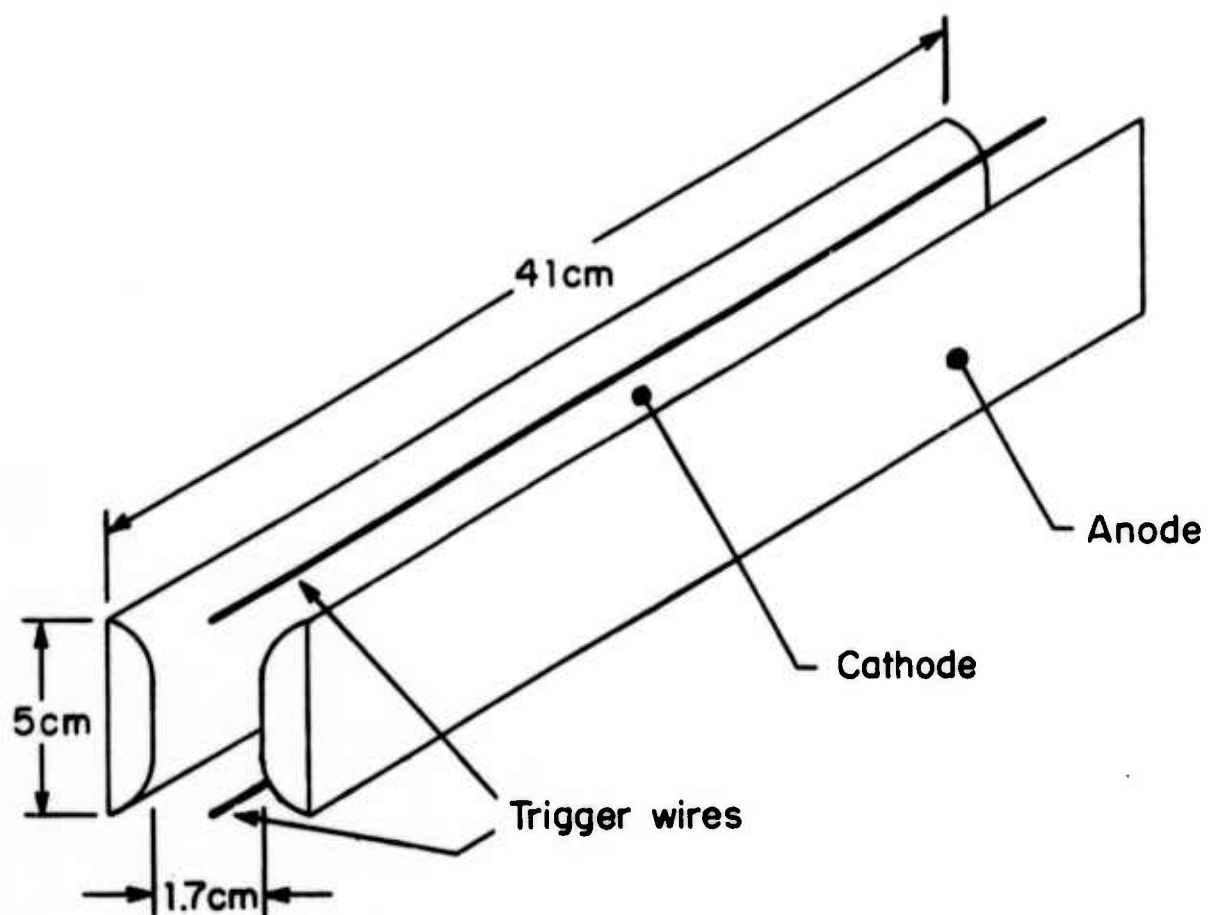
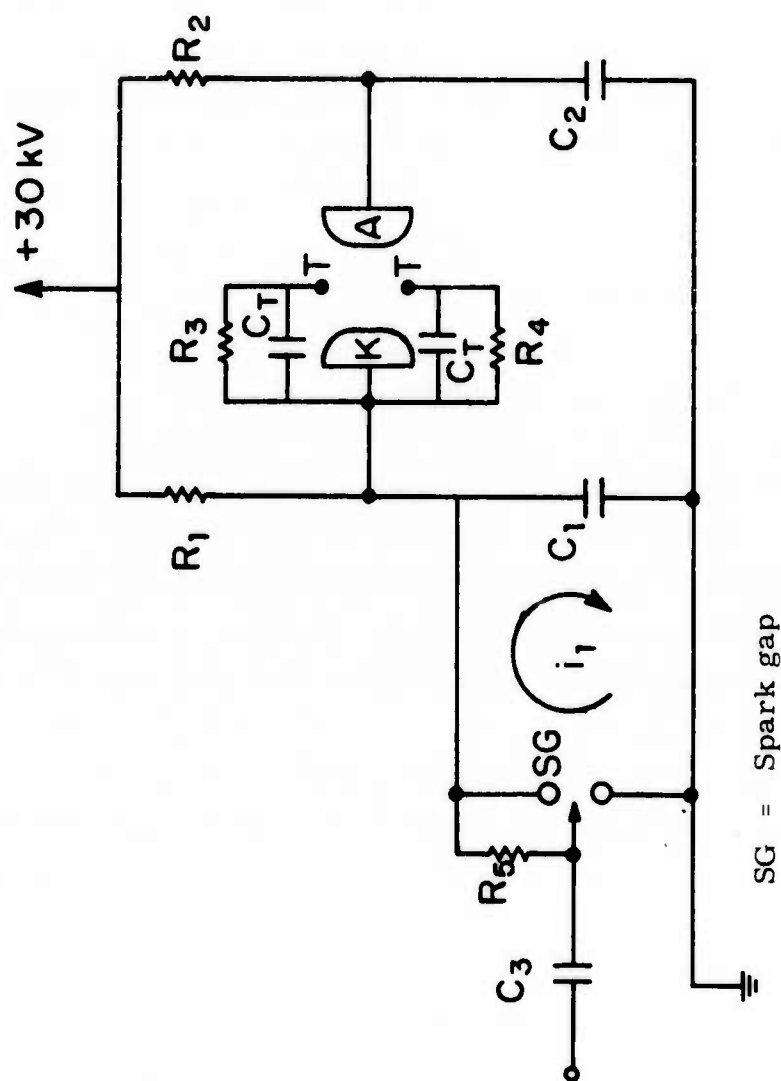


Fig. 1 Rogowski Shaped Graphite Electrodes. Each electrode was polished to remove sharp edges. The trigger wires were 9 mil tungsten.



SG = Spark gap

$R_1 = R_2 = 75\text{k}\Omega, 100\text{ W}$

$R_3 = R_4 = 1\text{k}\Omega, 2\text{ W [(2) } 500\ \Omega, 2\text{ Watt resistors in series]}$

$R_5 = 10\text{ M}\Omega\text{ High voltage}$

$C_1 = C_2 = 0.0432\ \mu\text{f [(12) } 3600\text{ pf, } 30\text{ kV Sprague capacitor]}$

$C_3 = 500\text{ Pf}$

Fig. 2 Schematic of Electrical Design of the Laser Discharge (see Ref. 2).

The physical design of the resonator was also modeled after Ref. 2. Figure 3 is a sketch of the resonator showing the placement of the charging capacitors and spark gap and the design of the electrode mounts. A photograph of the actual laser is reproduced in Figs. 4 and 5. Because of the use of thick resonator walls, the laser could be operated with other gases at well below atmospheric pressure.

Initial tests on this resonator (Fig. 6) produced about 0.7 joules of multimode laser output at  $10.6\text{ }\mu\text{m}$  with peak powers of about 0.6 mW for an input electrical energy of 29 joules. By optimizing the mirrors (germanium mirror 100 percent reflective at  $10.6\text{ }\mu\text{m}$ , 10 meter radius, and a germanium mirror 80 percent reflective at  $10.6\text{ }\mu\text{m}$ , flat) we were able to obtain 0.8 joules of multimode energy with a cavity spacing of 1.2 meters and an input electrical energy of 26.5 joules. Firing at about 1 pps, the pulse energy stability was about 5 percent. (Figure 7)

### C. Optical Design of the Resonator

Performance requirements for the  $\text{CO}_2$  laser were determined by its intended use as a light source for optical damage experiments. It was essential for our purposes that the laser operate in a  $\text{TEM}_{00}$  mode and that it achieve peak powers in excess of about 150 kW. It was desirable that the laser output contain a single longitudinal mode or that it be made completely time-resolved as in the work of Yablonovitch,<sup>9</sup> particularly if the damage mechanism involves inclusion absorption<sup>11</sup> with nanosecond or sub-nanosecond thermal time constants. Spectral purity is less critical for electron avalanche breakdown<sup>10</sup> as the effect of high-frequency mode beating tends to average out.

A number of optical configurations can be used to produce  $\text{TEM}_{00}$  mode operation. The simplest is a stable resonator having mirrors with radii of curvature larger than the resonator length and having an intra-cavity aperture constraining the cavity Fresnel number.

Another resonator configuration we considered was an unstable resonator with annular output coupling.<sup>12</sup> Initial tests, however, clearly

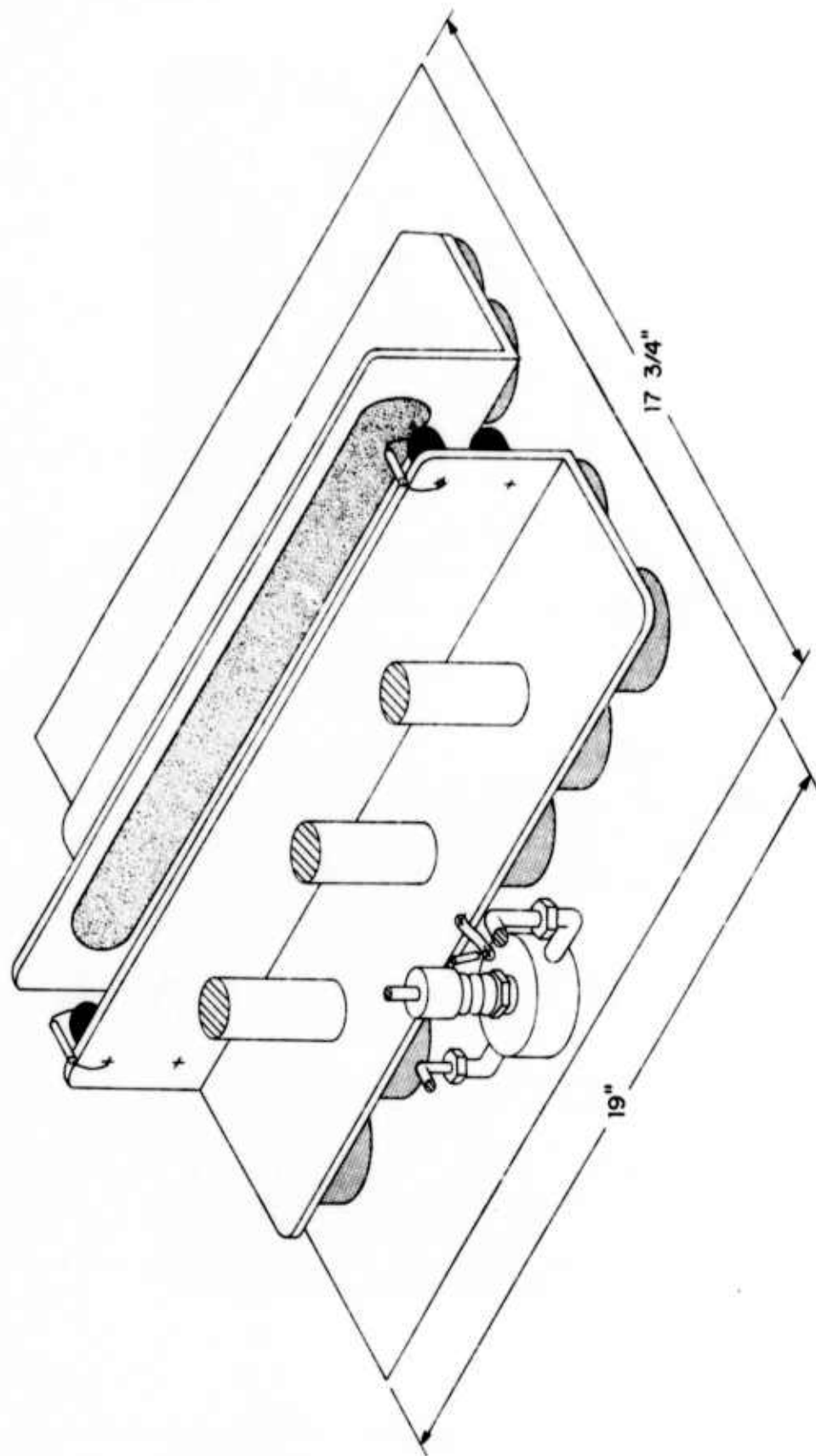


Fig. 3 Pictorial View of CO<sub>2</sub> Laser with Discharge Circuit.

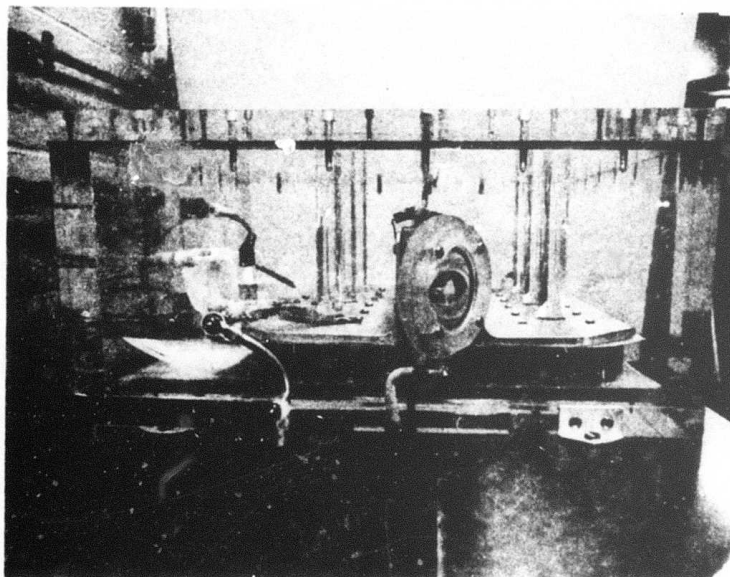
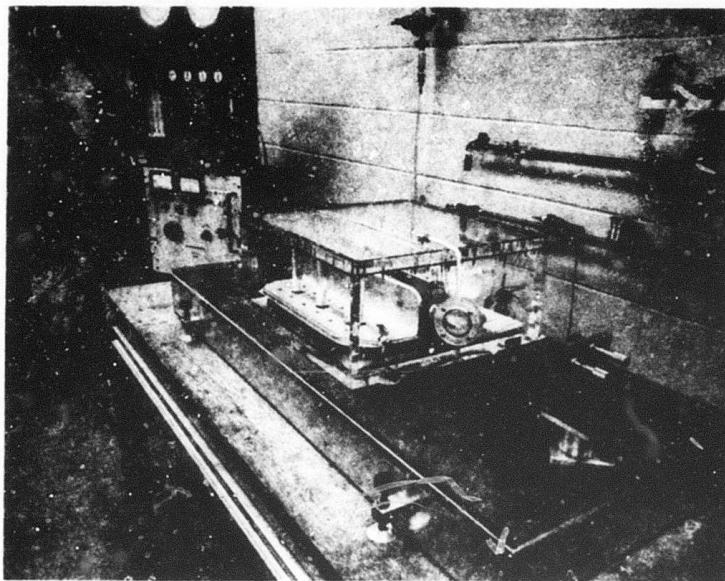


Fig. 4 Two Views of the Actual CO<sub>2</sub> Laser Built for this Program.

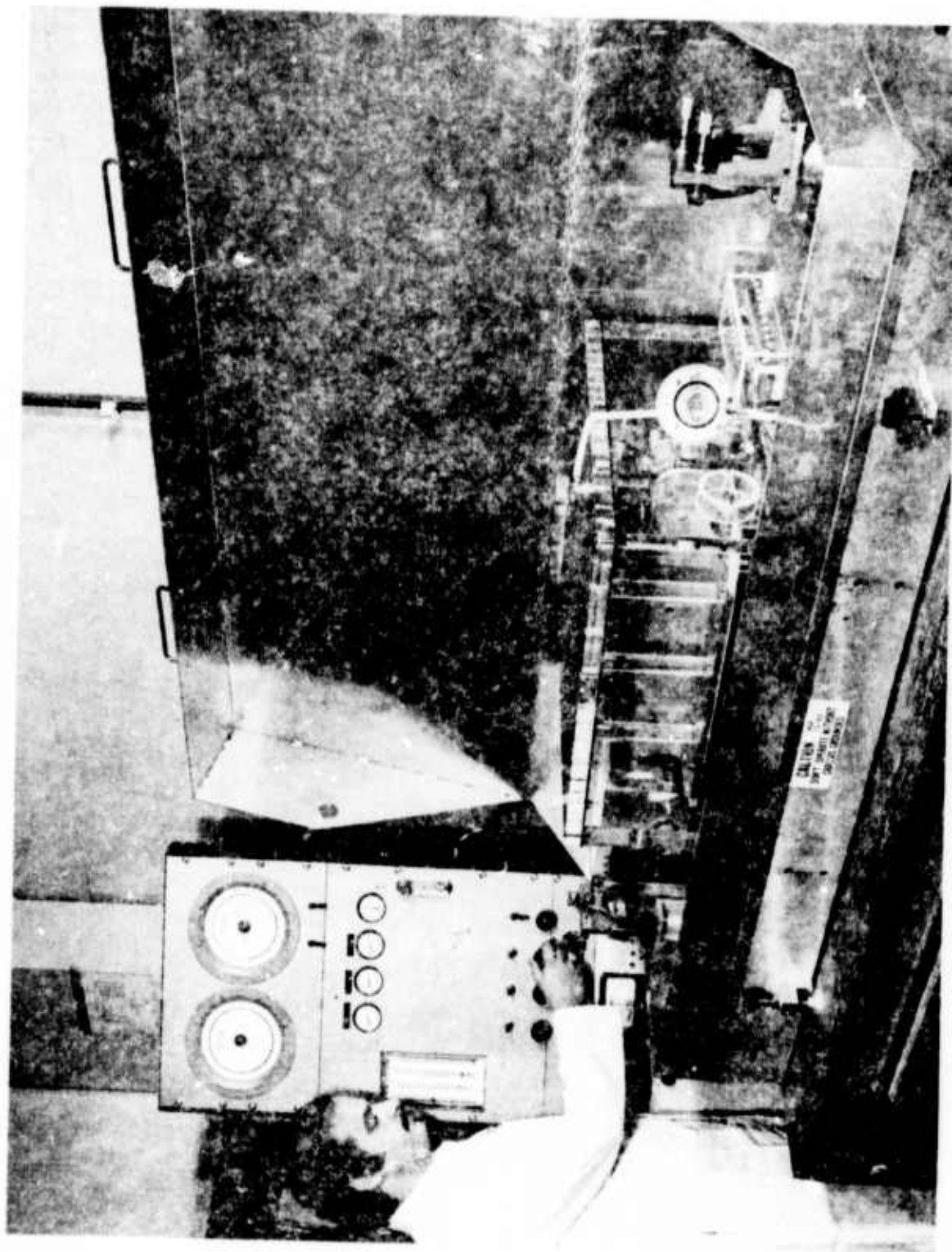


Fig. 5 Complete  $\text{CO}_2$  TFA laser system.

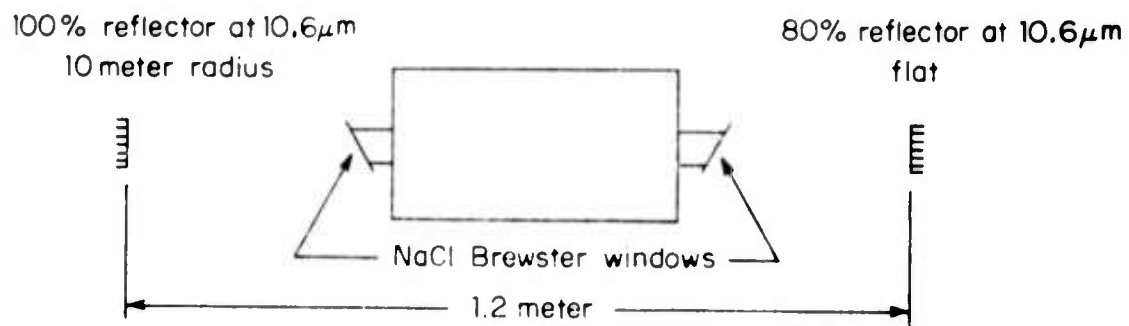


Fig. 6 Multimode Resonator Configuration

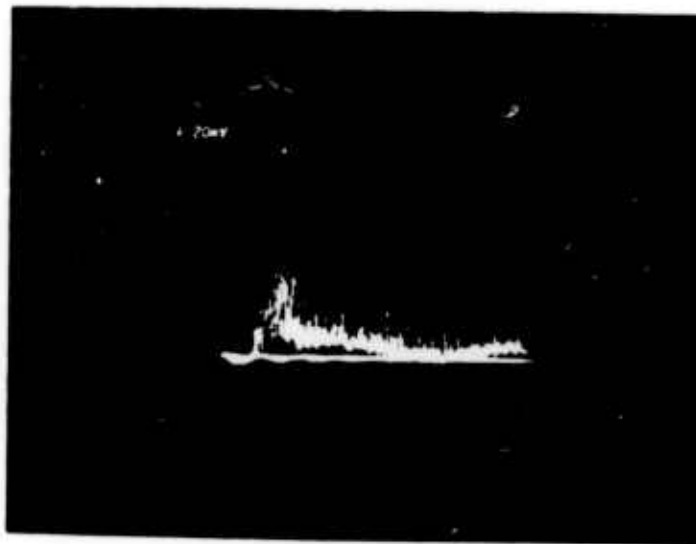


Fig. 7 Multimode Laser Output (200 ns/cm)

indicated that the first method, using a curved mirror and an aperture in a stable resonator, would supply us with more than enough energy for our experiments. The beam profile obtained with a stable resonator was more conducive to damage work since the output intensity distribution of the  $TEM_{00}$  stable resonator was very easily handled analytically. Since our earlier damage work had been conducted with Gaussian beams, comparative analytical interpretations were clearer with the stable resonator geometry.

A third resonator configuration considered was a stable resonator with intracavity optics to enlarge the mode.<sup>13</sup> This technique was complicated and unnecessary for our purposes.

Figure 8 shows the laser cavity with aperture installed. As the aperture size was decreased, the pulse time-structure (as observed with a GHz pyroelectric detector) was seen to improve to the point where the laser output became simultaneously mode-locked (Fig. 9). This change in time-structure was a good indication that the laser was operating  $TEM_{00}$  mode. The fact that the beam intensity distribution is gaussian was demonstrated by sweeping a pinhole across the beam diameter while monitoring the energy transmitted through the pinhole. A plot of the log of transmitted energy versus the beam radius squared produced a straight line (Figs. 10 and 11). With an input of electrical energy of 26 joules, an output of 120 mJ of  $TEM_{00}$  mode laser light was obtained.

Even though longitudinal mode selection was not necessary for our damage studies, some short experiments were conducted with this laser to determine if longitudinal mode selection could be easily accomplished.

With the laser operating  $TEM_{00}$  mode, longitudinal mode selection was accomplished by using an intracavity germanium etalon aligned normal to the cavity axis<sup>14, 15</sup> (Fig. 12). This same technique had been used previously to restrict the number of lasing modes in ruby and Nd:YAG lasers. In a solid state laser an intracavity etalon can be formed by the highly reflecting end mirror and the plane, antireflection-coated front surface of the laser rod.<sup>14</sup> The high gain of the medium enhances the

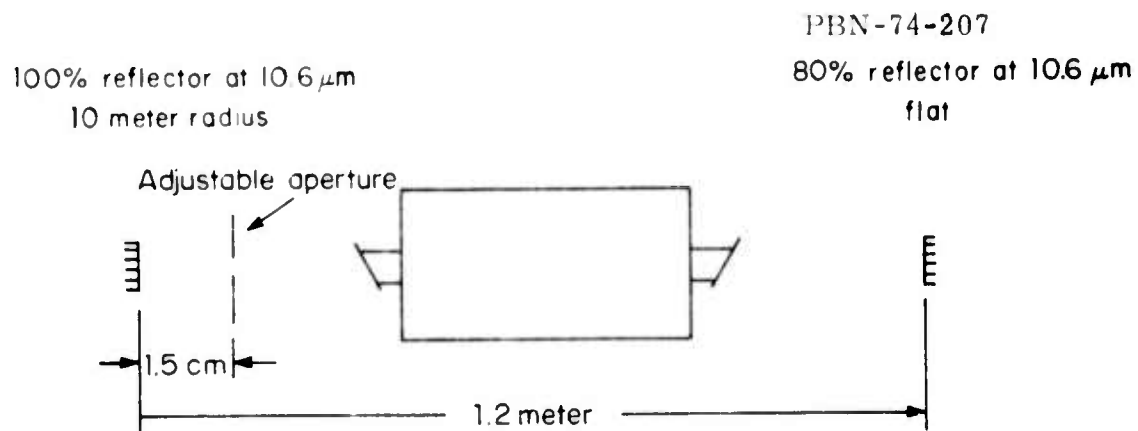


Fig. 8  $\text{TEM}_{00}$  Resonator Configuration



Fig. 9  $\text{TEM}_{00}$  Mode Laser Output (200 ns/cm)

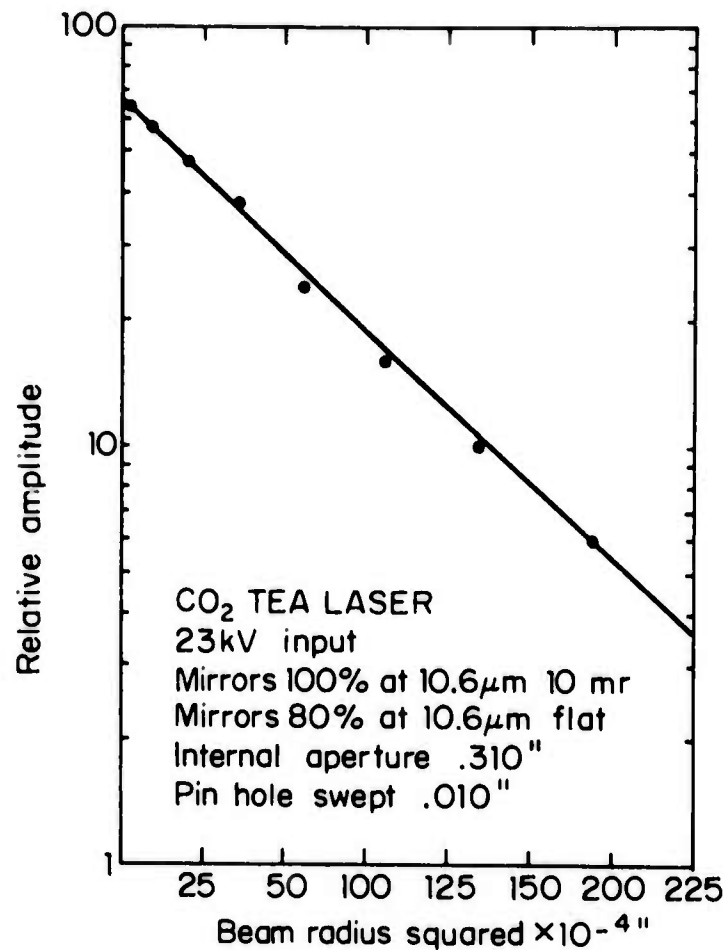


Fig. 10 Logarithmic Plot of Intensity Distribution of TEM<sub>00</sub> Mode Laser Output. The straight line represents a Gaussian distribution.

PBN-74-208

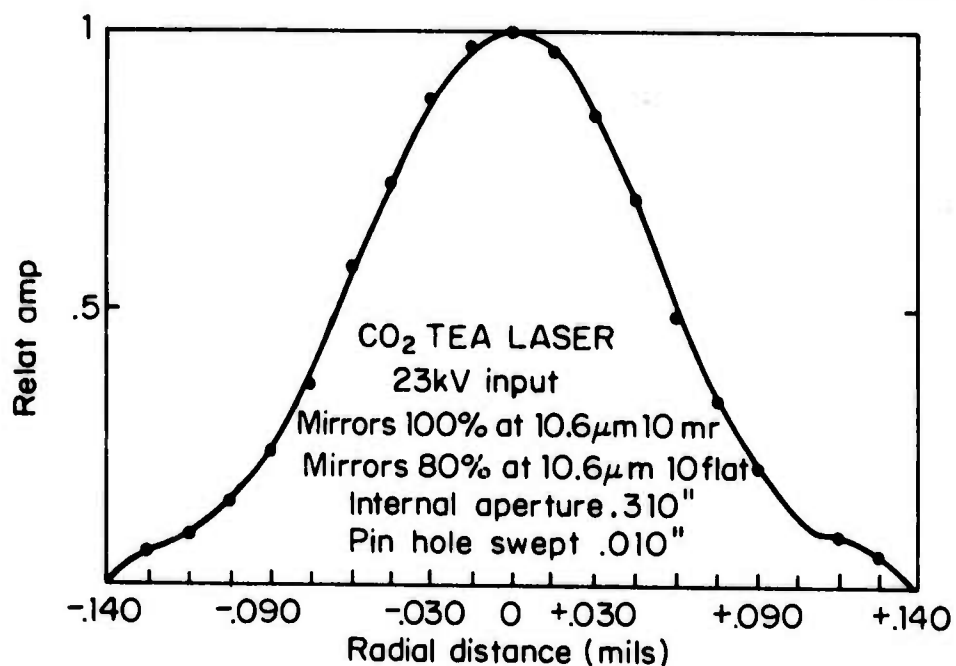


Fig. 11 Intensity Distribution of the TEM<sub>00</sub> Mode Laser Outputs Vertical Scale Arbitrary Units.

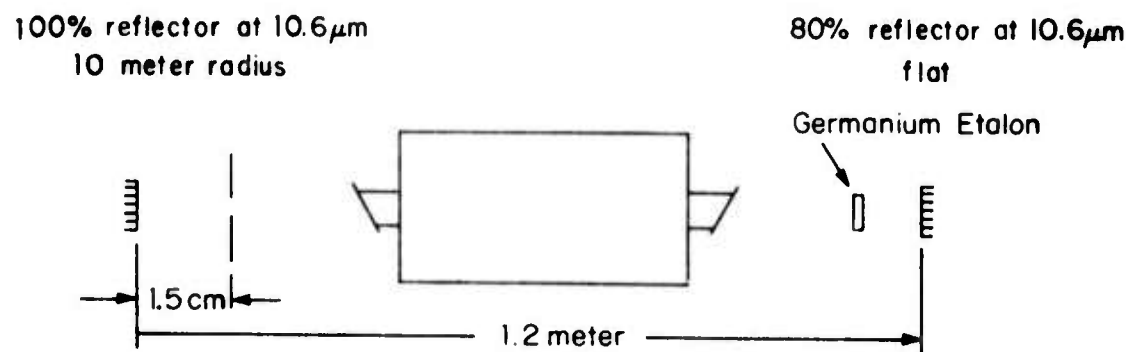


Fig. 12 TEM<sub>00</sub> Single Longitudinal Mode Resonator Configuration.

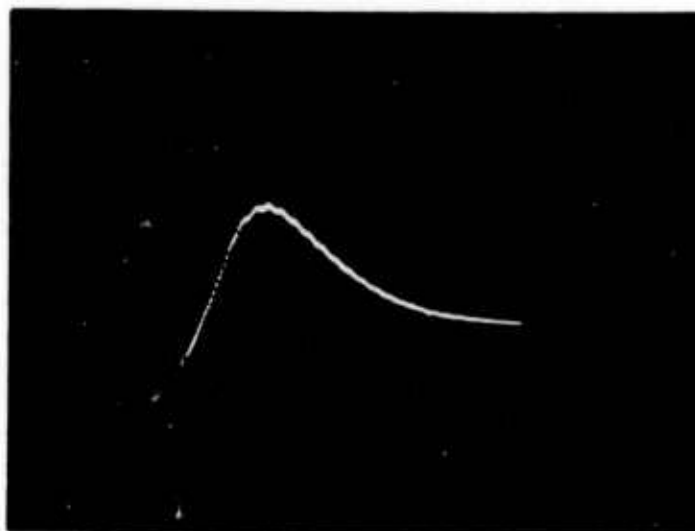


Fig. 13 Single-Frequency, TEM<sub>00</sub> Laser Output (40 ns/cm).

effective reflectivity of the rod face sufficiently to produce an effective etalon with a finesse of about 6 and a free spectral range comparable to that of the total resonator. In this manner, the number of longitudinal modes in YAG and ruby lasers were restricted to four or less. In CO<sub>2</sub> TEA lasers, an uncoated germanium flat positioned between the discharge region and the output mirror produces similar spectral selection.<sup>15</sup> Figure 13 is a picture of the laser output obtained with the germanium etalon in place. The photograph was made with a 500 MHz pyroelectric detector/oscilloscope combination.

While the germanium etalon did produce single frequency output, it also caused a loss in the laser output energy and output stability. The loss in output stability was apparently mechanical in origin and could have been solved by mounting the etalon in a more stable mount. In order to improve the resonator stability, different materials with lower indices of refraction and hence lower surface reflectivity were tested. NaCl did, in fact, lead to greater laser stability, but the reflectivity from its surfaces was so low that single frequency operation could not be attained.

ZnSe, whose index of refraction lies between that of sodium chloride and germanium, appeared to present a good compromise between spectral selectivity and laser stability. We did not adequately pursue the use of ZnSe, however, because the optical quality of the material available was low. Significant pulse smoothing was nonetheless observed with the ZnSe etalon. Experiments with SF<sub>6</sub> and chlorotrifluoroethylene gases were not successful because these gases produced only selected line absorption without an intracavity grating; their use merely forced the laser to change its oscillation to a different vibrational-rotational line.

Pulsed CO<sub>2</sub> lasers may operate on more than one rotational line. Since the lines of the P branches of either rotational band are separated by about 50 GHz, simultaneous lasing on more than one rotational line will produce ultrahigh frequency beating. Such fast time structure cannot affect the results of optical damage measurements. For this reason, no special attempt was made to restrict lasing to a single rotational branch.

#### D. Conclusion

We have completed the design and construction of an operating CO<sub>2</sub> TEA laser that more than meets the requirements needed to perform optical damage experiments. Figure 14 shows the arrangement we used in our experiments. The laser operated TEM<sub>00</sub> mode with approximately 120 mJ of energy of which 60 mJ was contained in the main pulse and approximately 60 mJ in the tail. A combination of a rotatable stack polarizer (two germanium flats) for fine adjustment and two-inch square pieces of calcium fluoride attenuators for coarse adjustments were used to control the laser power incident on test sample. The output beam was focused with antireflection coated germanium lenses having various focal lengths. All energy measurements were made with a fast response Jen/Tec energy meter. Pulse response was monitored with a 500 pic second pyroelectric detector manufactured by Molectron (model P5E) and a Tektronix type 7904 oscilloscope.

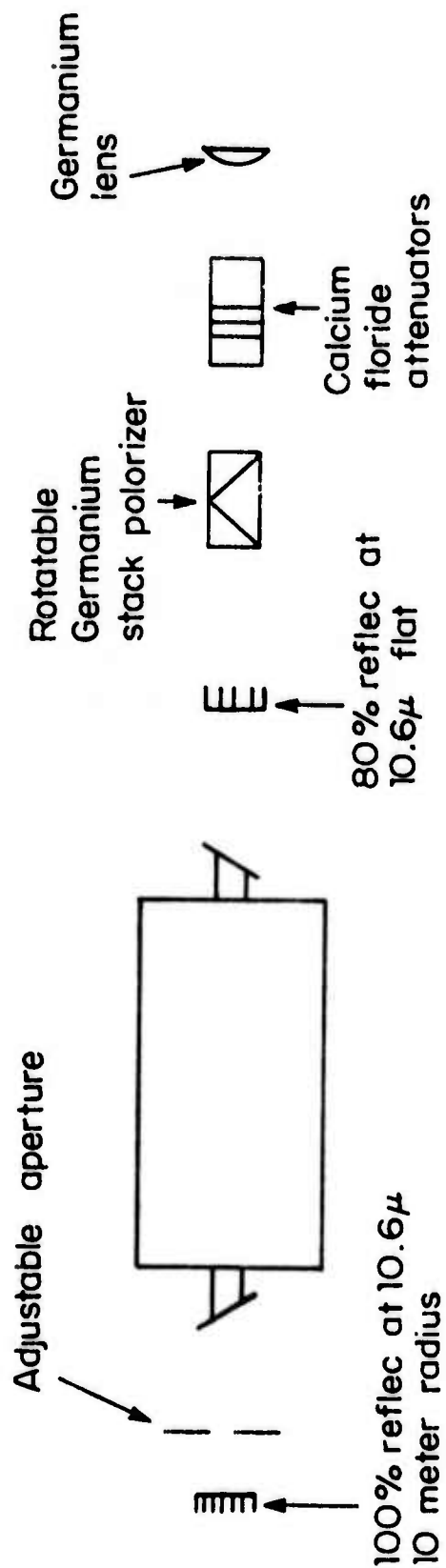


Fig. 14 Schematic of Arrangement for Laser Damage Studies with a  $\text{CO}_2$  TEA Laser.

### III. EFFECTS OF LATTICE DISORDER ON THE INTRINSIC OPTICAL DAMAGE FIELDS OF SOLIDS

#### A. Introduction

Intrinsic damage fields have previously been determined only for pure single crystals. Recent interest has developed, however, in disordered solids as possible new materials for high power laser optics. Disordered solids, particularly polycrystals and alloys, are attractive because of their superior physical properties. In addition, certain materials such as ZnSe are more easily produced in polycrystalline form than as single crystals. There are, then, practical reasons for measuring the intrinsic breakdown fields of disordered solids.

A more fundamental reason for such measurements concern the nature of the intrinsic damage process. It has been demonstrated that electron avalanche breakdown is responsible for intrinsic damage of transparent solids. Since our previous work had established that effective electron collision times are on the order of  $10^{-16}$  to  $10^{-15}$  sec, it appears that the hot electrons involved in the avalanche are changing their moments rapidly by effectively colliding with every atom in their paths. This fact implies that only severe lattice disorder should affect the avalanche. It is argued in Sec. B, in fact, that the intrinsic damage field does not change unless disorder exists on the scale of 10 atomic units or less. If such severe disorder exists, it will be more difficult to heat the electron population and hence the damage field will rise. A measurement of the intrinsic damage in disordered materials, therefore, is a test of our physical conception of electron avalanche breakdown.

We have measured the intrinsic optical damage fields of three systems having different degrees of disorder - polycrystal KCl, single-crystal KCl-KBr alloys, and glass solids. It was found that extreme lattice disorder such as present in a highly amorphous material such as fused quartz causes the damage field to increase whereas less severe disorder does not measurably affect the breakdown strength. This result is consistent with our predictions based on avalanche breakdown as being the damage mechanism. It demonstrates, in addition, that the intrinsic limits for light propagation in single crystals and polycrystals of the same materials are identical.

## B. Effects of Lattice Disorder on the Intrinsic Optical Damage Fields of Solids

Measurements of the effects of lattice disorder on the intrinsic laser-induced damage fields of transparent solids are reported. Extreme lattice disorder such as present in a highly amorphous material such as fused quartz causes the damage field to increase whereas less severe disorder does not measurably affect the breakdown strength. This is consistent with an electron avalanche intrinsic damage mechanism.

Studies of dc dielectric breakdown have shown that severe lattice disorder can increase the electric strength of solids.<sup>16</sup> Since it has recently been observed that intrinsic optical damage in transparent solids appears to develop from the same mechanism that is responsible for the dc dielectric breakdown,<sup>9,10,17</sup> severe lattice disorder should also increase the optical damage fields of solids.<sup>9</sup>

Measurements are reported in this paper of optical bulk damage in three systems having different degrees of disorder -- polycrystal KCl, single-crystal KBr-KCl alloys, and glassy solids. In each case the damage field for the disordered system was compared to the optical strength of the corresponding crystal. It was found that severe lattice disorder such as present in the completely amorphous system (fused quartz) causes the intrinsic optical damage fields to increase. This observation is consistent with dc breakdown experiments<sup>16</sup> and with simple models of electron avalanche breakdown.<sup>19</sup>

The laser system and the experimental techniques used here are described in Ref. 10. A Q-switched, TEM<sub>00</sub> Nd:YAG laser was used to induce damage inside the bulk of various samples. Self-focusing was avoided by restricting the laser input power,<sup>9,10</sup> and damage from inclusions was distinguished from intrinsic damage by examining both the morphology of the damage sites<sup>9,10</sup> and the temporal shape of light pulses transmitted through the sample.<sup>18</sup> Only data obtained from intrinsic damage events were considered in the present work. The damage field was defined as that value of on-axis, root-mean-square electric field necessary to induce damage on a single shot with a probability of 0.5.<sup>10,20</sup>

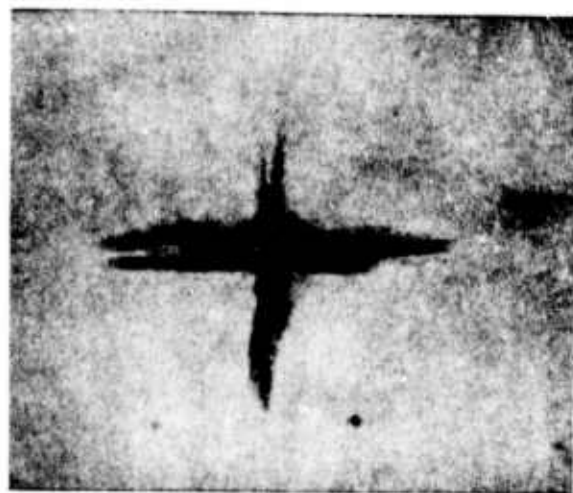
The damage field of the large-grain ( $20\text{ }\mu\text{m}$ ) polycrystal was the same as that measured in the single crystal, and the damage fields for the alloys were intermediate between the damage fields of the constituents. In quartz, on the other hand, the disordered form was noticeably stronger than the crystal, the ratio of damage intensities being  $5 \pm 1$ . This ratio is identical to the corresponding ratio of surface damage fields measured in previous work.

Damage data were taken on a second amorphous-crystal pair,  $\text{Ba}_2\text{MgGe}_2\text{O}_7$  (BMGO). Several measurements had indicated that the BMGO glass was distorted. An X-ray Laue pattern of the glass gave no evidence of crystallinity. Similarly, the directions of the stress-induced fractures that normally accompany optical damage<sup>10</sup> (Fig. 15) were random in the amorphous BMGO as expected for a glass, whereas fracture in the crystal occurred along well-defined crystal directions. Disorder on a local scale in BMGO glass was evident in the luminescence studies of Munasinghe and Linz.<sup>21</sup> When our sample was carefully studied with electron reflection diffraction,<sup>22</sup> however, it was found that regions ( $\gtrsim 2000\text{ \AA}$ ) of crystal ordering existed. Within the volume irradiated by the laser, therefore, the BMGO glass was not completely amorphous. It was actually a mixed crystal-amorphous phase. For the BMGO system, the damage fields of the glass and the crystal were the same within experimental error.

Table I and Fig. 16 summarize the measured optical damage fields.

It is to be expected that the large-grain polycrystal should have the same damage field as the single crystal. The average grain ( $20\text{ }\mu\text{m}$ ) and the laser focal volume were comparable so that in the high intensity region near the beam axis where breakdown is observed to initiate, the sample looks like a single crystal.

By a simplified argument we can estimate the degree of disorder necessary to affect the breakdown strength. Classical theories of avalanche breakdown<sup>19</sup> predict that the dynamics of electrons with energies



(a)

(b)

100  $\mu$ m

Fig. 15 Stress Induced Fractures in Crystalline and in Glassy  $\text{Ba}_2\text{MgGe}_2\text{O}_7$

Residual damage morphology from laser induced damage consists of a small melted region surrounded by stress induced fractures. The direction of light propagation is normal to the plan of the figure.

(a) Fracture in the crystal BMGO occurred along well-defined crystal planes.

(b) In the BMGO glass the directions of fracture were random and different at different damage sites. This behavior is to be expected for an amorphous solid.

TABLE I  
MEASURED OPTICAL DAMAGE FIELDS

System	$E_p/E_{\text{xtal}}$	$I_p/I$	Damage Intensity*
polycrystal KCl -- single-crystal KCl	$= 1.0$	$= 1.0 \pm 0.02$	$I_p = 8.3 \text{ GW/cm}^2$
fused quartz -- single-crystal quartz	$E_g/E = 2.2$	$I_g/I = 5 \pm 1$	$I_g = 108 \text{ GW/cm}^2$
$\text{Ba}_2\text{MgGeO}_3$ glass -- single crystal	$E_g/E_{\text{xtal}} = 0.9$	$I_g/I_{\text{single crystal}} = 0.8 \pm 0.2$	$I_{\text{xtal}} = 7 \text{ GW/cm}^2$

\* For comparison, the damage intensity for sapphire has been measured in D. Fradin and M. Bass, Appl. Phys. Lett. 22, 157 (1973) to be  $110 \text{ GW/cm}^2$  at  $1.06 \mu\text{m}$  with a 10 ns laser pulse. The damage intensity for NaCl, which was used as the standard for the present measurements, is  $18 \text{ GW/cm}^2$  as determined in Ref. 10.

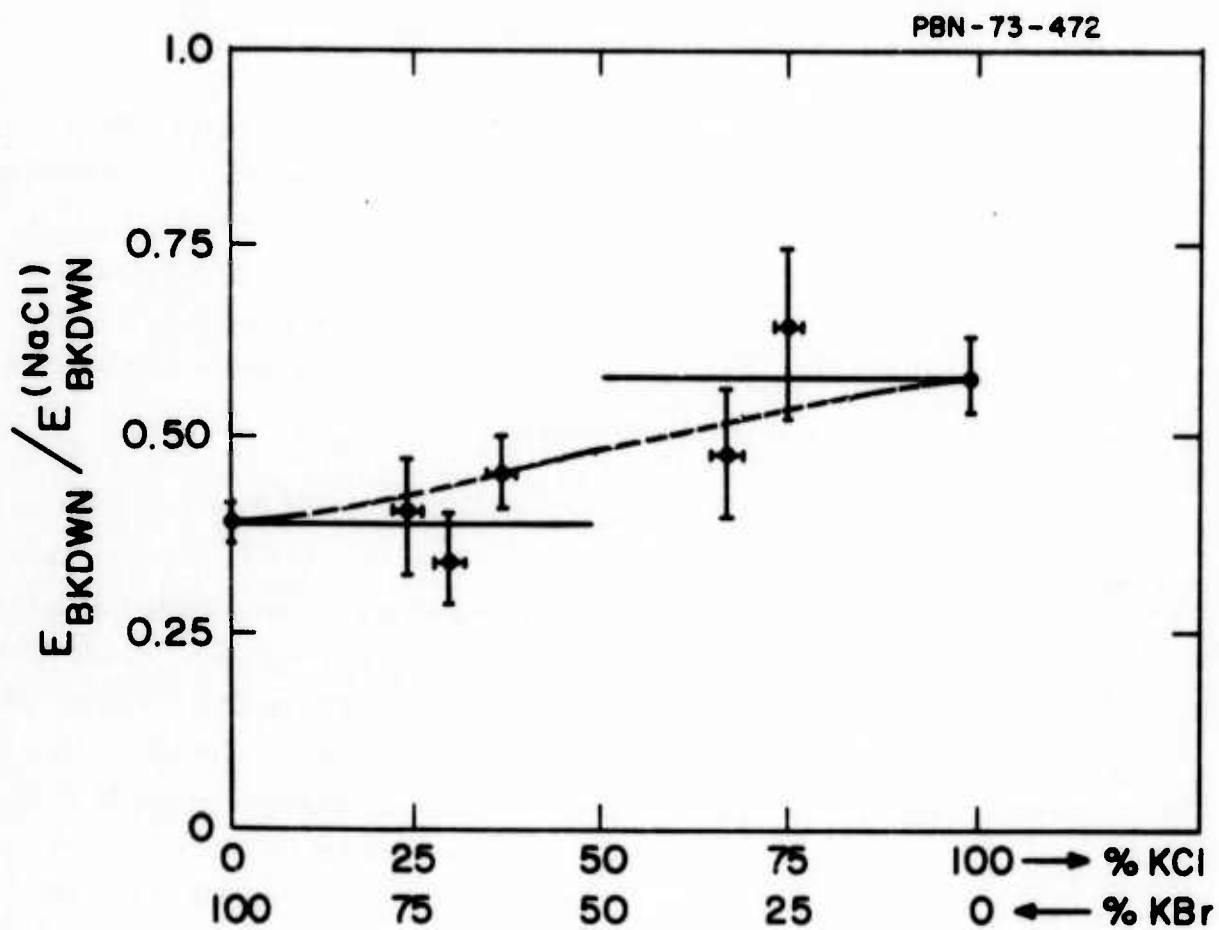


Fig. 16 Intrinsic Breakdown Fields for  $KBr_xKCl_{1-x}$  Alloys. The rms breakdown fields are normalized to the breakdown field of  $NaCl \approx 2.2 \times 10^6$  volts/cm.

greater than the longitudinal optical (LO) energy determine the characteristics of the avalanche. The LO energy in the alkali halides corresponds to electron momenta,  $k$ , of about 0.1 times the reciprocal lattice vector,  $G$ . Thus the important electrons have  $k \gtrsim 0.1G$  and their interaction with the lattice will be dominated by phonons having wave number  $\gtrsim 0.1G$ . Because such lattice vibrations have wavelengths equal to 10 lattice constants or less, this simple model suggests that the damage field should not be affected by disorder unless the disorder appears on the scale of about 10 lattice constants ( $\sim 50\text{\AA}$ ).<sup>a</sup>

Amorphous systems may be disordered on such a scale. Our observation that fused quartz is more resistant to damage than crystalline quartz is, therefore, consistent with the argument just presented. The data on the  $\text{Ba}_2\text{MgGe}_2\text{O}_7$  system is also explained by this argument since that system had regions within the focal volume which were locally ordered on the scale of  $> 10$  lattice constants. Electron avalanche is apparently initiated in these crystalline regions.

The breakdown fields for various single crystal alloys of KBr and KCl are summarized in Fig. 16. It is seen that the damage strengths of the alloys are intermediate between those of the constituents. There is no evidence that alloying caused disorder sufficient to increase the breakdown strength of these materials. The variation of damage strength with composition can be qualitatively understood by noting that many material parameters such as bandgap, lattice constant, dielectric constant, and phonon frequencies have values intermediate between those of the constituents.<sup>23</sup> According to simple models of avalanche breakdown,<sup>19</sup> the breakdown field depends on these various material parameters so that it is reasonable to expect the breakdown strengths of the alloys to also be intermediate between those of the constituents.

---

<sup>a</sup> The larger breakdown field for the amorphous quartz can be understood by another physically equivalent argument. As noted in Refs. 9 and 10, the rate of energy input into the electron population decreases with decreasing electron mobility  $\mu$ . In low fields  $\mu$  is smaller in highly disordered systems than it is in crystals with the same chemical composition. If the effective mobility in disordered media is also lower in the ultra-high fields characteristic of avalanche breakdown, then it should be more difficult to heat the electron distribution in fused quartz, and, as observed, fused quartz should be more damage resistant than crystalline quartz.

It thus appears that extreme lattice disorder such as present in highly amorphous systems has a measurable effect on intrinsic damage fields. This results is qualitatively predicted by simple models of electron avalanche breakdown.

The advice and assistance of D. Bua, R. Newberg, D.W. Howe, C. Willingham and R.R. Monchamp are gratefully acknowledged. A. Linz generously provided several of our samples and J. VanderSande conducted the electron reflection diffraction studies.

#### IV. DEPENDENCE OF LASER INDUCED BREAKDOWN FIELD STRENGTH ON PULSE DURATION

##### A. Introduction

Intrinsic damage fields from avalanche breakdowns have been determined for a number of materials using Q-switched laser pulses.<sup>9, 10, 24</sup> It was found that the damage fields are nearly independent of pulse duration  $t_p$  when  $t_p \geq 5$  ns. When high frequency ( $\geq$  GHz) mode beating occurs, however, the resulting time structure is averaged out by the damage process,<sup>10</sup> thus suggesting that characteristic development times of the electron avalanche are on the order of  $10^{-9}$  sec.

Measurements of avalanche breakdown with subnanosecond laser pulses have not been made prior to the present work. Since laser breakdown and dc dielectric breakdown appear to result from the same fundamental process, data at dc can, in principal, be used to estimate the pulse duration dependence to the laser induced avalanche. Yablonovitch and Bloembergen<sup>25</sup> have, in fact, made such estimates based on measured values of dc breakdown for thin samples of NaCl. Their estimates, however, were based on uncertain limits of an effective, high-field electron drift velocity and ignored important experimental uncertainties such as space charge development which can influence dc breakdown fields but not laser breakdown fields.

There is no reliable data in the literature, therefore, on the laser pulse width dependence of intrinsic optical damage. Such data is useful to our understanding of avalanche breakdown because it provides information on the time development of the electron avalanche. Such data also has practical importance in that it establishes measured upper limits for the propagation of mode locked laser pulses in solids.

We have measured the intrinsic breakdown strength of NaCl at  $1.06 \mu\text{m}$  using four pulse durations between 10.3 ns and 15 ps. It was found that the intrinsic breakdown field increases by a factor of about

6 to over  $10^7$  V/cm as the pulse duration is changed by about three orders of magnitude. From these measured damage fields, an ionization rate for the electron avalanche can be inferred and compared to the predictions of Yablonovitch and Bloembergen.

B. DEPENDENCE OF LASER INDUCED BREAKDOWN FIELD  
STRENGTH ON PULSE DURATION <sup>17</sup>

D.W. Fradin\*  
Raytheon Research Division  
Waltham, Massachusetts 02154

N. Bloembergen\*  
Gordon McKay Laboratory, Harvard University  
Cambridge, Massachusetts 02138

and

J.P. Letellier†  
Naval Research Laboratories  
Washington, D.C.

Abstract

Field strengths at which optical damage is initiated in NaCl have been measured with a mode-locked Nd:YAG laser with pulse durations of 15 and 300 picoseconds. Comparison with previously reported data with a Q-switched laser shows that the field strength required for intrinsic optical damage increases by almost one order of magnitude from  $10^6$  v/cm at  $10^{-8}$  sec to over  $10^7$  v/cm at  $1.5 \times 10^{-11}$  sec. This is in qualitative agreement with published estimates based on the electron avalanche breakdown mechanism.

---

\* Supported by the Joint Services Electronics Program at Harvard University under Contract No. N00014-67-A-0298-0006 and by the Advanced Research Projects Agency at Raytheon Research Division as monitored by the Air Force Cambridge Research Laboratories under Contract No. F19628-73-C-0127.

† Supported by NRL Problem K03-08.502, ARPA Project Order 2062, Project 62301D.

Damage produced by laser beams of high intensity in transparent materials has been studied intensively for many years. It is only recently, however, that the effects of absorbing inclusions and self-focusing have been carefully eliminated, and the intrinsic breakdown mechanism in transparent condensed dielectric media has been positively identified as electron avalanche ionization.<sup>9-10,18,20</sup> On the basis of this mechanism and known characteristics of dc breakdown by avalanche ionization, Yablonovitch and Bloembergen<sup>25</sup> predicted a characteristic dependence of breakdown field strength on laser pulse duration. In this note an experimental determination of this dependence in the subnanosecond regime is presented, which turns out to be in general agreement with those predictions.

The measurements were performed by focusing mode-locked YAG: Nd laser pulses having durations of 15 and 300 picoseconds inside a single crystal of NaCl. Because the experimental procedures used in the present work were identical to those used in recent studies with a Q-switched YAG: Nd laser,<sup>10</sup> the subnanosecond measurements can be directly compared to the results of these studies. It is found that the intrinsic breakdown field increased by almost an order of magnitude to over  $10^7$  volts/cm as the laser pulsewidth was decreased from 10 nanoseconds to 15 picoseconds. Previous data with pulse widths typical of Q-switched lasers had demonstrated that the dependence on pulse width in the nanosecond regime is small so that relatively little information on the time dependence of the avalanche process was available.\* Our results demonstrate again that lasers can be used to measure properties of dielectric breakdown which are difficult to obtain by dc techniques.<sup>26-28</sup>

---

\* A pulsewidth dependence to optical damage in thin films was first observed by E.S. Bliss and D. Milam, 4th ASTM Symp. on Damage in Laser Materials, NBS Spec. Pub. 372, 108 (1972).

The mechanism of damage was not identified, however. Since it is known that thin films can have a large residual absorption and significant structural defects and that both effects can change the damage characteristics of surfaces, it is not clear that the change in damage fields which were observed by Bliss and Milam reflect a property of an intrinsic bulk damage mechanism.

The laser used for the present work was a passively mode-locked YAG:Nd laser operating in a TEM<sub>00</sub> mode at 1.06  $\mu\text{m}$ . Without intercavity etalons, this oscillator produced bandwidth-limited light pulses of 15 picosecond duration. By replacing the output mirror with a sapphire etalon, the pulsewidth was lengthened to about 300 picoseconds. Two-phonon fluorescence measurements failed to detect substructure with pulses of either duration. A laser-triggered spark gap<sup>29</sup> was used to select a single light pulse which, after attenuation, was focused through a 14-mm focal length lens about 2 mm into the sample. Care was taken to insure that spherical aberrations from both the lens and the plane entrance surface of the sample being tested were unimportant. An energy monitor recorded the energy in each laser pulse.

The intrinsic damage process is statistical in nature<sup>18,20</sup> because of the fluctuations in the formation of the first few hot electrons in the small focal volume (about  $10^{-7} \text{ cm}^3$ ). The damage threshold can be defined as that value of the RMS electric field inside the sample which produces damage during one pulse with a probability of 0.5. In NaCl the threshold is quite sharp and damage was identified by the occurrence of a faint spark and concomitant melting of a small region ( $\sim 2 \times 10^9 \text{ cm}^3$ ) inside the crystal. At least 20 data points were taken at each pulse duration at the 0.5 probability point.

Beam distortion from self-focusing was avoided by confining the laser input powers to well below the calculated critical powers for catastrophic self-focusing.<sup>9,10</sup> (See Table II). To verify the absence of self-focusing, two different lenses (focal lengths of 14 and 25 mm) were used to focus the laser radiation. As expected from diffraction effects alone, the input damage powers scaled with the square of the focal lengths. If catastrophic self-focusing had been present with the subnanosecond pulses, the input damage power would have been independent of focal length.<sup>10</sup>

A number of tests have been developed to distinguish between damage from absorbing inclusions and damage from intrinsic breakdown.<sup>9,18</sup> Two of these tests -- examination of the damage morphology and examination of the transmitted laser light -- could not be used in the present work because of the small volumes of the damaged sites and the short durations of the laser pulses. But because breakdown is virtually threshold-like in NaCl, other tests were possible. It was observed that the damage

TABLE II

## EXPERIMENTAL BREAKDOWN FIELDS AND CALCULATED SELF-FOCUSING

## PARAMETERS IN NaCl

Pulsewidth ( $10^{-12}$ sec)	$P_{\text{input}}$ ( $10^6$ watts)	$P_c$ ( $10^6$ watts)*		$E_{\text{rms}}$ ( $10^6$ volts/cm)	
		electrostriction	electronic	relative	absolute
15	1.5	$2.9 \times 10^4$	18	$E(15 \text{ ps})/E(300 \text{ ps})$	$12.4 \pm 3.7$
300	0.22	82	18	$= 2.6 \pm 0.7$	4.7
$4.7 \times 10^3$ †	0.030	1.8	18	$E(4.7 \text{ ns})/E(10.3 \text{ ns})$	$2.3 \pm 0.4$
$10.3 \times 10^3$ †	0.033	1.8	18	$= 1.1 \pm 0.05$	2.1

\*  $P_c$  is the calculated critical power for catastrophic self-focusing. The calculation of the electrostrictive value is discussed in Ref. 10. The electronic value is estimated from measurements of third harmonic generation.

† Results taken from Ref. 10.

field was well defined and did not change as different regions of the sample were probed and lenses with different focal lengths were used to focus the radiation. Also, only one spark occurred with each damaging laser pulse, and the spark always appeared to form at the geometrical focal plane. These observations contrasted with those obtained under conditions where inclusion damage was seen.<sup>30</sup> It was therefore concluded that except possibly for occasional damage sites, inclusion damage was absent in highly pure NaCl under the conditions of our measurement as it had been in previous work<sup>10</sup> where Q-switched lasers were used.

Table II summarizes the results of the present measurements and those of Ref. 10. An increase in breakdown strength was observed as the duration of the laser pulse was decreased. As the pulse duration was changed from 10.3 ns to 15 ps, there was a total change by a factor of 5.8 in damage field strengths or a factor of 33 in damage intensity. The experimental points are plotted in Fig. 17, together with some semi-empirical predicted curves taken from Ref. 25.

In the subnanosecond regime electron diffusion and self-trapping may be ignored. The density of the conduction electrons in the avalanche changes exponentially with time,

$$N(t) = N_0 \exp\left[\int \alpha(E)dt\right] = N_0 M_c(t). \quad (1)$$

When the electron density exceeds about  $10^{18} \text{ cm}^{-3}$ , requiring a multiplication factor of roughly  $M_c \sim 10^8$ , breakdown is said to occur. According to Eq. (1) the ionization rate  $\alpha(E)_{\text{rms}}$  is related to the pulse duration as follows:

$$\alpha(E_{\text{rms}}) = t_p^{-1} \ln M_c \approx 18 t_p^{-1}. \quad (2)$$

This relation has been used to convert the quantity  $\alpha(E)$  used along the vertical axis in the figure of Ref. 25 to our figure which uses  $t_p^{-1}$ . We have shifted the curves along the horizontal axis to obtain agreement with the experimental values for the breakdown field  $E_{\text{rms}}$  for the long pulses. It

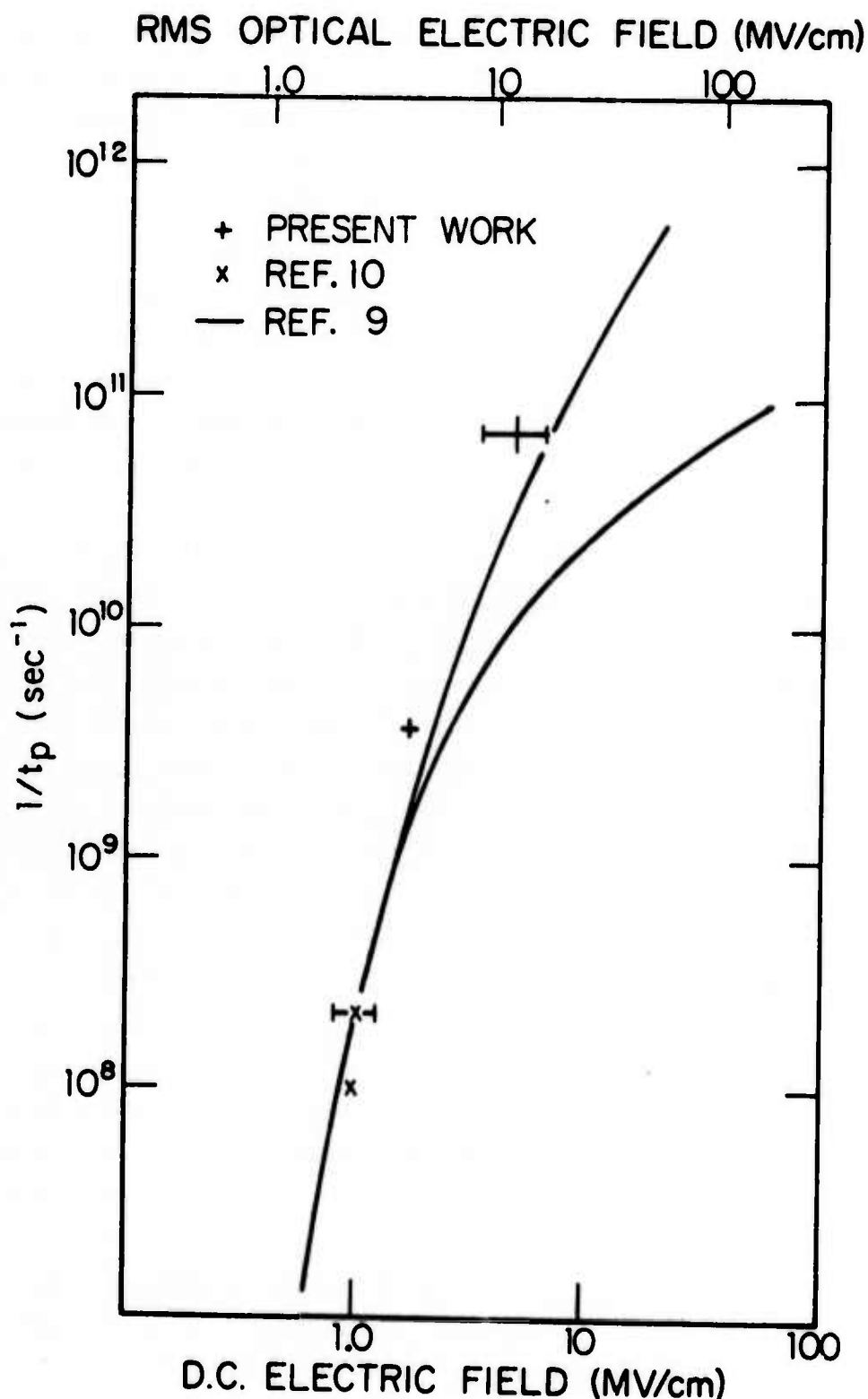


Fig. 17

The Functional Relationship Between the Optical Breakdown Field Strength and the Pulse Duration. The experimental points are compared with two semi-empirical drawn curves. (A discussion of these curves is given in the text and in Ref. 25). The experimental error bars reflect experimental uncertainties in the absolute field strengths.

should be noted that the dc breakdown fields quoted in Refs. 26-28, on which the curves in Ref. 25 were based, are about a factor 2.3 lower than our laser values for  $E_{rms}$ . There are reasons to suspect that this factor is due to systematic errors in the dc experiment. First, this factor of 2.3 is nearly the same for all nine alkali halides studied at  $10.6 \mu m^9$  and  $1.06 \mu m,^{10}$  and second, dc field values are average values without regard for field inhomogeneities from space charge effects which can be important in dc experiments.\*<sup>31,32</sup> Consistent with the approach of Ref. 9 and 10, it is therefore more meaningful to compare trends in breakdown fields as different materials are investigated or as parameters are varied than to compare the absolute values of breakdown fields.

It is seen that the experimental points fall close to the upper curve of Ref. 25, which was derived on the assumption that the mobility in the hot electron gas is independent of  $E_{rms}$ . Quantitative agreement should not be emphasized, however, because the analysis is based on assumptions which are questionable over the range of damage fields considered. As mentioned before, space charge and electrode effect may considerably alter the interpretation of the dc results<sup>19</sup> and consequently to transition from  $E_{dc}$  to  $E_{rms}$  along the horizontal axis. Furthermore the breakdown field at the shortest pulse durations becomes so high that it is possible that frequency-dependent tunneling (or multiphoton ionization) takes over as an intrinsic damage mechanism. In Ref. 25 it was estimated that this change over would occur for fields higher than  $2 \times 10^7$  V/cm or pulse durations shorter than one picosecond. If this estimate is inaccurate and this other intrinsic breakdown mechanism begins to compete with avalanche ionization, the trend would be to push the experimental points upward and to the left of the prediction curves based on the avalanche effect alone.

In summary, intrinsic laser-induced damage has been shown to be a time-dependent process. As the laser pulsewidth was decreased to 15 ps, the damage field in NaCl increased to over  $10^7$  V/cm. From the pulsewidth

---

\* Prof. Y.R. Shen has suggested (private communication) that local field effects may be important in an electron avalanche and may explain the difference in absolute field strengths between dc and optical frequencies. The damage fields reported in the literature, however, are not corrected for local fields because it is normally assumed that any local field effects are averaged out by the electron's rapid movement across the unit cell. The validity of this latter assumption has not been established.

dependence of the optical damage field, a field-dependent ionization rate was determined and found to agree at least qualitatively with experiments using dc fields. The agreement underscores the basic similarity between intrinsic laser-induced damage at  $1.06\text{ }\mu\text{m}$  and dc dielectric breakdown and adds further support to the existence of avalanche ionization in self-focusing "filaments", where effects also occur of a picosecond time scale.

We wish to thank M. Bass, L. Holway, E. Yablonovitch and J.M. McMahon for numerous helpful discussions. M. Bass and J.M. McMahon were particularly helpful in establishing arrangements for this work.

## V. THE ROLE OF INCLUSIONS AND LINEAR ABSORPTION IN LASER DAMAGE TO DIELECTRIC MIRRORS

### A. Introduction

Recent optical damage studies have established intrinsic limits for light propagation inside transparent solids.<sup>9, 10, 30</sup> The relationship between surface and bulk damage fields has been determined in previous work by direct comparison of measured intrinsic surface and bulk damage fields<sup>24</sup> and by theoretical analysis.<sup>33</sup> Surface finishing techniques now exist which for selected materials and highly focused laser light, produce effectively imperfection-free surfaces whose damage fields are identical to those of the bulk.<sup>24</sup>

Our understanding of damage to optical coatings, on the other hand, is not nearly as advanced as our understandings of surface and bulk damage. The reason for this difference is that material imperfections such as structural defects, inclusions, and residual absorption have not been sufficiently characterized in dielectric coatings nor have they, in fact, been sufficiently controlled in the manufacturing process.

The present work helps clarify the role of material imperfections in dielectric coating damage. By studying the residual damage morphology and the pulse duration dependence of the damage intensity it is shown that damage thresholds for weakly focused laser lights are determined by highly absorbing inclusions and that there is a large range of inclusion sizes present in the coatings. It is further established that residual absorption in coatings produced from transparent bulk material does not contribute to optical damage.

B.                   The Role of Inclusions and Linear Absorption  
                      in Laser Damage to Dielectric Mirrors

David Milam and R. A. Bradbury<sup>†</sup>  
Air Force Cambridge Research Laboratories  
Laser Physics Branch  
L. G. Hanscom Field  
Bedford, Massachusetts 01730

and

Michael Bass<sup>\*</sup>  
Raytheon Research Division  
Waltham, Massachusetts 02154

By studying the morphology of threshold damage and observing the predicted "pulse duration-inclusion size" relationship we have found that laser damage to dielectric coatings is primarily determined by the presence of metallic or highly absorbing nonmetallic inclusions. It is also shown that linear absorption does not determine the damage resistance of coatings when they are properly prepared from materials which do not show bulk absorption.

Key Words: Dielectric mirror, laser-induced damage, inclusions, Linear absorption.

---

<sup>†</sup> This research was supported jointly by the Air Force and the Advanced Research Projects Agency of the Department of Defense.

<sup>\*</sup> Supported in part by the Advanced Research Projects Agency of the Department of Defense and monitored by the Air Force Cambridge Research Laboratories under Contract No. F19628-73-C-0127.

## 1. Introduction

By studying the morphology of damage produced at threshold and observing the predicted<sup>11,34</sup> "pulse duration-inclusion size" relationship we have found that laser damage to dielectric coatings is primarily determined by the presence of metallic or highly absorbing non-metallic inclusions. Specifically, inclusions less than  $\sim 0.4 \mu\text{m}$  in diameter are most easily damaged by single 20 psec duration ruby laser pulses while inclusions with diameters greater than  $\sim 3.5 \mu\text{m}$  determine damage resistance due to 20 nsec pulses. This suggests that coating damage resistance to Q-switched pulses can be improved by eliminating the larger inclusions.

To study linear absorption in films, experiments were performed in which the mirror sample was irradiated by a pair of pulses separated by an interval of several nanoseconds. Significant linear absorption would be indicated if neither pulse alone could produce damage, but damage occurred when both pulses were used. These experiments showed that linear absorption in films does not determine the damage resistance of coatings when they are properly prepared from materials which do not show bulk absorption.

## 2. Experimental Conditions

### 2.1 Damage Apparatus

Experiments have been performed at a wavelength of  $0.69\ \mu\text{m}$  using Gaussian-mode pulses with durations between 20 psec and 20 nsec. The picosecond pulses were selected from a mode-locked pulse train, while the longer pulses were generated in a dye-Q-switched oscillator. For both systems, the temporal profile, pulse energy, and a magnified image of the laser spot incident on the damage specimen are recorded for each firing. Details of the two systems are reported elsewhere.<sup>35, 36</sup>

The Q-switched system has recently been modified by the installation of an electro-optic pulse shaper between the oscillator and the amplifier. This has allowed generation of strictly bandwidth-limited pulses 1.4 nsec in duration<sup>37</sup>, and pairs of pulses separated by a predetermined and reproducible interval. All damage experiments with shutter-shaped pulses were monitored in the same fashion as has been described elsewhere.<sup>35, 36</sup>

### 2.2 Damage Specimens

With a single exception noted in the next paragraph, all damage specimens were electron-gun deposited, quarter-wave stacks of either  $\text{TiO}_2/\text{SiO}_2$  or  $\text{ZrO}_2/\text{SiO}_2$  on fused silica substrates. The reflectivity of each of the mirrors exceeded 90 percent at  $0.69\ \mu\text{m}$ . A large number of samples from several manufacturers were examined; the data presented is generally true for all specimens.

A single set of experiments was performed on a  $\text{ThF}_4/\text{ZnS}$  reflector. This exception will be noted in the text.

## 3. Inclusion Damage in Coatings

### 3.1 Damage at 20 psec

Characteristic "near-threshold" damage induced by a 20 psec pulse<sup>35, 38</sup> focused to a spot  $190\ \mu\text{m}$  in diameter (FWHM of the intensity distribution)

is exhibited in the scanning electron micrograph (SEM) of Figure 18.\* The large ridges in the photo on the left are imperfections in the gold coating applied to permit scanning electron microscopy, and are not properties of the dielectric coatings or the laser damage. The laser damage is the array of small craters in the center of this photograph, which corresponds to the central part of the irradiated region. The fact that damage is not produced in the weakly irradiated outer regions is consistent with the assignment of damage threshold to this level of irradiation ( $3.5 \text{ J/cm}^2$  in 20 psec, or  $1.7 \times 10^{11} \text{ watts/cm}^2$ ).

A magnified view of several of the small craters is shown in the photo on the right. Craters are randomly located in the plane of the coating, but restricted primarily to the top two layers of the stack. There are between 2 and  $10 \times 10^6$  such craters per  $\text{cm}^2$ .

Since the size at the top of the craters may be characteristic of explosive rupture of the material, a more meaningful measure of the size of the damage site can be obtained at the bottom of the crater. The mean site diameter obtained using this criterion is  $0.2 \mu\text{m}$ . In no case with a single 20 psec pulse has a site with diameter greater than  $0.5 \mu\text{m}$  been observed.

It should be emphasized that the damage described in this section is caused by a single 20 psec pulse and is not necessarily characteristic of damage produced by a train of several such pulses. The distinction between these two cases will be discussed in Section 4.

### 3.2 Damage at 1.4 nsec

The SEM in Figure 19 illustrates threshold damage caused by a laser pulse 1.4 nsec in duration focused to a diameter of  $130 \mu\text{m}$  at the mirror sample surface. The energy density was  $14 \text{ J/cm}^2$ . Again we see that the damage is an array of randomly located small craters,

---

\* Damage sites shown in SEM's used as illustrations in this report are distorted since the specimen is viewed at an angle of  $45^\circ$ . True dimensions are obtained by measurements on a diagonal aligned on the long axis of the ellipse.



Fig. 18

Laser Damage in a Dielectric Mirror Produced by a Single 20 psec Duration Pulse Focused to a Spot Size of  $190\mu\text{m}$  (FWHM) in Intensity Profile. Left side: Near-threshold damage consisting of many small craters in the center of the most intensely irradiated area. The large dark features are defects in the gold coating applied to allow electron microscopy. Right side: Magnified view of a portion of the irradiated area.



Fig. 19 Laser Damage in a Dielectric Mirror Produced by a Single 1.4 nsec Duration Pulse Focused to a Spot Size of  $130\mu\text{m}$  (FWHM in the intensity profile). Left side: Near-threshold damage consisting of approximately 20 small craters near the center of the most intensely irradiated area. Dark spots are defects in the gold coating applied to allow scanning electron microscopy. Right side: Magnified view of the damaged region.

only now the mean crater diameter is  $1.5\text{ }\mu\text{m}$ . The density of these craters,  $10^6$  per  $\text{cm}^2$ , is less than the density of damage sites produced by picosecond pulses. These craters often extend further into the coating than the first one or two layers.

Smaller craters, such as those resulting from irradiation with picosecond pulses, were never produced by these longer laser pulses.

### 3.3 Damage at 20 nsec

The SEM in Figure 20 illustrates threshold damage caused by a laser pulse 23 nsec in duration focused to a diameter of  $400\text{ }\mu\text{m}$  at the sample surface. The energy density was  $16\text{ J/cm}^2$ . The mean site diameter was  $4.5\text{ }\mu\text{m}$  and the site density was  $10^4$  per  $\text{cm}^2$ . In order to measure so low a site density, it was necessary to irradiate a larger area of the sample. Craters produced by 20nsec pulses frequently extend into several layers of the coating.

### 3.4 Interpretation of Threshold Damage

It has been shown that small impurity inclusions, opaque at the laser frequency and in good thermal contact with the surrounding medium can be heated by a laser pulse to temperatures in excess of the melting point of the medium.<sup>11</sup> The material near such inclusions can undergo a phase change and so laser damage results. When damage due to the presence of inclusions occurs, the residual morphology is characterized by an array of many damage sites randomly located within the irradiated volume.<sup>9, 10, 39</sup> A similar morphology would be expected if the damage were due to any other type of localized material or physical defect.<sup>40</sup>

A morphology characterized by randomly located sites is precisely that of the threshold coating damages shown in Figures 18, 19, and 20. We conclude therefore that localized defects are the principal cause of laser damage to these optical coatings.

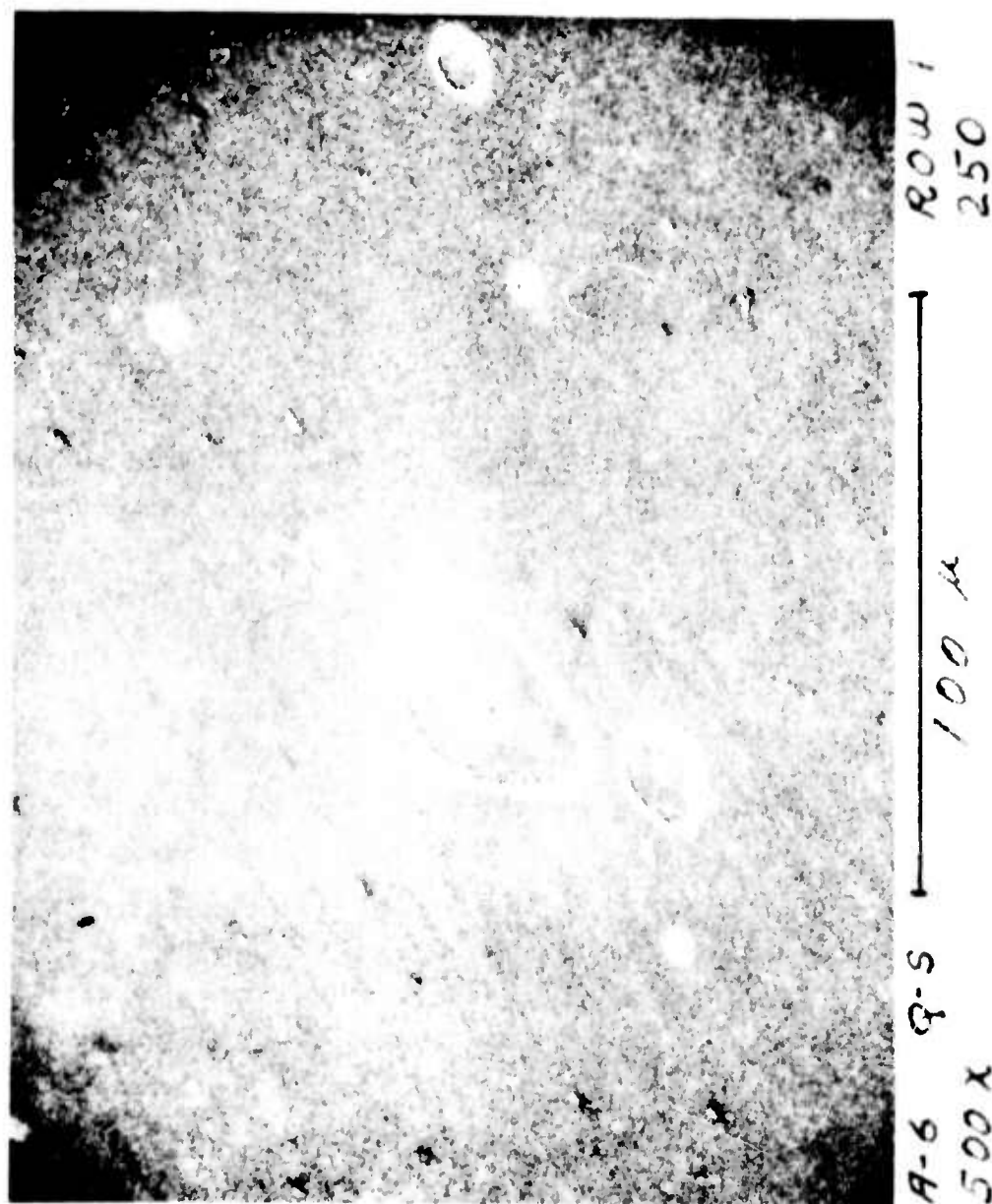


Fig. 20 Near-Threshold Damage in a Dielectric Mirror Produced by 23 nsec Duration Pulse Focused to a Spot Size of 400  $\mu$ m (FWHM in the intensity profile).

A hint that the defects are impurity inclusions is obtained from the size of the sites damaged by laser pulses of different durations. By considering both the heating and cooling of spherical, metallic inclusions in laser glasses, Hopper and Uhlmann<sup>11</sup> and Bliss<sup>34</sup> have shown that for a particular laser pulse duration a particular size of inclusions will be most easily heated to damaging temperatures. \* These studies show that short pulses can more easily damage small inclusions than long pulses and vice versa. From Eq. 4 in Ref. 11 for the inclusion temperature as a function of the radius,  $R_i$ , one can easily show that to a first approximation the inclusion which is most readily heated by a laser pulse of duration  $\tau_p$ , has radius proportional to  $(\tau_p)^{1/2}$ . Thus, for the three pulse durations used in this work we would expect the damaged inclusions to have radii in the ratios

$$R_i(23 \text{ nsec}): R_i(1.4 \text{ nsec}): R_i(20 \text{ psec}) = 34:8.3:1$$

Note that for a particular pulse duration a range of sizes of "easily damaged inclusions" can be expected because the relationship between the temperature reached and the inclusion size is not a very sharply peaked function.<sup>11</sup> In addition, if the level of irradiation is even slightly above the absolute minimum required for damage then several different sizes of inclusions can be heated to damaging temperatures.

Because there is this range of site sizes in each case, the ratios of the mean site diameters,

$$\bar{R}_i(23 \text{ nsec}): \bar{R}_i(1.4 \text{ nsec}): \bar{R}_i(20 \text{ psec}) = 22:7.5:1$$

are to be compared with the expected ratios. These sets of ratios are in acceptable agreement in view of the difficulty in finding the exact size of the inclusions which produced the damage sites.

Hopper and Uhlmann have also shown that for non-metallic inclusions having moderate absorptivity there is no "pulse duration-inclusion

---

\* The treatments in Refs. 11 and 34 require that the inclusion be completely embedded in the surrounding material. The morphology of the damage indicates that this condition is satisfied for almost all of the inclusions which contribute to coating damages.

size" relationship as above.<sup>11</sup> However, if the absorptivity of the inclusion is very high (i.e.  $1/\alpha < R_i$  where  $\alpha$  is the absorption coefficient in  $\text{cm}^{-1}$  at the laser wavelength) the same model as used for metallic inclusions can be applied. Thus, the observed damage morphology and "pulse duration-inclusion size" relationship suggest that the damaging defects are either metallic or very highly absorbing non-metallic included impurities.

Inclusions of either type may arise from impurities in the starting material, incomplete oxidation of the high index material (particularly in the case of  $\text{TiO}_2$ ), introduction of material from the electron gun,<sup>41</sup> dust, or general deposition of dirt from the chamber. All of these indicate the possibility of improving the damage resistance of optical coatings by improving the coating process control. Note that long pulse damage resistance can be increased simply by eliminating the large inclusions.

Non-metallic absorbing inclusions are likely to be more strongly absorptive at shorter wavelengths and in the infrared than they might be near  $1\ \mu\text{m}$ . Thus, their importance in damage problems will grow as the need for high peak power devices in these spectral regions increases.

### 3.5 Above-Threshold Damage

The morphology of damage sites produced by irradiation at levels significantly above threshold is consistent with the conclusion that damage is caused by metallic or highly absorbing inclusions. In Figure 21 there are four SEM's of damage produced by single 20 psec pulses of successively higher energy. These photographs are highly suggestive that damage for above-threshold irradiation is the result of the compounding of damage at many independent sites. Above-threshold damage with single 1.4 nsec pulses appears to follow the same pattern.

A possible exception to the observation that massive damage is a compounding of damage at many small inclusions occurs with the 20 nsec duration pulses. Above-threshold damage sites at this pulse duration frequently consist of a smooth area, one or two layers deep which is similar

Reproduced from  
best available copy.

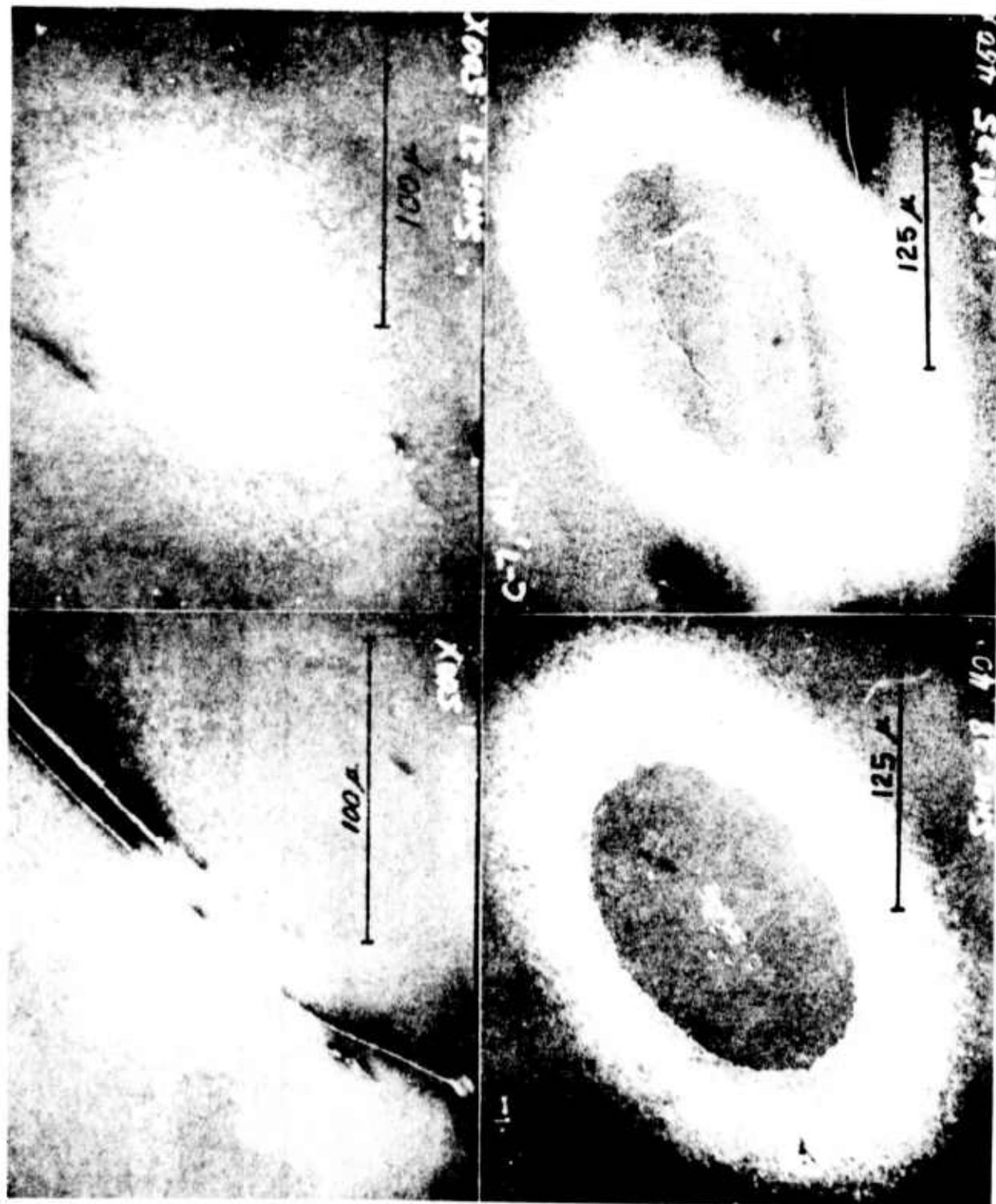


Fig. 21 Damage in a Dielectric Mirror Produced by Single 20 psec Pulses of Successively Higher Energy.

in size and shape to the incident laser beam (see Figure 22). A number of inclusion damage craters may occur either within or outside the edges of the large site. Since the inclusion craters are seldom centered on the larger area, it is not clear that the larger area results from massive inclusion damage. In addition, the material surrounding these sites is not strewn with small inclusion damages as in Figure 21.

The appearance of these large damage sites suggest that other damage interactions might take place with 20 nsec pulses. Numerous mechanisms involving combinations of inclusion damage and/or intrinsic processes can be invoked to account for the correlation between the shape of the laser beam and that of the larger sites. One possibility is that the outer layers are simply heated to a damaging temperature due to irradiation of the great number of small absorbing inclusions present. Linear absorption by the coating materials will also contribute to a damage morphology similar to the laser beam cross-section. This is explored in detail in the double-pulse experiments described below.

It is to be emphasized that observations concerning the potential importance of other mechanisms for 20 nsec irradiation in excess of threshold in no way effects the conclusion that threshold at this pulse duration is determined by large inclusions.

#### 4. Double-Pulse Damage Experiments

If a damaging quantity of energy,  $H$ , is absorbed from a single 1.4 nsec pulse of energy,  $E$ , the same energy,  $H$ , can be supplied by two pulses each of energy  $E_p$  ( $E/2 < E_p < E$ ) provided that the interpulse interval is shorter than the cooling time of the absorbing volume. Addition of the two pulses to produce damage can occur in a uniformly absorbing film or at inclusions too large to be effectively heated by single 1.4 nsec pulses. This would not occur at small inclusions which could cool during the interpulse interval, or if damage is due to a fast response mechanism such as an electron avalanche breakdown.

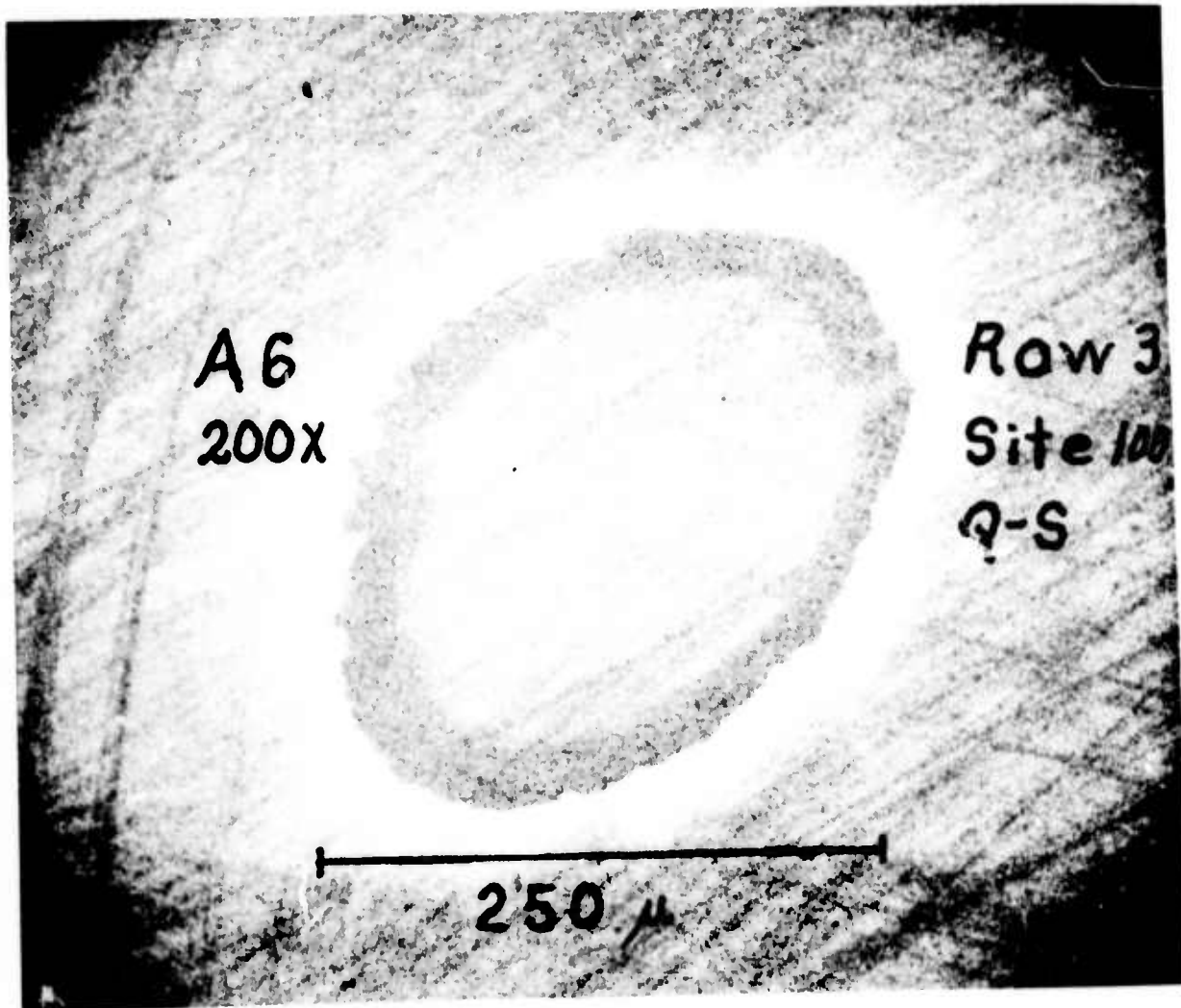


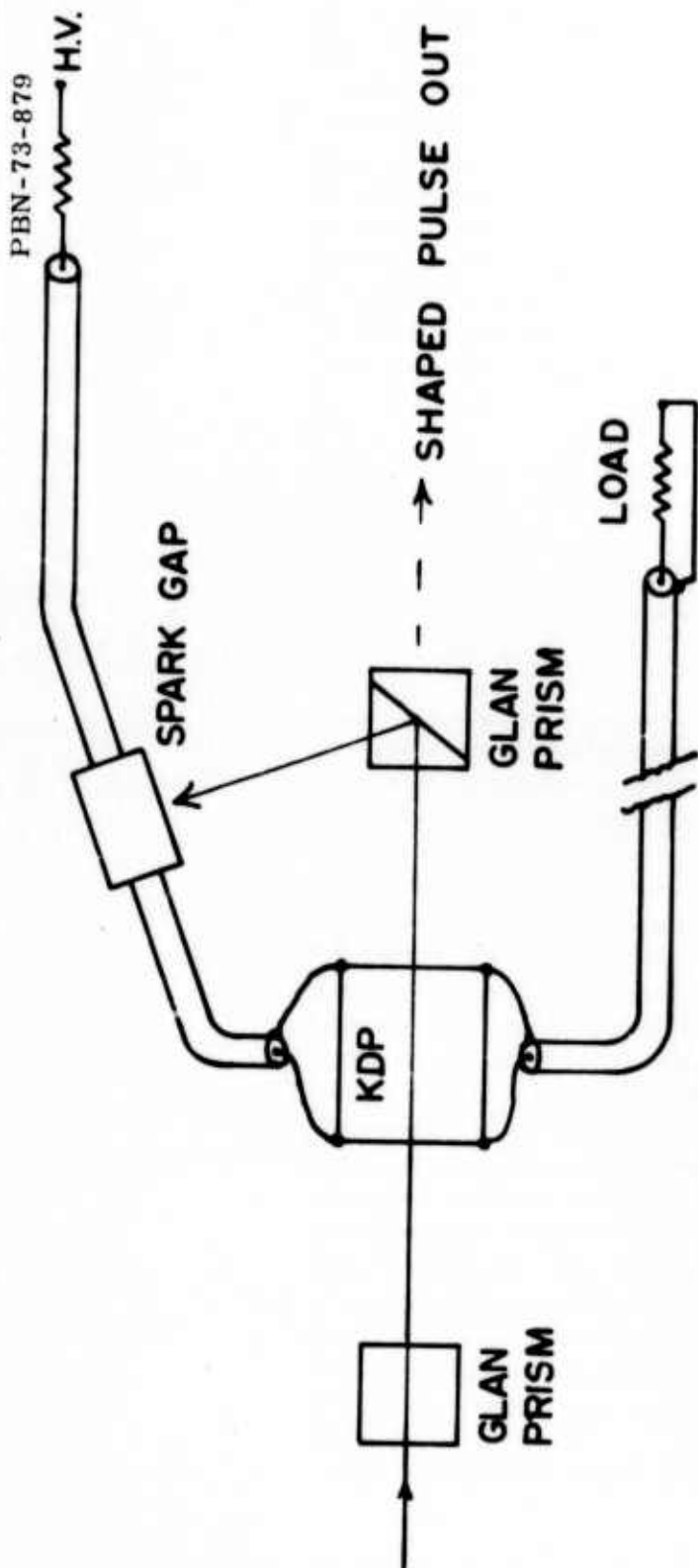
Fig. 22 Above-Threshold Damage in a Dielectric Mirror Produced by a 23 nsec Duration Pulse Focused to a Spot Size of  $400\mu\text{m}$ . Five small inclusion craters are located within the damaged area which is itself two layers deep. The area has a shape like that of the incident laser beam, and is not centered on the obvious inclusion damage.

As noted in Section 2.1, pairs of optical pulses are readily generated by the pulse-shaping shutter. The Pockels cell in this shutter is constructed as an electrical transmission line element. The driving voltage pulse propagates through the Pockels cell into a cable terminated by an impedance-matched load. Removing the load results in a reflection of the voltage pulse, which in turn opens the shutter a second time. Single- and double-pulse operation of the shutter are both illustrated in Figure 23.

During the experiment, a mirror was probed by single 1.4 nsec pulses at a number of sites to determine the energy  $E_t$ , required to produce damage with single pulses. A given site was irradiated only once during this sequence. Additional sites were irradiated with a series of several single subthreshold pulses at intervals greater than one minute. As a general rule, even several pulses with intensities less than that required for single pulse damage produced none. This implies that permanent damage, undetectable by optical microscopy, did not occur with single subthreshold pulses. Subsequent observations of damage due to the addition of two closely spaced pulses could therefore be of thermal origin.

A record of an experiment performed in this fashion is shown in Figure 24. An approximate threshold for damage by single pulses is indicated by the horizontal dashed line, and a lack of cumulative undetected damage by sequences of near-threshold shots which were fired on a given site without causing damage.

A record of some of the double-pulses experiments performed on the same mirror is shown in Figure 25. The total energy ( $2E_p$ ) of each pair of pulses satisfies the requirement  $2E_t > 2E_p > E_t$ , so that damage was possible only if summation occurred. In several cases, damage did indeed occur. Damage sites produced by addition on this mirror were characteristic of damage due to large inclusions. Such inclusions would not be expected to damage upon irradiation by single 1.4 nsec pulses. This observation, coupled with the failure of addition at many sites is taken as evidence that there is no severe linear absorption present in this mirror beyond that presented by the localized inclusions.



→ 20 nsec ←



SHAPED OUTPUT

INPUT

Fig. 23 Shutter for Generating Single Pulses of 1.4 nsec Duration, or Pairs of 1.4 nsec Pulses Spaced by a Reproducible Interval. Removing the load from the cable causes a voltage reflection which gates the Pockels cell a second time.

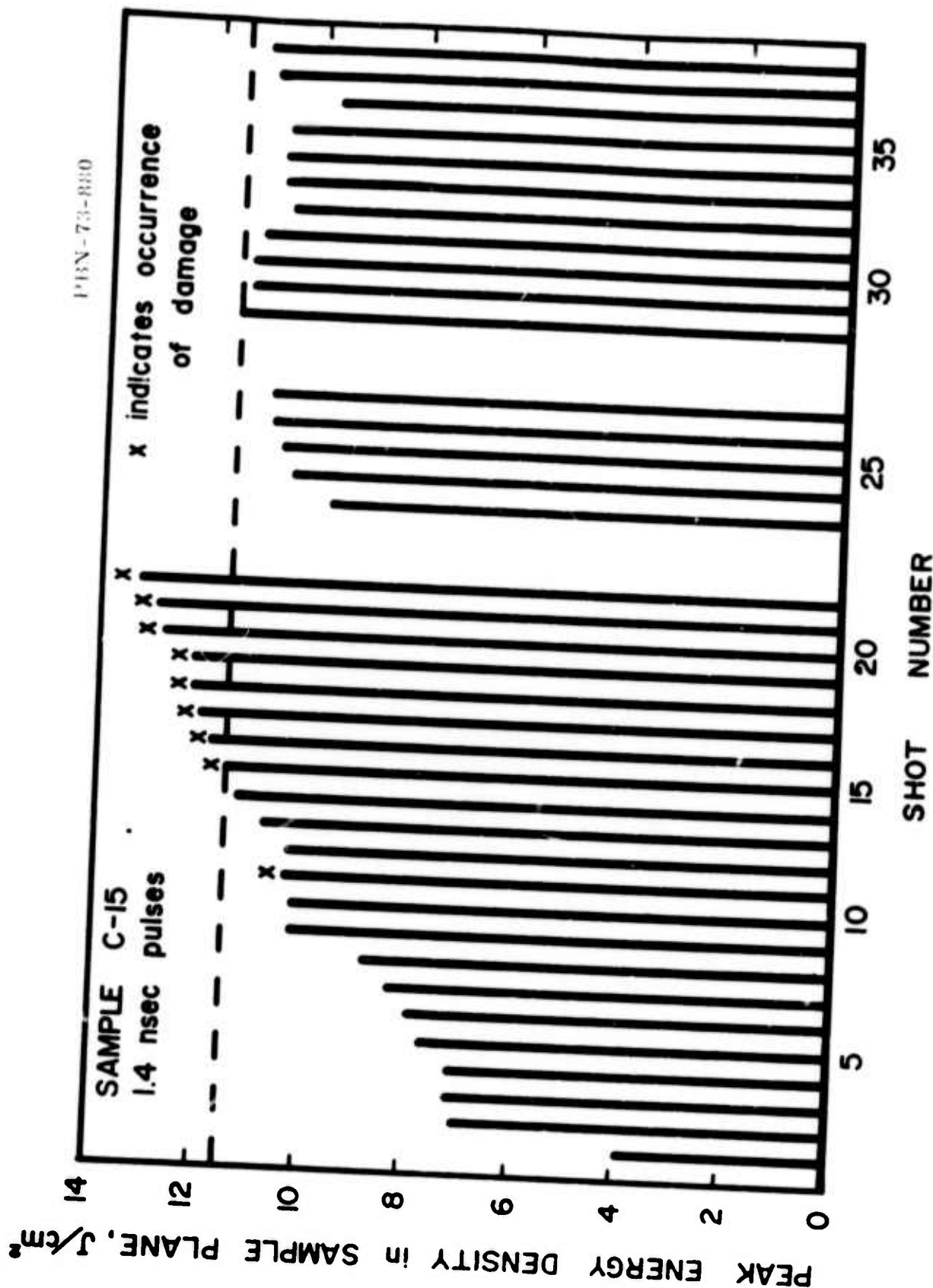


Fig. 24 Histogram of a Damage Experiment on a  $ZrO_2/SiO_2$  Mirror. Shots 1-22 were single shots each fired on a different site to determine single-pulse threshold (indicated by a horizontal dashed line). The set of shots 23-27 were fired onto a single site at one minute intervals to verify that detectable damage did not occur as a result of accumulation of undetected permanent damage. No damage could be detected after the five firings. Shots 28-38 were fired onto a second site at one minute intervals without causing damage.

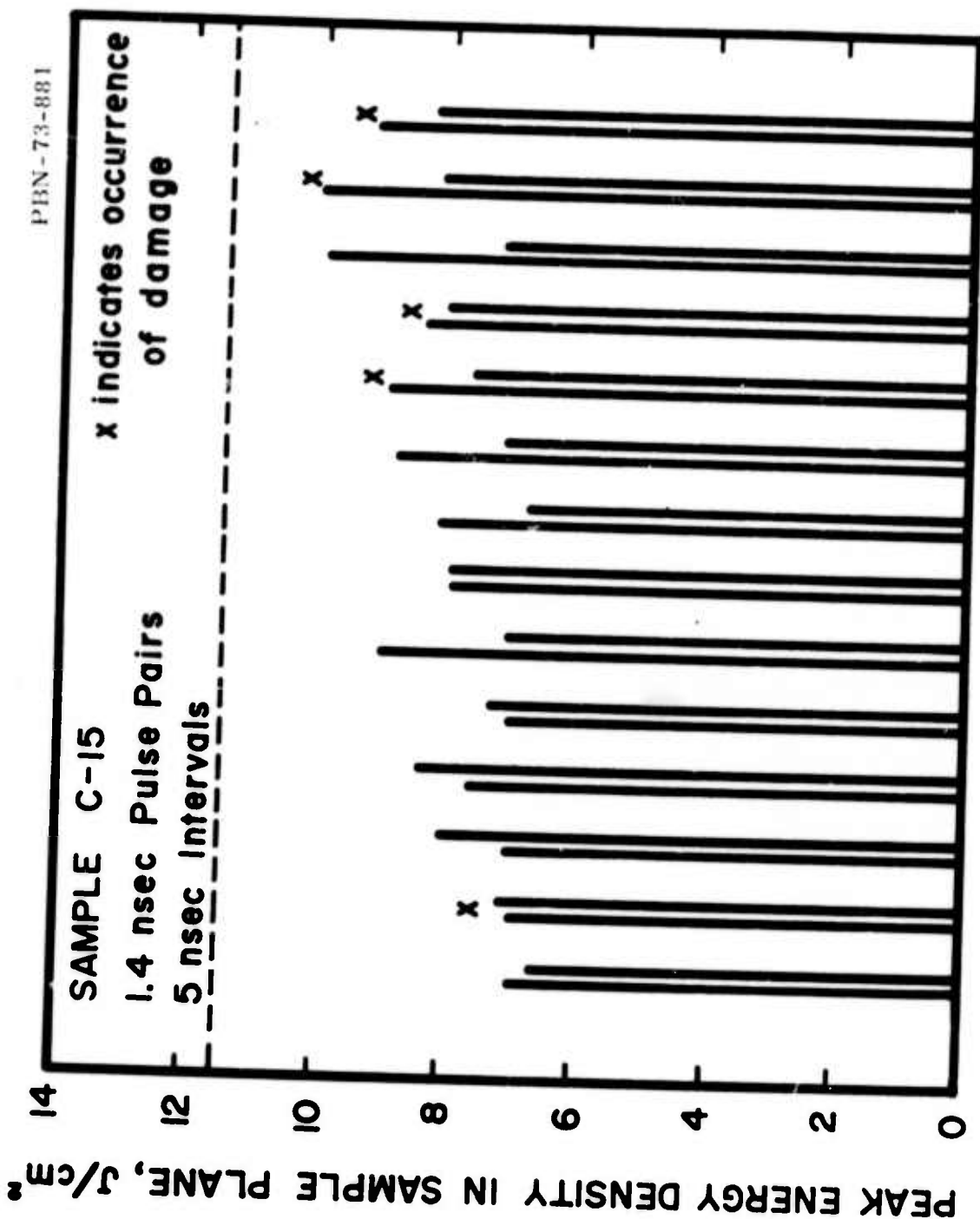


Fig. 25

Record of Some Double-Pulse Experiments on the Sample for Which Single-Pulse Data is Shown in Fig. 26. The failure to observe a consistent pattern of damage due to pulse-pair summation indicates that linear absorption in the film itself is not a limiting problem. A study of the morphology of the sites at which damage did occur by summation shows that damage was due to a class of larger inclusions than would have been damaged by single 1.4 nsec duration pulses.

The observation that large inclusions can be damaged due to cumulative heating by successive pulses can be generalized to explain damage by a train of mode-locked pulses. If the intensity of each of the pulses is such that singly they cannot produce damage, damage to large inclusions can still be the principal failure mechanism. This may explain the difference between the damage threshold found for single 20 psec pulses,  $\sim 10^{11}$  watts/cm<sup>2</sup>, and the intensity limits of mode-locked oscillators set by coating damage,  $\sim 1-4 \times 10^9$  watts/cm<sup>2</sup>.

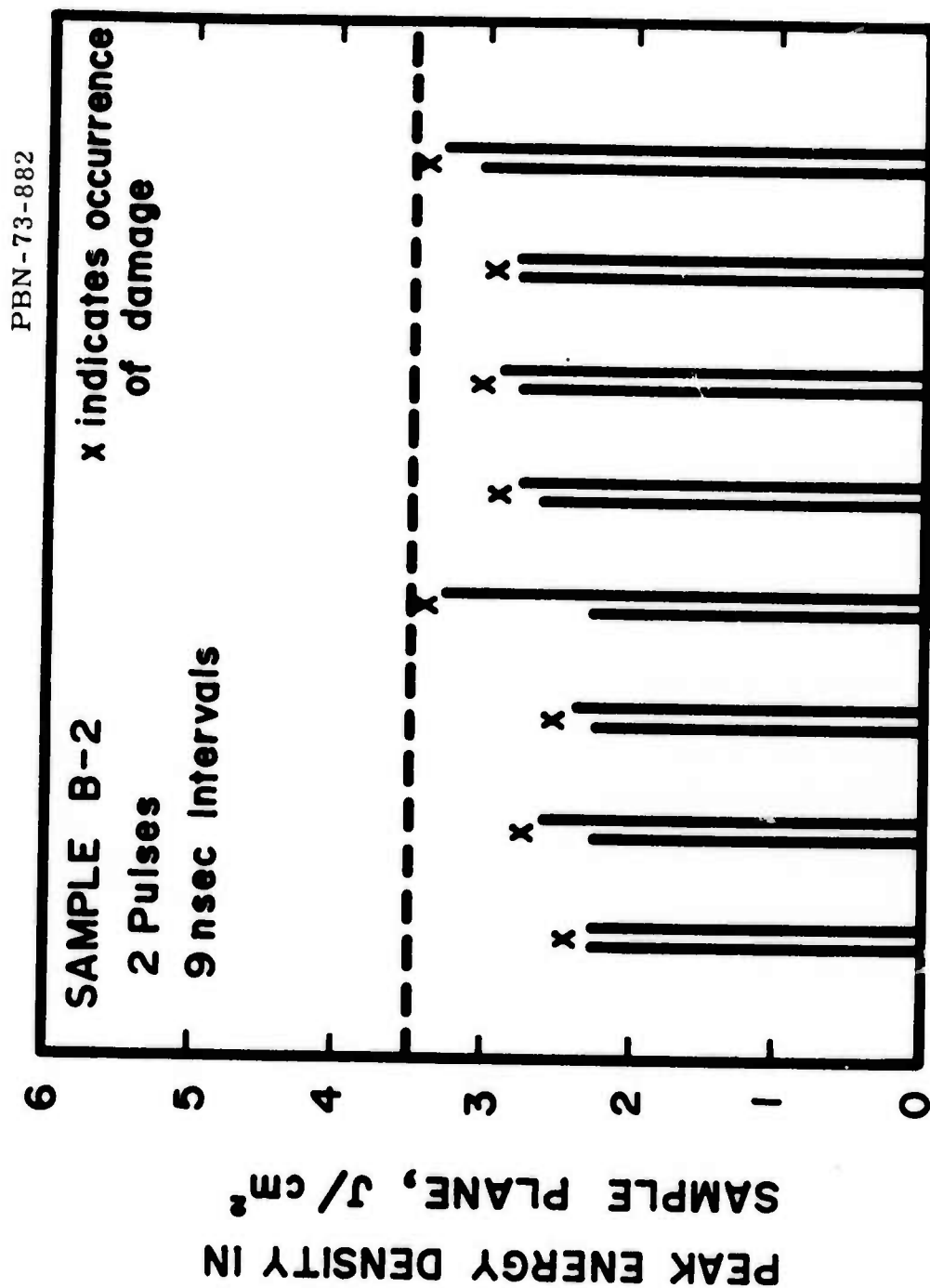
It was a general observation that there was no consistent pattern of pulse-pair addition indicative of material absorption in the mirrors used in this study.

In order to ascertain that the double-pulse experiment does indeed detect absorption, we have used the technique to study a ThF<sub>4</sub>/ZnS reflector which is known to be linearly absorptive at  $\lambda = 0.69 \mu\text{m}$ . Typical double-pulse data for this mirror is shown in Figure 26, where the single-pulse damage threshold is again represented by the dashed line. For this reflector, the expected consistent addition of pulses is seen to occur.

These results indicate that if the coating materials are non-absorbing than a combination of linear absorption and/or absorption by small inclusions cannot be invoked to explain results such as those shown in Figure 22. It is possible therefore that this type of damage was caused by an intrinsic process. To study this possibility, experiments in which a spot size sufficiently small such that the irradiated area of the coating is not likely to contain inclusions which are easily damaged by the pulses used are in progress.

## 5. Conclusions

The principal conclusions of this work are:



Double-Pulse Damage Experiments on a  $ThF_4/ZnS$  Mirror. Single-pulse threshold is indicated by the dashed horizontal line. A consistent pattern of damage due to addition of two subthreshold pulses indicates linear absorption in the coating.

Fig. 26

1. The practical damage threshold for optical coatings at  $0.69\ \mu\text{m}$  is determined by the presence of absorbing impurity inclusions.
2. The predicted "pulse duration-inclusion size" relationship for metallic or highly absorbing non-metallic inclusions was observed.
3. Very small ( $< 0.3\ \mu\text{m}$ ) inclusions are the limiting factor in coating damage resistance to single 20 psec ruby laser pulses.
4. Larger inclusions ( $> 4\ \mu\text{m}$ ) are responsible for threshold coating damage when long duration pulses ( $\approx 20\ \text{nsec}$ ) or trains of mode-locked pulses are used. Damage resistance to such irradiation would be improved if only this class of larger inclusions could be eliminated. Inclusions of these sizes are appropriate to laser radiation in the visible or near infrared. For other wavelengths the limiting inclusion sizes must be scaled according to the wavelength.
5. Linear absorption in films does not determine the damage resistance of coatings when they are properly prepared from materials which do not show bulk absorption.

## 6. Acknowledgments

The authors wish to acknowledge the use of data collected by E. S. Bliss (currently with Lawrence Livermore Laboratories) while he was employed at Air Force Cambridge Research Laboratories. They also acknowledge the assistance of C. C. Gallagher in design and construction of the laser-triggered spark gaps and fast pulse circuitry, and the assistance of E. E. Hoell and H. Miller in collecting some of the data presented here. The latter three individuals are employed at Air Force Cambridge Research Laboratories.

## VI. RELATIONSHIP BETWEEN SELF-FOCUSING AND OPTICAL DAMAGE

### A. Introduction

A number of researchers have analyzed the self-focusing effect by using a paraxial ray formula. This approach has been found to be inadequate in the ultra-high-power regime where small-scale beam distortions can lead to effects that are absent at lower laser powers. However, the paraxial ray model has been useful in describing both incipient self-focusing at moderate laser powers and the competition between self-focusing and diffraction at low laser powers near the critical power  $P_{cr}$  for catastrophic beam collapse.

The relationship between self-focusing and optical damage is discussed in this section within the framework of a paraxial ray model. Because of the low laser powers considered ( $P < P_{cr}$ ), the paraxial ray model appears to provide an adequate description of beam propagation. The analysis summarizes the effects of the index nonlinearity on a focused, low-power laser beam and shows how this effect can be used to measure self-focusing parameters. As an illustration of the application of this measurement technique, the self-focusing parameters for sapphire are determined.

B. THE MEASUREMENT OF SELF-FOCUSING PARAMETERS  
USING INTRINSIC OPTICAL DAMAGE\*

David W. Fradin<sup>†</sup>  
Division of Engineering and Applied Physics  
Harvard University  
Cambridge, Mass. 02138

Abstract

A new method for measuring the self-focusing parameters of transparent materials is reported. The technique consists of using lenses with different focal lengths to induce intrinsic bulk damage at low powers where catastrophic self-focusing is absent and then comparing the results to analytical calculations. Using this technique, the self-focusing parameters for sapphire are determined.

---

\* Supported by the Joint Services Electronics Program at Harvard University under Contract No. N00014-67-A-0298-006 and the Advanced Research Projects Agency of the Dept. of Defense monitored by the Air Force Cambridge Research Labs. under Contract No. F19628-70-C-0223.

<sup>†</sup> Present address: United Aircraft Research Labs., East Hartford, Conn. 06108

It has been observed that a third-order optical nonlinearity can lead to catastrophic self-focusing of light.<sup>42</sup> This nonlinearity causes the index of refraction to increase by an amount  $n_2(E_{rms})^2$  in the presence of an optical electric field. Values of  $n_2$  for various materials can be determined from measurements of induced birefringence,<sup>43</sup> by studies of the movement<sup>44</sup> or positions<sup>45</sup> of optical damage tracks in crystals, or by observing the changes in the intensity distribution of a transmitted laser beam as the input power is increased.<sup>46</sup> The electric contribution to  $n_2$  can also be inferred from measurements of optical third harmonic generation.<sup>47</sup>

Reported here is a new technique for measuring self-focusing parameters consisting of determining the powers necessary to induce intrinsic bulk damage as lenses with different focal lengths are used to focus the radiation and compare the results to analytical calculations. High input powers are not needed so that relatively small, stable lasers can be used. This technique is described below, and as an illustration of its application, the self-focusing parameters for sapphire are determined.

We consider a low power laser beam with input power  $P < P_{cr}$  where  $P_{cr}$  in esu units is<sup>48-50 \*</sup>

$$P_{cr} = \lambda_0^2 c / 32 \pi^2 n_2 \quad (1)$$

The vacuum laser wavelength is  $\lambda_0$  and  $c$  is the vacuum light velocity. For such powers catastrophic self-focusing is absent, and the focused beam diameter is decreased from its diffraction limit of  $d_0$  to a smaller value,  $d_1$ , because of the index nonlinearity. As a result of this reduction in beam diameter, the on-axis intensity is increased by the factor  $(d_0/d_1)^2$ , a factor which is a function of both the laser input power and the nonlinear index  $n_2$ . (See Fig. 27)

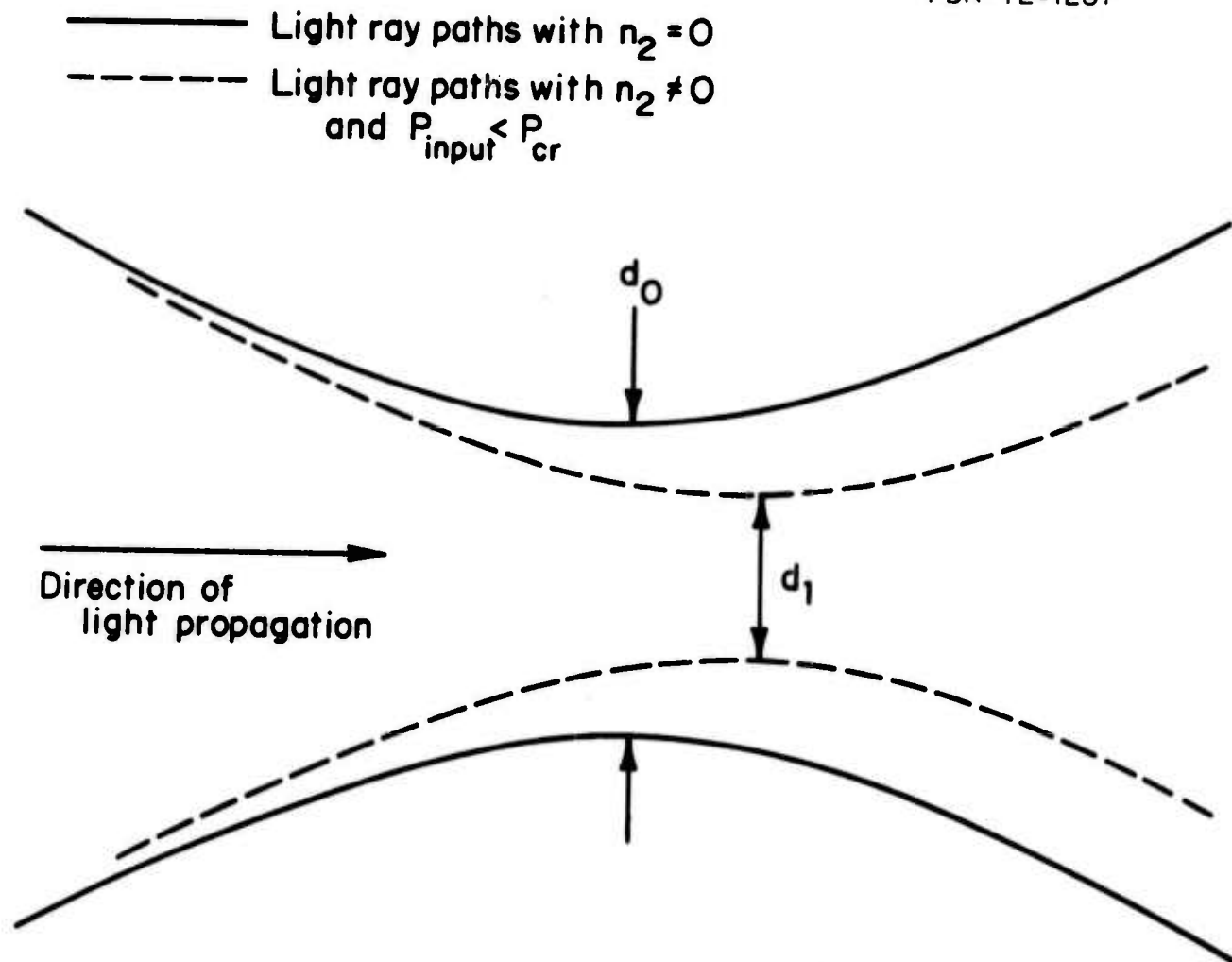


Fig. 27 The Effect of the Index Nonlinearity on the Diameter of the Focal Point. The tendency to self-focus acts in opposition to diffraction. Whereas diffraction produces a positive ray curvature, self-focusing produces a negative ray curvature. The focal diameter inside a nonlinear medium ( $n_2 \neq 0$ ) will be effectively reduced, therefore, from  $d_0$  -- its value with  $n_2 = 0$  -- to  $d_1$ , and the on-axis light intensity at the focus will be correspondingly increased. As shown by Wagner et al.<sup>49</sup>, the presence of the index nonlinearity also causes the point of minimum beam radius to be displayed to the right toward the geometrical focus.

Calculations of  $d_0/d_1$  have been made for Gaussian beams from a steady-state, paraxial ray analysis. These calculations show that if  $I_0$  is the on-axis intensity of a strongly focused laser beam when  $n_2 = 0$ , then the on-axis intensity  $I_d$  in the presence of the index nonlinearity is \*

$$I_d = I_0 (1 - P/P_{cr}) . \quad (2)$$

As the input power is increased to within a few percent of  $P_{cr}$ , corrections to Eq. (2) may become important<sup>48</sup> and numerical calculations may be required to accurately establish the relationship between  $I_d$  and  $I_0$ .

The steady-state analysis summarized by Eq. (2) is appropriate for tightly focused laser beams, because the electronic contribution to  $n_2$  is in its steady-state whenever the laser pulsewidth  $t_p$  is greater than a response time  $\tau$  given by the ratio of the radius of the focused laser beam and the radial compression wave velocity  $v_s$ .<sup>51</sup> In sapphire  $\tau = 10^{-8}$  sec when the focused beam diameter is 220  $\mu\text{m}$  and the propagation direction is along the crystalline c-axis. If electrostriction is slightly transient, Eq. (1) may be used with  $P_{cr}$  corrected in a manner discussed by Kerr.<sup>52</sup>

Having this determined the intensification produced by the index nonlinearity, we look for a process which is sensitive to a constant value of on-axis laser intensity. The powers necessary to reach this intensity will be recorded as  $d_0$  (see Fig. 27) is varied by using lenses with different focal lengths. Intrinsic optical damage from avalanche breakdown is a convenient choice for this intensity-sensitive process.<sup>9,10</sup> Although laser-induced avalanche breakdown is an inherently statistical process,<sup>18,20</sup> it is virtually threshold-like for many materials. A damage intensity  $I_d$  can be defined<sup>10</sup> as that value of intensity inside the material which is necessary in order to induce damage on a single shot with a probability of 0.5. The damage power is the incident power necessary to reach  $I_d$  under particular external focusing conditions. Breakdown leads to a spark and local melting of the material and is therefore easily observed.

---

\* Prof. J. Marburger has pointed out that Eq. (2) is an approximate result. Using Eqs. (2.16) and (3.2) of Ref. 49, a more accurate relationship between  $I_d$  and  $I_0$  can be derived. The difference between Eq. (2) in the text and this more accurate results is unimportant, however, when  $P < P_{cr}$  and the incident laser beam has been focused sufficiently to induce intrinsic optical damage.

$P_{cr}$  is determined from measurements of the damage power  $P$  made with various lenses having different focal lengths. Complications from aberrations in the focusing optics<sup>52</sup> and inaccuracies in determining the input powers can be greatly reduced by the use of a reference crystal such as NaCl which can be damaged over a large range of input powers before self-focusing becomes important.<sup>10</sup> Approximate values of  $P_{cr}$ , which are useful for the initial selection of focusing optics, can be calculated theoretically.<sup>47,52</sup>

To analyze the data, it is convenient to rewrite Eq. (2) as

$$1/P = (2n_0/\pi I_d) \frac{1}{w^2} + 1/P_{cr} \quad (3)$$

Here we have assumed that the intensity distribution at the focus in the absence of the index nonlinearity is  $I(r) = I_0 \exp(-2r^2/w^2)$  where  $w = d_0/2$ , and we have replaced  $I_0$  in Eq. (2) by  $2n_0 P/\pi w^2$ . The focal lengths of the various lenses can be related to the corresponding values of  $w$ . The damage intensity  $I_d$  does not depend on  $w$  for avalanche breakdown.<sup>10</sup> A plot of  $1/P^2$  as a function of  $1/w^2$  then yields a straight line with  $1/P_{cr}$  as the intercept and  $2n_0/I_d$  as the slope.

Two precautions should be taken when using this measurement technique. The first is to avoid damage from absorbing inclusions, and the second is to account for any dependence of avalanche breakdown on the laser pulse width. Methods for distinguishing between inclusion and intrinsic damage are detailed in Refs. 10 and 18. The laser pulsewidth dependence to the damage field has been measured.<sup>17,54 \*</sup>

As an illustration of the use of this technique, we consider data accumulated in two different experiments on optical damage in sapphire. In the first experiment<sup>53</sup> a Q-switched TEM<sub>00</sub> ruby laser was used by Giuliano et al. to damage sapphire with three different lenses. In the second<sup>24</sup> a measurements of  $I_d$  was made with two different lenses and

---

\* An increase in damage intensity of no more than about 15 percent was predicted as the laser pulsewidth is varied from 20 to 5 ns. This prediction was confirmed in Refs. 51 and 24. A frequency dependence to the breakdown intensity will, if present, act to compensate this change. Because of possible inaccuracies introduced from the pulsewidth and frequency dependence to breakdown, experiments designed to use the technique reported in the text should be conducted at a single frequency with the pulsewidth being held reasonably constant.

a Q-switched TEM<sub>00</sub> YAG:Nd laser. The pulse widths were 20 nsec and 5 nsec, respectively.<sup>54</sup> Table III summarizes the relevant results of these studies.

In order to compare the data, the wavelength dependence of  $P_{cr}$  must be considered. It can be seen from Eqs. (2) and (3) that the data can be plotted together if the coordinate axes for the YAG data are properly scaled relative to those for ruby. In the plot of  $1/P$  versus  $1/w^2$  in Fig. 28, the axes are scaled by  $[\lambda_0(\text{YAG})/\lambda_0(\text{ruby})]^2 = 2.35$ . The intercept on the vertical ruby axis is  $P_{cr}$  at  $0.6943 \mu\text{m}$ , and the slope measured relative to either pair of axes is  $(2/\pi I_d)n_0$ .

$P_{cr}$  is found to be  $0.83 \times 10^6$  watts at ruby wavelength;  $n_2 = 0.56 \times 10^{-13}$  esu; and  $I_d$  is  $1.1 \times 10^{11}$  watts/cm<sup>2</sup>. The value of  $n_2$  lies within the range of values reported in Ref. 44 and  $I_d$  agrees with the results of Ref. 24.

The plot in Fig. 28 curves downward when  $1/w^2 \lesssim 0.02 \times 10^{-2} (\mu\text{m})^2$  because the electrostrictive contribution to the critical power is becoming transient. Even though Eq. (3) is not valid for transient effects, we can modify it to approximate slightly transient behavior by letting  $P_{cr}$  in Eq. (1) become a function of  $w$  as described by Kerr.<sup>52</sup> If it is assumed that the electrostrictive nonlinearity is much larger than the electronic effect,<sup>55</sup> a damage power of about  $1.1 \times 10^6$  watts is thereby predicted for  $w = 140 \mu\text{m}$ . This value compares favorably to the measured value of  $1.2 \times 10^6$  watts in Table III.

The electronic contribution to  $n_2$  can in principle be determined by the present technique if electrostriction is negligible because conditions of measurement have been chosen so that  $t_p/\tau \ll 1$ . Because of the requirement that the input power be less than  $P_{cr}$ ,  $t_p/\tau \ll 1$  cannot be achieved by increasing  $\tau$  even though the use of weakly focusing optics. This extreme transient limit for electrostriction can be achieved, however, by using single, mode-locked laser pulses with time durations of the order of  $10^{-11}$  sec. Such pulses must be temporarily smooth and hence transform-limited so that a YAG:Nd system is a natural choice for the laser.

TABLE III

DAMAGE POWER IN SAPPHIRE FOR DIFFERENT BEAM SIZES

<u>Wavelength</u>	<u>w (<math>\mu\text{m}</math>)<sup>*</sup></u>	<u>P (MW)</u>
0.6943 $\mu\text{m}$ (ref. 15)	20	0.51 $\pm$ .04
	53	0.74 $\pm$ .07
	140	1.23 $\pm$ .10
1.064 $\mu\text{m}$ (ref. 16)	9.0	0.24 $\pm$ .05
	4.1	0.05 $\pm$ .02

\* The beam radius is defined to be the  $1/e^2$  radius for the intensity. In both experiments Gaussian laser beams were used.

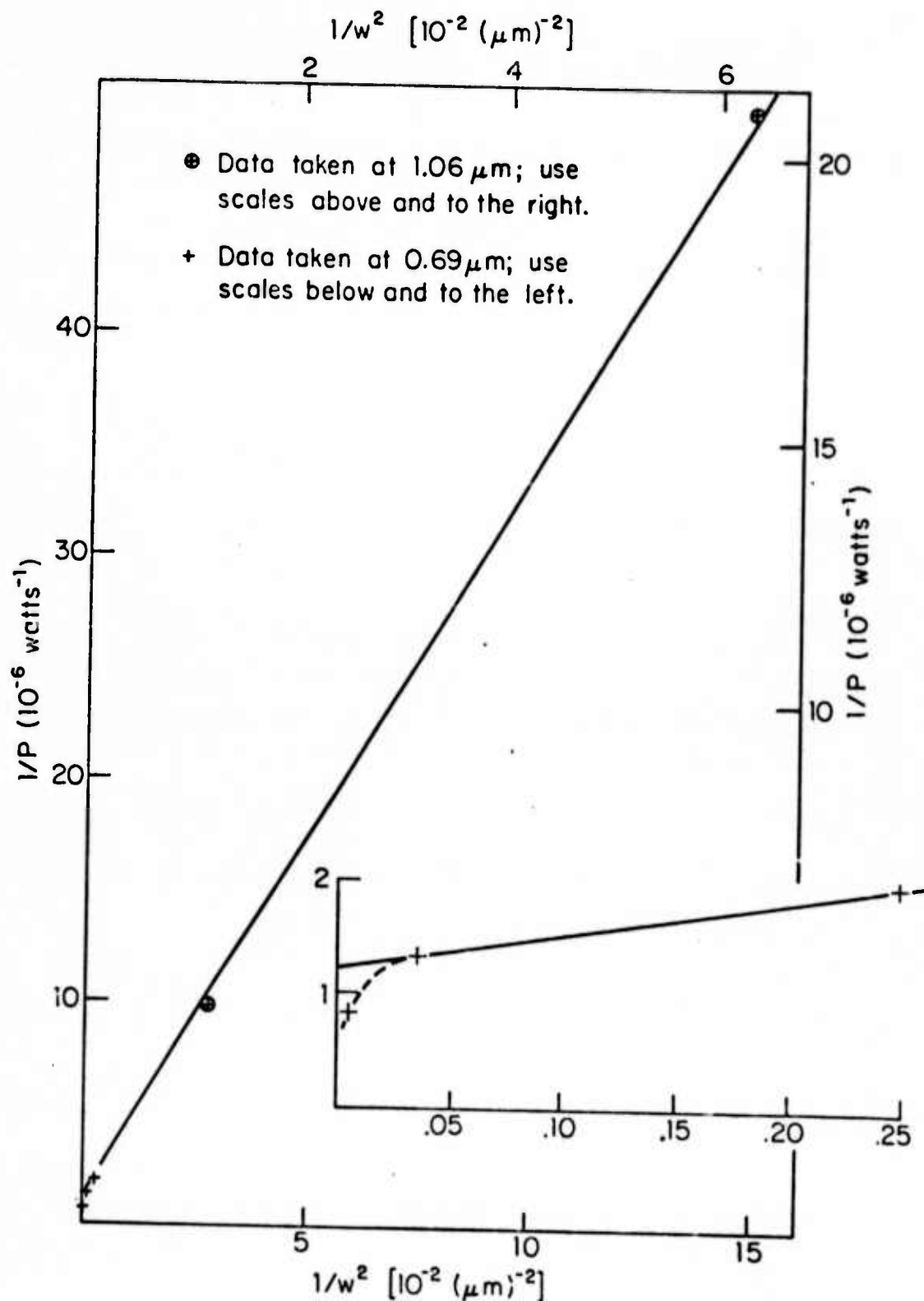


Fig. 28 The Dependence of Damage Power for Sapphire on Beam Focal Diameter. A plot of  $1/P$  as a function of  $1/w^2$  produces a straight line according to Eq. (3).  $P$  is the input damage power, and  $w$  is the Gaussian beam radius. For large  $w$  ( $1/w^2 \lesssim 0.02 \times 10^{-2} (\mu\text{m})^{-2}$ ), departures from a linear relationship are expected because electrostriction becomes transient. This is experimentally observed as seen in the insert where the scales for the ruby data have been expanded.

It should be noted that the analysis summarized by Eqs. (2) and (3) is based on the assumption of an infinite self-focusing medium. In fact, the tendency to self-focus begins at the sample entrance face.<sup>57</sup> A correction to Eq. (2) that accounts for the finite medium has been evaluated using the method of Ref. 56.\* It was found that the error introduced by the assumption of an infinite medium is less than 10 percent provided that the distance  $\Delta z$  between the beam focus and the entrance face satisfies

$$\Delta z > 5.4 \times 10^{-3} \left( \frac{P}{P_{cr}} \right)^{\frac{1}{2}} (f^2) . \quad (4)$$

The lens focal length  $f$  and  $\Delta z$  are expressed in millimeters. Equation (4) appears to have been easily satisfied in the experiments of Refs. 53 and 24.

In summary, a new technique for measuring self-focusing parameters in transparent solids has been developed which uses optical damage induced by low-power lasers. This technique has been applied to previously reported measurements of breakdown intensities in sapphire to infer a value for  $n_2$ .

The author wishes to acknowledge numerous helpful discussion with M. Bass, J.H. Marburger and Y.R. Shen.

---

\* Equation (2-9) in Ref. 56 was integrated from  $z_0$  to  $z$  instead of  $-\infty$  to  $z$ . Here  $z_0$  is the coordinate of the sample entrance surface.

## VII. INCLUSION DAMAGE IN ZnSe

### A. Introduction

This section summarizes an analysis of inclusion damage and a short experimental study of 10.6  $\mu\text{m}$  laser damage in ZnSe grown by chemical-vapor-deposition. The analysis is based on a model of inclusion damage in which the probability of finding a damaging inclusion inside the high intensity portion of the laser focal volume is calculated. A statistical aspect to inclusion damage is predicted, and an operational threshold (probability  $\frac{1}{2}$  point) is calculated in terms of the damage intensity of an individual inclusion and appropriate beam parameters. Data is presented that describes 10.6  $\mu\text{m}$  laser damage in ZnSe induced by external focusing with lenses having two different focal lengths. The damage intensity was lower with the longer focal lens as expected from an inclusion damage mechanism. This observation is quantitatively explained.

B. LASER DAMAGE FROM INCLUSION ABSORPTION IN ZnSe<sup>\*</sup>

David W. Fradin<sup>†</sup> and Dominic P. Bua  
Raytheon Research Division  
Waltham, Massachusetts 02154

ABSTRACT

The inclusion damage studies, conducted at 10.6  $\mu\text{m}$  in ZnSe, show a dependence of bulk inclusion damage levels on the degree of external beam focusing. This same effect, previously seen and explained in thin film damage studies, is quantified for bulk inclusion damage by using a simple model based on a statistical approach to inclusion damage.

---

<sup>\*</sup> Supported by the Defense Advanced Research Projects Agency and monitored by Air Force Cambridge Research Laboratories under Contract No. F19628-73-C0127.

<sup>†</sup> Present address: United Aircraft Research Laboratories, East Hartford, Conn. 06108.

## 1. Introduction

When optical damage results from inclusion absorption, the damage intensity will depend on the focused beam diameter.<sup>60</sup> This dependence exists because the inclusions responsible for damage are randomly dispersed in the material. When the beam diameter  $2\omega_0$  is of the same order of magnitude as the average inclusion separation  $d_0$ , this dependence is pronounced and can be calculated from the probability of illuminating a damaging inclusion with the high intensity portion of the light beam.<sup>60,61</sup> In the limit of sufficiently large beam diameters ( $2\omega_0 \gg d_0$ ) or sufficiently small diameters ( $2\omega_0 \ll d_0$ ), however, the damage intensity will be independent of beam size. Constant damage intensity results, in the former case, from the fact that the probability of intercepting an inclusion in the intense portion of the light beam approaches unity for large beam diameters. In the latter case, the damage intensity becomes independent of  $\omega_0$  because inclusions will be missed by most tight focused laser pulses and damage will thus normally result from an intrinsic process.

In Sec. 2 analytical expressions will be derived for the probability of bulk inclusion damage induced by Gaussian laser beams. These expressions will allow us to quantify the ideas just expressed and to interpret the 10.6  $\mu\text{m}$  ZnSe damage data presented in Sec. 4.

## 2. Theory

In order to more accurately clarify the inclusion damage problem considered here, the following questions are posed: If optical damage from inclusion absorption develops when the laser beam is focused to an on-axis intensity  $I_0^D$ , what is the threshold intensity  $I_1$  necessary to damage an individual inclusion? How does  $I_0^D$  vary with the degree of external focusing?

Two simplifying assumptions will be made in the analysis. First,  $I_0^D$  will be assumed to be less than the intrinsic breakdown intensity  $I_2$ . Second, all the inclusions are assumed to be identical in the sense that each has the same damage intensity  $I_1$  when the laser pulse duration is held constant.

This second assumption, although it might appear at first to be an unphysical restriction, can be a useful approximation to the inclusion damage problem. As shown by Hopper and Uhlman,<sup>11</sup> the damage intensity for highly absorbing inclusions is lowest when the thermal diffusion time  $\tau$  and the pulse duration  $\tau_p$  are comparable. Since  $\tau \sim R^2/D$  where  $R$  is the inclusion radius and  $D$  is the host thermal diffusivity, threshold damage is principally determined by inclusions having

$$R \sim (Dt_p)^{\frac{1}{2}}. \quad (1)$$

These inclusion have a well-defined damage intensity  $I_1$ . At longer pulse durations, larger inclusions, if present, will be responsible for threshold damage and  $I_1$  will scale as  $(t_p)^{-\frac{1}{2}}$  as long as Eq. (1) can be satisfied.

We will see that even when  $I_1$  is a well-defined quantity, inclusion damage can appear to be a statistical process because of the random placement of inclusions inside the solid. For this reason it is necessary to define an operational damage threshold  $I_0^D$  as that intensity at which the probability for damage is  $\frac{1}{2}$ . This same convention was used in the ZnSe experiment in Sec. 3.3 as well as in intrinsic damage studies where statistics result from the physical nature of the damage process itself<sup>18, 20</sup> and not from the inhomogeneous nature of the medium as in the present case.

To derive the bulk damage probability, we begin with the two-dimensional problem of points randomly distributed on a plane. DeShazer, et al.<sup>60</sup> have considered this same starting point in their approximate calculations of the damage intensity of thin film optics.

Analysis shows that the probability that no points will be within a circle of radius  $r$  on the plane is<sup>60</sup>

$$p_0 = e^{-\sigma \pi r^2} \quad (2)$$

where  $\sigma$  is the average surface density of points. Consider a Gaussian light beam that is incident on this plane and that has the intensity distribution

$$I(r, z) = I_0 \left[ \frac{\omega_0}{\omega(z)} \right]^2 \exp \left[ -\frac{2r^2}{\omega(z)^2} \right] \quad (3)$$

where  $\omega(z) = \omega_0 [1 - (z/z_R)^2]^{1/2}$  and  $z_R$  is the Rayleigh distance  $\pi \omega_0^2 / \lambda$ . If each of the points of the plane corresponds to an inclusion with damage intensity  $I_1$ , then the probability that optical damage will occur on this plane is just the probability that an inclusion will lie with the region where  $I(r, z) \geq I_1$ . This region is bounded by a circle of radius  $r_T$  defined by the intersection of the surface

$$I(r_T, z) = I_1 \quad (4)$$

with the plane at constant  $z$ .

From Eqs. (3) and (4),  $r_T$  is found to be

$$r_T = \omega_0 \sqrt{\frac{1}{2} [1 + (z/z_R)^2] \ln \gamma / [1 + (z/z_R)^2]} \quad (5)$$

where  $\gamma = I_0/I_1 \geq 1$ . The probability  $P_D$  that damage will occur is just

$$P_D(I_0, \omega_0) = 1 - p_0 = 1 - \exp(-\pi \omega_0 r_T^2). \quad (6)$$

If the plane is located at the beam focus ( $z = 0$ ), then  $r_T$  simplifies and  $P_D$  can be expressed as

$$P_D(I_0, \omega_0) = 1 - e^{-\bar{n}} \quad (7)$$

Here  $\bar{n}$  is the average number of inclusions inside the circle of area  $\pi \omega_0^2 / 2$ .  $\bar{n}$  and  $\omega_0$  are related by

$$\bar{n} = \sigma \left( \frac{\pi \omega_0^2}{2} \right) \quad (8)$$

Equations (7) and (8) give the probability that a focused Gaussian beam will induce damage on the surface of a solid or in a thin film layer.

The analysis can now be extended to three dimensions. Before calculating  $P_D$  exactly, consider an idealized gaussian beam that remains perfectly collimated over a distance  $\ell_{\text{eff}}$ . For this geometry  $P_D$  is still given by Eq. (6), but  $\sigma$  is replaced by  $\rho \ell_{\text{eff}}$ . The volume density of inclusions  $\rho$  is treated as an exogeneous variable that has been determined by an independent technique such as the light scattering measurement described in the next section. With this substitution

$$\begin{aligned} P_D &= 1 - \exp(-\pi \rho \ell_{\text{eff}} r_T^2) \\ &= 1 - \exp(-\rho V_{\text{eff}}) . \end{aligned} \quad (9)$$

$V_{\text{eff}}$  is that portion of the focal volume in which the laser intensity is high enough to cause inclusion damage.

For a true focused beam,  $P_D$  still has the form of Eq. (9). The basic form of the probability is unchanged for complicated geometries because of the exponential behavior of  $p_0$  and the multiplicative nature of compound probabilities.  $V_{\text{eff}}$  can be approximated by cones of revolution as noted in Fig. 29. The radius of the base of either cone is  $r_T$  and the cone height is  $z_T$  defined by

$$I(0, z_T) = I_1 \quad (10)$$

or

$$z_T = z_R (\gamma - 1)^{\frac{1}{2}} = -\frac{\pi \omega_0^2}{\lambda} (\gamma - 1)^{\frac{1}{2}} . \quad (11)$$

$V_{\text{eff}}$  becomes, in this approximation,

$$V_{\text{eff}} (\text{cones}) = \frac{2}{3} \pi r_T^2(0) z_T \quad (12)$$

where  $r_T(0)$  is given by Eq. (5) with  $z = 0$ . Alternately,  $V_{\text{eff}}$  can be calculated exactly as we now show.

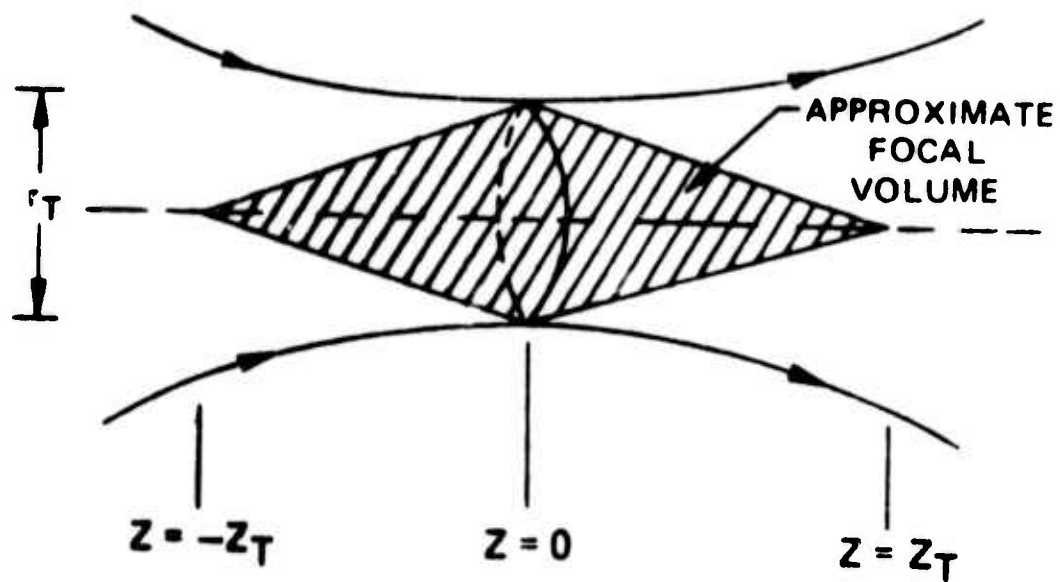


Fig. 29 Approximate Focal Volume for a Gaussian Beam.

$V_{\text{eff}}$  is the cylindrically symmetric region bounded by the surface of Eq. (4). Making use of the cylindrical symmetry,  $V_{\text{eff}}$  can be written as

$$V_{\text{eff}} = 2 \int_0^{z_T} \pi r_T^2(z) dz. \quad (13)$$

Inserting Eqs. (5) and (11) into  $V_{\text{eff}}$  gives

$$V_{\text{eff}} = \pi \omega_0^2 \int_0^{z_F} [1 + (z/z_R)^2] \ln \left[ \gamma / [1 + (z/z_R)^2] \right] dz. \quad (14)$$

This integral can be expressed in closed form using standard integral tables with the result that

$$V_{\text{eff}} = (\pi \omega_0^2) z_F \left[ \frac{2}{9} (\gamma - 1)^{\frac{1}{2}} (\gamma + 5) - \frac{4}{3} \tan^{-1} (\gamma - 1)^{\frac{1}{2}} \right] \quad (15)$$

Since  $p_0 = (-\rho V_{\text{eff}})$  and  $P_D = 1 - p_0$  from Eq. (6), it follows that

$$\begin{aligned} P_D &= 1 - \exp(-\rho V_{\text{eff}}) \\ &= 1 - \exp \left\{ -\rho \frac{(\pi \omega_0^2)^2}{\lambda} \left[ \frac{2}{9} (\gamma - 1)^{\frac{1}{2}} (\gamma + 5) - \frac{4}{3} \tan^{-1} (\gamma - 1)^{\frac{1}{2}} \right] \right\}. \end{aligned} \quad (16)$$

As before,  $\gamma = I_0/I_1$ , and only the region  $\gamma \geq 1$  is considered.

Equation (16) expresses the probability that inclusion damage will occur in a solid and shows how this probability depends on focused beam radius ( $\omega_0$ ), the on-axis intensity at the focus ( $I_0$ ), the damage intensity for an individual inclusion ( $I_1$ ), and the measured inclusion density ( $\rho = N/d_0^3$ ).

$P_D$  is not a step function except in the limit  $\omega_0 \rightarrow \infty$ . There exists a range of conditions in which  $0 < P_D < 1$  so that optical damage will appear to be a statistical process as different damage sites are probed. Unlike the statistics resulting from avalanche breakdown,<sup>18,20</sup> however,  $P_D$  is a function of laser intensity, not peak field, and the damage intensity is well-defined at each damage site. Statistics are

apparent in the inclusion problem because each damage site is different. For a perfect single-mode laser held to constant peak intensity, each site will damage on the first shot or not at all. Referring to Eqs. (7) and (9), it is seen that the intensity range over which  $P_D$  is measurably different from 0 or 1 depends on the average number of inclusions  $\bar{n}$  inside the focal volume. When  $\bar{n}$  is large, as expected for weakly focused laser beams,  $P_D$  approaches a step function with the discontinuity located at  $I_0 = I_1$ . The dependence of  $P_D$  on  $\bar{n}$  is illustrated schematically in Fig. 30.

Because the statistical nature of inclusion damage precludes the observation of a well-defined threshold for focused beams, an effective damage threshold  $I_0^D$  must be defined.<sup>10</sup> We let  $I_0^D$  be that value of  $I_0$  which induces damage with a probability of  $\frac{1}{2}$ . When  $P_D = \frac{1}{2}$  is inserted into Eq. (16), an equation results which relates  $I_0^D$  to  $I_1$ . From Eq. (13) we find

$$(\gamma - 1)^{\frac{1}{2}} (\gamma + 5) - 6 \tan^{-1} (\gamma - 1)^{\frac{1}{2}} = \frac{9\lambda}{2\rho(\pi\omega_0)^2} \ln 2. \quad (17)$$

The right hand side of this equation can be evaluated in terms of known parameters giving an equation for  $\gamma = I_0^D/I_1$ .

Equation (17) is our basic result. If  $\omega_0$ ,  $\rho$  and  $I_0^D$  are measured, then Eq. (17) allows us to calculate  $I_1$ , the damage intensity for a single inclusion. Having obtained  $I_1$ , it is then possible to predict the damage intensity measured under different conditions of focusing using Eq. (17) and

$$\omega_0 = \frac{2}{\pi} \frac{\lambda}{D} f. \quad (18)$$

$D$  is the gaussian  $1/e^2$  diameter at the lens of focal length  $f$ . Alternately,  $\rho$  can be calculated from two or more measurements of  $I_0^D$  made with different lenses.

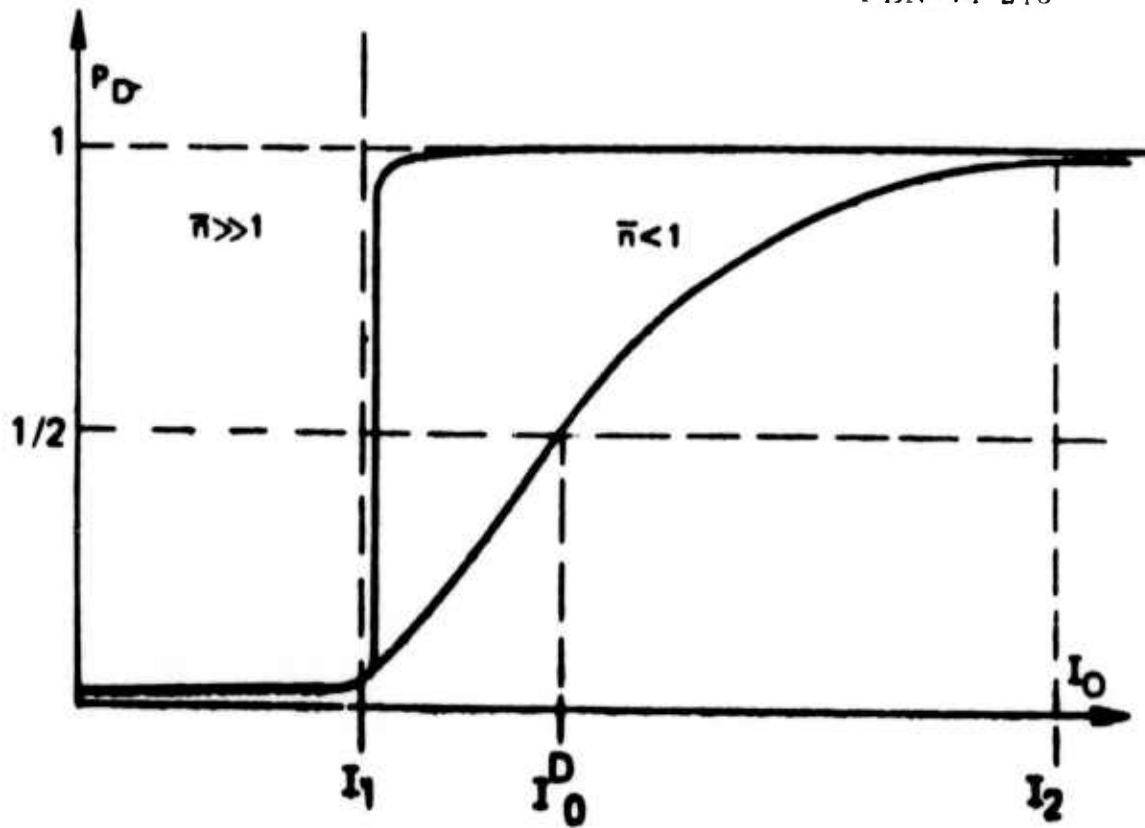


Fig. 30 Schematic Showing the Relationship Between  $P_D$  and  $I_0$  for Two Different Values of  $\bar{n}$ .

When  $\gamma$  approaches unity (weak focusing), Eq. (17) can be approximated by

$$(\gamma - 1)^{3/2} \approx \frac{9 \ln 2 \lambda}{4 \rho (\pi \omega_0^2)^2} \quad (19)$$

In the next section we will use Eq. (17) to analyze the results of inclusion damage studies in ZnSe.

### 3. Intrinsic damage statistics

The intrinsic damage process has been found to have a statistical character.<sup>18</sup> Although these statistics are less pronounced than the statistics associated with inclusion damage, they should, in principle, be included in a complete model of damage statistics.

To illustrate the manner in which intrinsic and inclusion statistics are combined, we calculate the total damage probability  $P_{tl}$  from the inclusion damage probability  $P_D^{inc}$  and the intrinsic damage probability  $P_D^{intr}$ .  $P_D$  is given by

$$\begin{aligned} P_{tl} &= 1 - (\text{probability that no damage occurs}) \\ &= 1 - (1 - P_D^{inc}) (1 - P_D^{intr}) . \end{aligned} \quad (20)$$

We have used the fact that the probability that no damage occurs is given by the compound probability that damage does not occur in either an intrinsic or an inclusion process. Expanding Eq. (20) gives

$$P_{tl} = (P_D^{inc} + P_D^{intr}) - P_D^{inc} P_D^{intr} . \quad (21)$$

In the limit where  $P_D^{intr}$  is a step function defined as

$$P_D^{intr} = h(I^{intr} - I_0) = \begin{cases} 0; & I_0 < I^{intr} \\ 1; & I_0 \geq I^{intr} \end{cases} . \quad (22)$$

Equation (21) reduces to

$$P_{tl} = \begin{cases} P_D^{inc}; I_0 < I^{intr} \\ 1; I_0 \geq I^{intr} \end{cases} \quad (23)$$

Since it has been found experimentally that Eq. (22) is nearly valid in ZnSe for the conditions of our measurement, Eq. (23) will be used for  $P_{tl}$  with  $P_D^{inc}$  given by Eq. (16). In experiments where the intrinsic limits are approached, however, it is necessary to explicitly consider the intrinsic damage probability in order to adequately describe the statistical aspects of laser damage.

#### 4. Experimental measurements of inclusion damage

ZnSe, grown by a chemical vapor deposition process at Raytheon Company, was probed with laser light at  $1.06 \mu\text{m}$  ( $t_p = 10 \text{ ns}$ ) and  $10.6 \mu\text{m}$  ( $t_p = 140 \text{ ns}$ ) from Q-switched lasers. The  $\text{TEM}_{00}$  outputs from both these lasers were examined with pinholes, as described in Ref. 10 and found to be gaussian in form to  $r \gtrsim 3\omega_0$ .

Damage studies at  $1.06 \mu\text{m}$  were conducted to establish intrinsic breakdown limits and to thereby provide a reference for additional damage studies. Because the  $1.06 \mu\text{m}$  beam could be highly focused ( $2\omega_0 \approx 16 \mu\text{m}$ ), it was possible to avoid inclusions at most damage sites. When inclusion damage did occur at individual damage sites, it was possible to distinguish between inclusion and intrinsic damage by studying the residual damage morphology.<sup>9,10</sup> Data corresponding to inclusion damage were discarded in the measurements at  $1.06 \mu\text{m}$ . Catastrophic self-focusing was precluded by the experimental design<sup>9,10</sup> and tests were conducted to confirm the absence of measurable beam distortion from either a steady-state or a transient index nonlinearity.<sup>10</sup> In this manner the incident intrinsic damage intensity,  $I_2$ , was measured at  $1.06 \mu\text{m}$  to be  $1.2 \pm 0.3 \text{ GW/cm}^2$ . Approximately 20 percent of the light was lost by reflection from the incident surface.

The temporal behavior of light transmitted through the sample when damage occurred is shown in the multiple exposure of Fig. 31. Unlike the attenuation observed during intrinsic damage in ionic solids,<sup>10</sup> the rate of attenuation is shown for the pulses which damage ZnSe, and subsequent laser pulses were not completely blocked by the damaged region. These observations at first led us to conclude that damage was occurring from submicrometer inclusions randomly dispersed in the focal volume. Such an interpretation was inconsistent, however, with calorimetric measurements of the low-field absorption coefficient ( $\alpha \approx 2 \times 10^{-3} \text{ cm}^{-1}$ ).<sup>63</sup> Although it is possible that finely dispersed submicrometer voids may locally enhance the damage intensity,<sup>64</sup> we found no experimental evidence to suggest that material defects played a role in the  $1.06 \text{ }\mu\text{m}$  measurements. The slow attenuation of the laser pulse may suggest fundamental differences between the temporal characteristics of avalanche breakdown in ionic materials and the temporal behavior of intrinsic damage in semiconductors. In the absence of reliable dc breakdown data on ZnSe and intrinsic laser breakdown data at other wavelengths, it is not possible to remove the ambiguity of our interpretation. The damage was well-defined, and any statistical character to intrinsic damage was marked by laser fluctuations.

When  $10.6 \text{ }\mu\text{m}$  laser light was used to damage ZnSe, bulk damage without self-focusing developed at  $I_0 = 340 \text{ MW/cm}^2$  when the beam was focused to  $2\omega_0 = 65 \text{ }\mu\text{m}$  and at  $260 \text{ MW/cm}^2$  when the laser beam was focused to  $130 \text{ }\mu\text{m}$ . Since intrinsic damage limits change very little with laser frequency in the infrared and do not change with the degree of focusing,<sup>10</sup> it appeared that inclusion damage was occurring. Microscopic investigation of the damage sites confirmed this interpretation.<sup>9, 10</sup> It should be noted that the experimental uncertainty in the absolute calibration of  $I_0$  was  $\pm 25$  percent but that relative values of damage intensities were determined to better than  $\pm 10$  percent. The inclusion density  $\rho$  was later determined by using both the bulk scattering of incoherent light as observed under a microscope and surface etching<sup>65</sup> initiated at inclusion sites. It was found that inclusion having diameters  $\gtrsim 1 \text{ }\mu\text{m}$  were spaced by an average distance of about  $45 \text{ }\mu\text{m}$  in ZnSe.

PBN-74-20

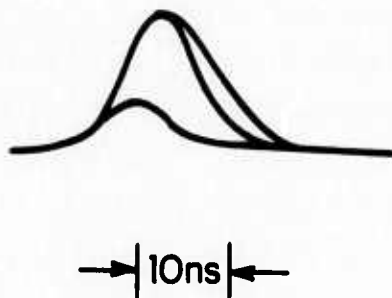


Fig. 31 Intrinsic Laser Damage at  $1.06\mu$  in ZnSe. Damage occurred on the second of three pulses. The transmitted light pulses shown here are line drawings that reproduce the pulse envelopes. High-frequency modulation from longitudinal mode beating is not shown.

Since  $I_0^D < I_2$  for both data points, the results of the preceding section can be used to explain the damage measurements at  $10.6 \mu\text{m}$ . Equation (17) can be solved numerically for  $\eta$  when  $\rho = 1/(45\mu\text{m})^3$ ,  $\lambda = 1.06 \mu\text{m}$  and  $\omega_0 = 130 \mu\text{m}$ .  $\eta = 1.05$  is obtained from either Eq. (17) or the approximate relationship of Eq. (19). Therefore,  $I_1 = (1/1.05) (260 \text{ MW/cm}^2) = 250 \text{ MW/cm}^2$ . Inserting the derived value of  $I_1$  into Eq. (17) with  $\omega_0 = 65 \mu\text{m}$ , we predict that  $I_0^D (65 \mu\text{m}) = 330 \text{ MW/cm}^2$  as compared to a measured value of  $340 \text{ MW/cm}^2$ . The experimental data, although not a strong test of the analytical model of the previous section, are thus seen to be explained quantitatively by the model.

From the present results we conclude that large diameter  $10.6 \mu\text{m}$  beams ( $2\omega_0 \gtrsim 150 \mu\text{m}$ ) with pulse durations of  $140 \text{ ns}$  will induce damage at  $250 \text{ MW/cm}^2$ . When other pulse durations are used, the damage intensity will change if there exists a distribution of inclusion sizes. As noted earlier,  $I_0^D \propto (t_p)^{-\frac{1}{2}}$  as long as Eq. (1) can be satisfied. An accurate estimate of the dependence of  $I_0^D$  on pulse width depends on a knowledge of the distribution of inclusion sizes and the absorption cross section of each inclusion.<sup>56</sup> Such a knowledge, coupled with the analysis of Hopper and Uhlman<sup>11</sup> and the results of Eq. (17) allow us to predict, at least in principle, the damage behavior of a solid for arbitrary values of  $t_p$  and  $\omega_0$ .

## 5. Conclusions

The basic approach to inclusion damage used in this section can be useful as a guide for materials evaluation studies in which the pulsed damage characteristics of initially transparent solids are to be determined. By measuring the intrinsic damage limit  $I_2$  with tightly focused laser beams, a useful reference is established for further damage studies with larger focal diameters. Under experimental conditions such that damage results from inclusion absorption, a dependence of  $I_0^D$  on the degree of focusing is predicted by the model developed here.

Careful measurements of  $I_0^D$  versus  $\omega_0$  and a determination of  $\rho$  by either light scattering or surface etching can be interpreted in terms of the model of Sec. 2 to provide a characterization of the inclusion content of the solid under study.

## 6. Acknowledgments

Many useful discussions were held with Drs. T.F. Deutsch, F.A. Horrigan, P. Miles, D. Readey and C. Willingham on various aspects of the present work. Their advice is greatly appreciated. The facilities of United Aircraft Research Laboratories were used in the preparation of this manuscript.

## VIII. EFFECTS OF ATOMIC IMPURITY CONCENTRATION ON INTRINSIC BREAKDOWN FIELDS

Previous measurements of intrinsic breakdown have been conducted on pure materials and, as reported in Sec. III, on one alloy system. The possible effects of atomic impurities on intrinsic breakdown limits have not been previously investigated.

In this section we report the results of a short series of measurements in which three laser host materials both pure and doped were damaged at 1.06  $\mu\text{m}$ . As in the experiment of the previous section, care was taken to insure that measurable self-focusing effects were absent and that only data from an intrinsic damage mechanism were used.

YAG and  $\text{YAlO}_3$  doped with  $\text{Nd}^{+3}$  at concentrations of up to 2 percent and ruby with  $\text{Cr}^{+3}$  concentrations of up to 0.5 percent were damaged with the Q-switched laser pulses. The damage intensities were compared to the intrinsic damage levels of the pure hosts. It was found that within experimental uncertainty, the doped materials had the same intrinsic optical damage intensities as the respective pure hosts. Incident damage intensities of 64, 71 and 210  $\text{GW}/\text{cm}^2$  were measured, respectively, for YAG,  $\text{YAlO}_3$  and ruby.

The results for the  $\text{Nd}^{+3}$  doping were expected since the 4f valence electrons of the trivalent rare earths overlap very little with the electron wave functions of the host solid. Avalanche breakdown is a bulk phenomenon, and the narrow bands of  $\text{Nd}^{+3}$  effectively remain decoupled from the host.

In the case of  $\text{Cr}^{+3}$  levels, however, substantial overlap exists between the valence electrons and the manifold of host states. The  $\text{Cr}^{+3}$  levels are correspondingly broad, and it might be expected that at extremely high doping levels, the presence of the additional  $\text{Cr}^{+3}$  states located effectively within the bandgap will affect the impact ionization process and lower the breakdown field. On the basis of the present results, it can only be concluded that a  $\text{Cr}^{+3}$  doping level of 0.5 percent, a value about 10 times the normal doping level of pink ruby laser material, produces a negligible perturbation of the intrinsic breakdown process.

The present damage results along with the results of the previous section serve to underscore the basic insensitivity of electron avalanche breakdown to material parameters. Although we have considered only two restricted types of impurities, it appears safe to predict that atomic contaminants of types other than those considered here will also have no measurable effect on intrinsic damage levels.

## IX. THEORY OF ELECTRON AVALANCHE BREAKDOWN

### A. Introduction

A complete theory of avalanche breakdown has not been developed. The models of breakdown formulated to date, which are based on relaxation-time approximations, avoid the enormous complexities of the various physical interactions involved in the avalanche process. Except for the work of Feynman et al., in fact, theories of hot electron effects in solids have been based on a perturbation theory formalism that is, in principle, inappropriate for electron avalanche theories.

It is now recognized that a realistic theory of avalanche breakdown in solids must contain both a modeling of the interactions between the electron and the electric and phonon fields and a statistical framework that accounts for the distribution of electron energies. Pioneering work by Seitz in breakdown in insulators and Baraff in studies of electron avalanching in semiconductors have shown that the development of an electron avalanche depends sensitively upon the energy dependence of the electron-lattice interaction. A statistical framework that accurately describes the electron distribution function is thus a critical aspect of a relevant theoretical model. On the other hand, the details of the electron dynamics, which involve the quantization of the EM fields or of electron energy, do not appear to strongly affect the predictions of theory. For this reason, avalanche models that use a classical relaxation-time approach and a Boltzmann or Fokker-Planck equation analysis are surprisingly successful in predicting many of the experimentally observed features of avalanche breakdown. Such models are not rigorous theories, however.

The analysis described in this section is an extension of a classical Fokker-Planck equation model of avalanche breakdown that was originally developed and published by Holway.<sup>72</sup> This work addresses, in a semi-quantitative manner, some of the ideas concerning avalanche breakdown in insulators that have been raised by Seitz, Fröhlich, and other workers

in the field. Among the ideas to be tested are the importance of the nonpolar electron-phonon interaction, the Fröhlich criterion for breakdown, and the sensitivity of breakdown thresholds to the electron ionization cross section. The predictions of the model are compared to the results of our recent experimental studies on intrinsic laser damage.

B. ELECTRON AVALANCHE BREAKDOWN GENERATED BY LASER  
RADIATION IN INSULATING CRYSTAL\*

Lowell H. Holway, Jr. and David W. Fradin†  
Raytheon Research Division  
Waltham, Mass. 02154

ABSTRACT

Recent experimental investigations into optical damage in the alkali halides have suggested that the damage is due to avalanche breakdown in its dc limit. Numerical computations have been carried out which indicate that the ionization rate can be accurately computed by a diffusion or Fokker-Planck approximation to the Boltzmann equation for ionization rates on the order of  $10^{12} \text{ sec}^{-1}$ . However, for hot electrons it is necessary to add a contribution to the collision frequency which is due to the deformation potential in order to explain the dc character of breakdown by  $1.06 \mu\text{m}$  radiation.

-----  
\*Supported partly by the Advanced Research Projects Agency of the Department of Defense, monitored by the Air Force Cambridge Research Laboratory under Contract No. F19628-73-C-0127 and partly by the Raytheon Independent Research Program.

†Present address: United Aircraft Research Laboratories, East Hartford, Conn. 06108

## 1. Introduction

In a recent series of experiments in which optical damage was studied in the alkali halides,<sup>9,17,18,20,25,30,66-68</sup> it was determined that intrinsic optical damage in transparent solids occurs as the result of electron avalanche breakdown. The experiments, which used laser wavelengths of 10.6, 1.06 and 0.69  $\mu\text{m}$ , were designed to keep the laser power below the critical power for self-focusing<sup>10,66,99</sup> since, without this precaution, the observed breakdown fields would have been measures of this critical power instead of the desired thresholds for electron cascade breakdown. Microscopic inspection of the damaged volume was used to distinguish intrinsic breakdown from breakdown induced by inclusions in the crystals. The experimental data shows that, within experimental error, laser-induced breakdown and dc dielectric breakdown in insulators appear to be virtually identical processes, a fact not previously anticipated in the literature.

Although dc dielectric breakdown in insulators has been studied for nearly half a century, uncertainties caused by surface conditions, electrode effects and space charges often confused the experimental results. The information attained by these studies was limited not only by experimental difficulties but also by the basic inability of experiments to provide information other than dc threshold fields. A true theoretical understanding of dielectric breakdown from electron avalanching was inhibited by the relative paucity of reliable experimental data at dc and the enormous complexity of the process itself. The basis of this complexity is the fact that the relevant interactions in avalanche breakdown cannot be treated separately. When considering avalanche breakdown, it is not strictly correct, for example, to treat electron excitations as being distinct from those of the lattice. The electron-phonon interaction during breakdown in NaCl is so strong that the effective collision rate appears to be more than  $10^{15} \text{ sec}^{-1}$ . In addition, distortion from the ultrahigh electric fields characteristic of breakdown thresholds cannot properly be treated as a perturbation on the energy spectrum of the electron-lattice system. A number of theories have been formulated for dielectric breakdown which largely ignore these difficulties. These

theories are based on an electron avalanche mechanism and normally use a relaxation-time approximation to model the electron-phonon interaction. Such theories are basically similar to classical treatments of breakdown in gases<sup>70</sup> and semi-conductors. The details of electron dynamics in insulators subject to ultrahigh electrical fields have been calculated quantum mechanically by Feynman, et al.,<sup>71</sup> but their treatment in its present form is not directly applicable to dielectric breakdown.

Interest in dielectric breakdown has recently increased with the discovery that intrinsic optical damage from laser irradiation develops from a mechanism that is fundamentally the same as dc breakdown. By utilizing the great versatility of the laser, it has been possible to explore the dependence of breakdown fields on frequency, laser pulse duration, and material characteristics. Such studies have provided new information on electron avalanche breakdown that serves both as a basis and a test for breakdown theories.

In the present work the results of dielectric breakdown measurements at dc and optical frequencies will be summarized and the results interpreted in terms of electron avalanche breakdown. A Fokker-Planck model, which was derived<sup>72</sup> without reference to the Boltzmann equation although it proves to be identical to the Legendre expansion of the Boltzmann equation<sup>70</sup>, will be used to provide a basis for this interpretation. Such a formalism was applied in order to answer the following questions:

1. Can a classical model of electron avalanche breakdown in insulators explain the basic features of the experimental results obtained at dc and optical frequencies?
2. How important are the details of the electron-phonon interaction in determining breakdown fields? In particular, does the introduction of nonpolar interactions change the predictions of breakdown theories for insulators as Seitz<sup>59</sup> suggested many years ago?

3. Is breakdown an average electron phenomenon and /or does the avalanche process depend upon the diffusion of hot electrons into the high energy tail of the distribution function?

Such questions cannot all be answered definitively by a classical calculation based on perturbation modeling since  $\hbar\omega$  becomes comparable to 1 eV for the higher laser frequencies and the collision frequency will approach  $10^{15} \text{ sec}^{-1}$  in the materials of interest. It will be seen, however, that avalanche breakdown appears to have the same fundamental characteristics whether it develops in solids, liquids or gases. For this reason, simplified models of the process can be successfully applied. Because electric breakdown is similar in different materials, the formalism applied here to electric breakdown in insulators is also applicable to avalanche breakdown in semiconductors and, with some modification, to avalanche breakdown in gases, which is important, not only for breakdown caused by laser beam propagating through the atmosphere, but also for microwave breakdown which can occur inside high power radar waveguides.

This paper begins with a brief review of some of the important data obtained in the laser experiments. The major implications of these data for a theoretical understanding of avalanche breakdown are noted.

In Sec. 3 and 4, the Fokker-Planck model for avalanche breakdown is applied to sodium chloride. Although the mathematical formalism for this model has been previously developed in the literature, the present calculation differs in a fundamental manner from the previous treatment. Whereas the previous treatment considered only the polar or Fröhlich model for the electron-phonon interaction, the present calculation adds a nonpolar, deformation potential effect to the interaction in an attempt to provide closer agreement between theory and experiment. The calculation is based on the evaluation of the electron distribution function  $f(u)$  and its growth in high electric fields, as described in an ionization rate  $\eta(E)$ . A simplified band structure is assumed in which conduction-band electrons can produce additional electrons when their kinetic energy, relative to the band edge, reaches values that exceed the band gap.

Numerical results for sodium chloride crystals are presented in Sec. 4-5. These results were obtained first using just the Fröhlich model for the polar contribution to the electron-phonon collision frequency  $\nu$  and then using both the polar and the nonpolar contributions to  $\nu$ . The latter contribution is modeled after a calculation by Seitz. In both cases comparison is made between calculated values of  $\eta(E)$  and values of  $\eta(E)$  inferred from optical damage experiments. It is found that the Fröhlich model alone is incapable of explaining the important experimental observation that the breakdown fields in NaCl and hence  $\eta(E)$  are the same within experimental error at  $10.6\mu$  and  $1.06\mu$ . On the other hand, by adding the nonpolar contribution to  $\nu$  and assuming peak values of  $\nu$  in excess of  $10^{15} \text{ sec}^{-1}$ , reasonably good agreement is obtained between the predictions of theory and the results of experiments.

The present work demonstrates that knowledge of average electron dynamics must be supplemented by the determination of a distribution function in order to obtain a quantitative description of electron avalanche breakdown. Avalanche breakdown is a statistical process in which the properties of electrons over a broad range of energies play a role in the avalanche development. This distribution, which is shown to be non-Maxwellian, leads to a diffusion of electrons to high energies. The diffusion contribution to electron heating and subsequent ionization is significant and can only be calculated from a knowledge of the electron distribution function. As a result, a statistical description of the avalanche is required in which  $f(u)$  is calculated from a kinetic equation. The present work suggests, in fact, that the basic kinetic modeling may have as much effect on the predictions of avalanche theory than as the precise theoretical modeling of the electron dynamics.

Considerable attention is given both to the physical meaning of the coefficients in the Fokker-Planck equation and to the range of validity of its use in Sec. 4-6 and the Appendix. The relationship between the present calculation and the works of Wolf, Shockley and others will be discussed. Also in the Appendix, an addition to the kinetic equation that was ignored in the present calculations although it becomes important for weak fields, is described, and its effect on the computed results is considered.

## 2. Experimental studies of optical breakdown

The experiments involving laser-induced breakdown in transparent solids have been described in several publications.<sup>9, 10, 17, 18, 20, 25, 30, 66, 67</sup> The observed damage is interpreted as an electron cascade process in which the electron density increases exponentially until the energy absorbed from the beam becomes large enough to cause a thermally-induced fracture or phase change which permanently damages the material.

The experiments show little dependence upon the laser frequency and a characteristic time dependence, which indicates that the damage process is electron avalanche breakdown rather than multiphoton absorption. In an avalanche breakdown the number of conduction-band electrons increases with time as

$$n(t) = N_0 \exp \left[ \int_0^t \eta(E)(t') dt' \right] \quad (1)$$

where  $E$  is the electric field and  $\eta$  is the ionization rate. Figure 32 shows ruby laser light transmitted through an NaCl sample is suddenly cut off when damage develops.<sup>66</sup> The damage can occur before, at, or after the peak of the laser pulse. The variation between apparently identical laser pulses shows the statistical fluctuations in the breakdown time. The breakdown after the peak intensity is consistent with a cascade process such as that described by Eq. (1). Since breakdown occurs with the electric field within 90 percent of its peak value,  $\eta(E)$  must be a rapidly increasing function of electric field. The suddenness of the attenuation also suggests that  $\eta$  must be large on a nanosecond time scale.

The most striking indication that optical damage is a manifestation of avalanche breakdown comes from a comparative study of the electric fields required to produce damage by dc breakdown in different alkali halides, and by comparing different frequency lasers with 10.6, 1.06 and 0.69  $\mu\text{m}$  wavelengths. The breakdown fields for different materials are shown in Fig. 33.<sup>10</sup> These fields have been normalized to the NaCl breakdown fields, which are

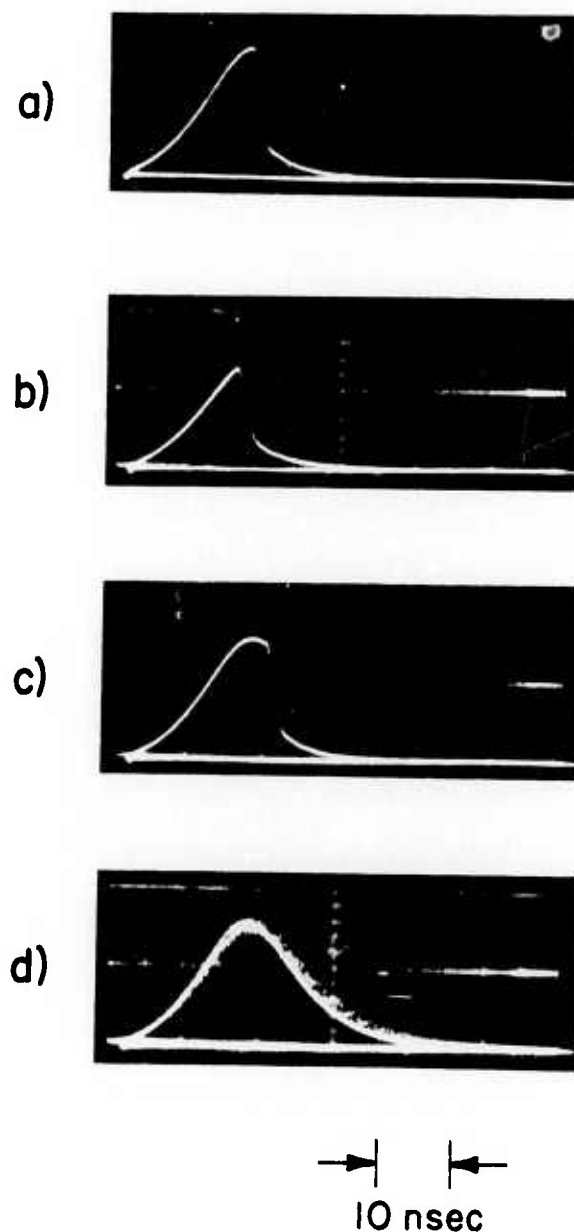


Fig. 32 Ruby Laser Pulses Transmitted Through a NaCl Sample. (a) Attenuation occurs when peak laser field is reached. (b) Attenuation before peak field is reached  $E_{\text{damage}} = 0.896 E_{\text{peak}}$ . (c) Attenuation after peak laser field was reached,  $E_{\text{damage}} = 0.954 E_{\text{peak}}$ . (d) Three successive pulses with same peak power, no damage.

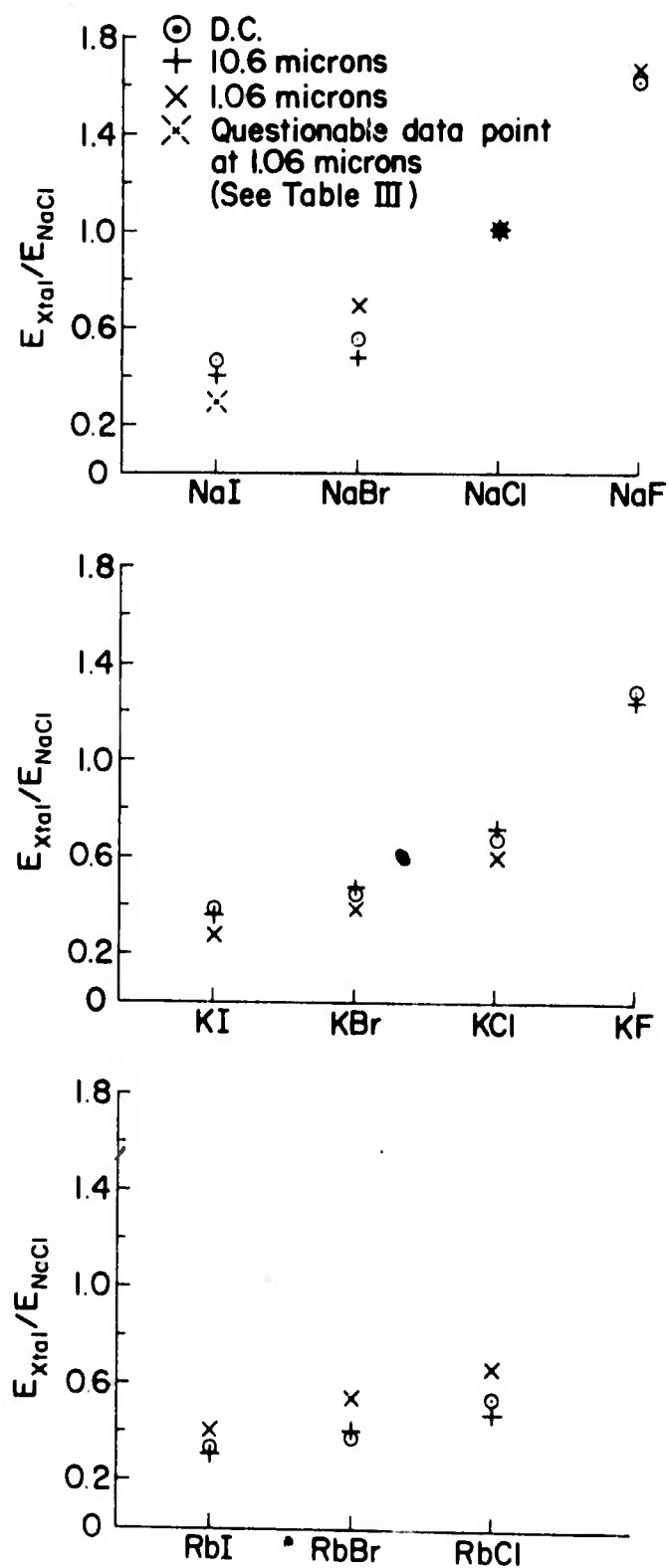


Fig. 33 RMS Electric Fields Necessary to Damage Nine Alkali Halides, Normalized to the Damaging Field for NaCl.

given at the appropriate frequency in Table IV, in order to make it easier to see the variation in trends as the laser frequency is increased. The breakdown fields shown in Fig. 33 are the same as dc breakdown within experimental uncertainty for laser wavelengths of 1.06  $\mu\text{m}$  or greater. However, when the wavelength is decreased to 0.69  $\mu\text{m}$ , there is an increase in the breakdown field (for all of the halides except NaCl) as would be expected from theories of frequency-dependent avalanche breakdown.<sup>70</sup> Although the similarity to dc breakdown makes the identification of the damage mechanism as an electron cascade seem quite certain, the lack of frequency dependence for the 1.06  $\mu\text{m}$  radiation seems to require the hot electrons to have a collision frequency on the order of  $2 \times 10^{15} \text{ sec}^{-1}$  for all energies up to the ionization energy.

Another sequence of measurements, which indicated that the ionization rate  $\eta$  as a function of field is consistent with dc measurements,<sup>69,70</sup> is compared with calculations in Sec. 5.

### 3. The physical model

The existence of a frequency dependence to avalanche breakdown intensities can be understood by a simplified argument. In the absence of electron losses from either defect trapping or electron diffusion, the essential features of the avalanche are determined by the rate at which energy is fed into the electron population. This rate is approximately given by the well-known formula for Joule heating

$$\frac{dW}{dt} = (ne^2\tau/m) E^2 / (1 + \omega^2 \tau^2) \quad (2)$$

where  $n$  is the time-dependent electron density,  $\omega$  the angular frequency of the ac electric field, and  $\tau$  the characteristic relaxation-time determined principally from electron collisions with lattice vibrations. In general,  $\tau$  must be considered to be a function of energy and, in some sense, Eq. (2) must be "averaged" over the electron distribution function. For the purposes of the present qualitative discussion,  $\tau$  will be taken as a constant,  $\tau = 1/\nu_{\text{eff}}$ .

TABLE IV

ABSOLUTE BREAKDOWN STRENGTH OF NaCl<sup>67</sup>

$E_{\text{peak}}$ (dc)	$1.5 \times 10^6$ V/cm
$E_{\text{rms}}$ (10.6 $\mu\text{m}$ )	$(1.95 \pm 0.20) \times 10^6$ V/cm
$E_{\text{rms}}$ (1.06 $\mu\text{m}$ )	$(2.3 \pm 0.46) \times 10^6$ V/cm
$E_{\text{rms}}$ (0.69 $\mu\text{m}$ )	$(2.2 \pm 0.44) \times 10^6$ V/cm

Eq. (2) shows that the energy input to the electrons scales with frequency and field as  $E^2/(1 + \omega^2 \tau^2)$ . Since the energy input determines the electron distribution function, the threshold for damage will scale in the same way. This scaling underlies the use of root-mean-square fields in comparing dc and laser dielectric breakdown. It indicates that the avalanche process will appear to be in its dc limit only for laser frequencies that satisfy  $\omega \tau(u) \ll 1$  for all electron energies involved in the electron cascade. Since the experiments indicated that laser breakdown at  $1.06 \mu\text{m}$  in the alkali halides is virtually indistinguishable from dc breakdown, but that a frequency dependence begins to appear at  $0.69 \mu\text{m}$ , it appears that  $\omega \tau \approx 1$  at the ruby laser frequency. For the electron energies characteristic of avalanche breakdown, therefore, the effective value of  $\tau$  is about  $0.5 \times 10^{-5}$  sec or less for the alkali halides. This effective relaxation time is much shorter than relaxation times inferred from low-field measurements of various transport properties in the same materials.

A rigorous model of avalanche breakdown would replace Eq. (2) with a formalism that treats the strong electron-lattice interaction quantum mechanically with a coupled electron-lattice excitation emerging instead of well-defined electron states perturbed by the lattice, the approximation that leads to Eq. (2). Except for the work of Feynman, et al, no such rigorous model has been formulated for insulators subject to high electric fields. Unfortunately, Feynman's rigorous model of electron dynamics is not directly relevant to the avalanche breakdown problem for two reasons. First, a statistical framework that takes account of the wide distribution of electron energies was not included in the calculation. As should become clear below, this statistical framework is fundamental to a proper description of avalanche breakdown. Second, the particular electron-phonon interaction important for Feynman's work; namely, the Fröhlich interaction, describes only part of the relevant interaction for the hot electrons involved in the avalanche development.

The present calculation bypasses the enormous complexities involved in the electron dynamics by using an energy-dependent relaxation time model.

A significant departure from previous treatments of avalanche breakdown in insulators is the introduction of a nonpolar electron-phonon interaction. We find that calculations based on the Fröhlich interaction alone are not capable of explaining the important experimental finding that the characteristics of laser-induced breakdown in the alkali halides do not change measurably with laser wavelength for wavelengths as short as 1.06 micron. Following a suggestion made by Seitz almost thirty years ago, but never tested with a statistical calculation, we show that the addition of a nonpolar interaction does explain this experimental fact. In addition, the use of simple perturbation formulas for the polar and nonpolar contributions to the electron-phonon collision frequency  $\nu$  (where  $\nu = 1/\tau$ ) led to reasonable quantitative agreement with the measured breakdown fields.

The nonpolar contribution to the collision frequency is taken to vary with electron energy in the manner predicted by Seitz from a deformation potential calculation. Its peak value is adjusted to  $3 \times 10^{15} \text{ sec}^{-1}$ . This contribution is important to avalanche breakdown in insulators, because it is large at high electron energies where the Fröhlich, longitudinal-optical-phonon interaction is much smaller than its peak which occurs near the LO phonon energy. In low-field transport processes in insulators, very few electrons reach such high energies so that the Fröhlich interaction sufficiently describes the electron dynamics for these processes. During avalanche breakdown, on the other hand, electrons must become extremely energetic in order to gain sufficient energy to cause impact ionization and concomitant avalanche growth. The dynamics of hot electrons thus become fundamental to a description of avalanche breakdown. These dynamics should be strongly affected by the nonpolar interaction.

In order to make a clear comparison between the polar and nonpolar interactions, we first carry out a calculation using only the polar interaction on defining the collision frequency. Next we carry out a calculation in which the deformation potential contribution to the collision frequency is added to the polar contribution. Only the gross features of those dynamics appear to be important and these gross features should be reasonably approximated by adding the contributions of Seitz' nonpolar interaction to the Fröhlich, polar interaction.

The present calculation uses a simple two-band model for the electron energy spectrum. Impact ionization occurs when a conduction-band electron has gained sufficient energy above the band minimum to excite a valence electron across the band gap. All energies are measured relative to the band minimum.

#### 4. The kinetic equation

Let  $f(u, t)du$  be the probable number of electrons (per unit volume) between energy  $u$  and  $u + du$ , with  $u$  measured from the bottom of the conduction band. Then, under fairly general conditions,<sup>81</sup> the kinetic equation can be written as

$$\frac{\partial f}{\partial t} = \frac{\partial}{\partial u} \left( \frac{\langle \Delta u \rangle}{\Delta t} f \right) + \frac{1}{2} \frac{\partial^2}{\partial u^2} \left( \frac{\langle (\Delta u)^2 \rangle}{\Delta t} f \right) \quad (3)$$

and, for the case of electrons gaining energy from an electric field and losing it by exciting phonons (or molecules) we have shown<sup>78</sup>

$$\frac{\langle \Delta u \rangle}{\Delta t} = A(\omega) Y(\omega) - \left( \frac{du}{dt} \right)_L, \quad (4a)$$

and

$$\frac{\langle (\Delta u)^2 \rangle}{\Delta t} = \frac{4}{3} u A, \quad (4b)$$

where

$$A = \frac{e^2 E^2}{m} \frac{\nu(u)}{(\nu(u))^2 + \omega^2}, \quad (5)$$

where  $E$  is the RMS electron field, or, for a steady field, is the magnitude of the field,  $\nu$  is the collision frequency for momentum transfer,  $\omega$  is the radial frequency of the field and  $m$  is the effective mass,

$$Y = 1 + \frac{2}{3} \frac{\omega^2 - \nu^2}{\omega^2 + \nu^2} \left( \frac{u}{\nu} \right) \frac{\partial \nu}{\partial u}, \quad (6)$$

and  $\frac{du}{dt}$ , the rate at which an electron of energy  $u$  loses energy to the lattice, has been calculated theoretically for alkali halides.<sup>59,74,75</sup> In principle, the energy loss should contribute to the dispersion also, but we have argued that this contribution is likely to be insignificant compared to the field term in Eq. (4b), if the field is strong enough, as is the case for elastic energy loss in electron-molecule collisions.<sup>72,76</sup> (When the field vanishes, the dispersion must balance the average energy loss in determining a thermal equilibrium distribution, but the thermal spread is tiny compared to the spread when breakdown is caused by a strong field.)

It can be shown that the field dependent terms in Eq. (3) are identical with the terms which are obtained by expanding the Boltzmann equation or Legendre polynomials<sup>70,77,78</sup>, when  $f$  is considered a function of time. One of the advantages of the Fokker-Planck derivation, besides some reduction in formal manipulation, is that the conditions for its applicability are well known. For example, it is necessary that the energy gained in one collision time,  $\nu^{-1}$ , be much less than the total energy, which amounts to the condition

$$\frac{e^2 E^2}{m(\nu^2 + \omega^2)} \ll I, \quad (7)$$

where  $I$  is the ionization energy. In other words, the diffusion formulation is limited to electric fields which are weak in the sense of Eq. (7). It is not difficult to show that if Eq. (7) is violated, the electron velocity will take on a considerable component antiparallel to the field in the time between collisions so the velocity distribution function will no longer be close to spherically symmetric. Thus the Legendre expansion method must similarly be expected to fail for strong fields, which is consistent with our assertion that the Legendre expansion and the Fokker-Planck approximation are identical. If we take  $I = 7.7$  eV and  $\nu^2 + \omega^2 = 10^{30}$ , the equality in Eq. (7) will only occur for fields as large as 66 MV/cm, which indicates that the Fokker-Planck equation is valid for the measured breakdown fields.

The amount of energy per unit volume absorbed by the electrons can conveniently be obtained by multiplying Eq. (3) by  $u$  and integrating over  $u$ . The second term on the right hand side vanishes upon integrating by parts, leaving

$$\begin{aligned} \frac{\partial}{\partial t} \int_0^{\infty} u f du &= \int_0^{\infty} \frac{\langle \Delta u \rangle}{\Delta t} f du \\ &= \int_0^{\infty} A(\omega) Y(\omega) f du, \end{aligned} \quad (8)$$

where we have dropped the energy loss term in Eq. (4a). Equation (8) denotes the total energy gained per unit volume from the field, and can be written as

$$\frac{\partial}{\partial t} \bar{n} u = \frac{e^2 E^2}{m} \frac{n \nu_{\text{eff}}}{\nu_{\text{eff}}^2 + \omega^2} \quad (9)$$

where  $\nu_{\text{eff}}$  is not the average collision frequency (except in the trivial case  $\nu = \text{constant}$ ). For example, if  $\nu = bu$  and if  $f$  were a Maxwellian at temperature  $T$ , we would obtain  $\nu_{\text{eff}} = \frac{5}{2} bkT$  for  $\omega \gg \nu_{\text{eff}}$  and  $\nu_{\text{eff}} = \frac{1}{2} bkT$  for  $\omega \ll \nu_{\text{eff}}$ . This last result is known in ionospheric propagation, where it is obtained after considerable algebraic manipulation of the integrals arising from the Boltzmann equation.<sup>79</sup> In general, if  $\nu = bu^m$  and  $m > -3/2$ ,  $\nu_{\text{eff}} = (1 + \frac{2}{3}m) \nu_{\text{ave}}$ , for  $\omega \gg \nu$ , which can be shown from Eqs.(5), (6) and (8) and holds for nonequilibrium distribution functions.

In order to carry out numerical calculations, we must assume some model for  $\nu$  since no entirely satisfactory model for hot electrons exists. The first model considered will be that of Fröhlich<sup>74</sup> which is derived by assuming that positive and negative charges situated at the lattice sites are perturbed by the electrons and has the form

$$\begin{aligned} \nu &= b u_0^{-1} u^{-1/2} & u < u_0 \\ \nu &= b u^{-3/2} & u > u_0 \end{aligned} \quad (10)$$

for electrons with energies somewhat greater than thermal where

$$b = 1 + \left( \frac{2}{\exp \frac{\hbar \omega_t}{kT} - 1} \right) \left( \frac{2^{1/6} \pi^3 e^4 \hbar}{4m^{1/2} M a^5 \omega_t} \right) \quad (11)$$

and  $u_0$  is a crossover energy, approximately equal to the electron energy corresponding to the boundary of a Brillouin zone, which we take as

$$u_0 = 2^{2/3} \pi^2 \hbar^2 / 8ma^2 \quad (12)$$

Our numerical examples are for NaCl crystals where<sup>75</sup> the nearest inter-ionic distance  $a = 2.81 \text{ \AA}$ , the effective mass is taken as the electron mass  $m = 9.109 \times 10^{-28}$ ,  $\omega_t = 3.09 \times 10^{13}$ ,  $T = 300^\circ\text{K}$ , and  $M = 23.2 \times 10^{-24} \text{ gm.}$  Equations (11) and (12) are Fröhlich's original formulas<sup>74</sup> which are larger by a factor of  $2^{2/3}$  than values given by O'Dwyer,<sup>75</sup> a numerical factor does not affect the results greatly. This collision frequency is plotted as curve (1) in Fig. 34, where  $u_0 = 1.89 \text{ eV.}$

For nonpolar crystals, the deformable atom hypothesis can be used to obtain a perturbation potential and Seitz<sup>59</sup> indicates this should be important, even in polar crystals, for hot electrons.

This contribution to the collision frequency has the form

$$\begin{aligned} \nu_s &= d u & u < u_0, \\ \nu_s &= d u_0^{3/2} u^{-1/2} & u > u_0, \end{aligned} \quad (13)$$

for energies much greater than thermal. For our purposes, we consider  $d$  a phenomenological constant and add the contribution of Eq. (13) to the polar contribution given by Eq. (10), so that

$$\begin{aligned} \nu &= b u_0^{-1} u^{-1/2} + d u & u < u_0 \\ \nu &= b u^{-3/2} + d u_0^{3/2} u^{-1/2} & u > u_0. \end{aligned} \quad (14)$$

Curves 2 and 3 are the result of choosing  $du_0 = 6.5 \times 10^{14}$  (so that (10) and (14) make equal contributions at  $u_0$ ) and choosing  $du_0 = 2 \times 10^{15}$ . Curve 4 is the form for a constant mean free path arbitrarily normalized to  $10^{15}$  at  $u = 1$  eV. Curves 1 and 4 bracket the extremes used in the literature since the  $u^{-3/2}$  form (Curve 1) was used by Keldysh<sup>80</sup> while the constant mean free path assumption (Curve 4) was made by Wolff<sup>77</sup> and Baraff.<sup>78</sup>

The net number of electrons per unit volume whose energy increases from a value less than  $u$  to a value greater than  $u$  per unit time can be defined as  $J(u)$ , the current in energy space. Then Eq. (3) is equivalent to

$$\frac{\partial f}{\partial t} = - \frac{\partial J}{\partial u} \quad (15)$$

where

$$J = \frac{\langle \Delta u \rangle}{\Delta t} f - \frac{1}{2} \frac{\partial}{\partial u} \left( \frac{\langle (\Delta u)^2 \rangle}{\Delta t} f \right) \\ = Gf - D \frac{\partial f}{\partial u} \quad , \quad (16)$$

where  $G = \frac{1}{3} A - \left( \frac{du}{dt} \right)_L$  plays a role like an average rate of energy change and  $D(u) = \frac{1}{2} uA$  plays the role of a diffusion coefficient in energy space.

Equation (16) is a convenient form for numerical purposes since  $\frac{\partial \nu}{\partial u}$ , the derivative of the collision frequency has cancelled. It is important to note that  $G$  is not the rate of change of energy for the average electron which is given by Eq. (3) in general (and equals  $A - \left( \frac{du}{dt} \right)_L$  if  $\nu$  is constant).

If diffusion could be neglected, breakdown would only occur if  $G > 0$ . Thus we find it more meaningful to plot  $\frac{1}{3} A$  and contrast it with the energy loss,  $\left( \frac{du}{dt} \right)_L$ , instead of contrasting  $A$  with the energy loss. This has been done in Fig 35a where Curves 1 and 2 plot  $\frac{1}{3} A$  based on the collision frequency of Curve 1 of Fig. 34. The energy loss rate is given by Curve 3 so that  $G > 0$  if Curve 1 exceeds (3). Curves 4 and 5 plot  $D(u) = \frac{1}{2} \frac{\langle (\Delta u)^2 \rangle}{\Delta t}$  for different fields. The diffusion constant, which has units  $\text{eV}^2/\text{psec}$ , cannot strictly be compared with  $G$  but its relative size plays an important role as can be shown by the following qualitative argument. If steady-state

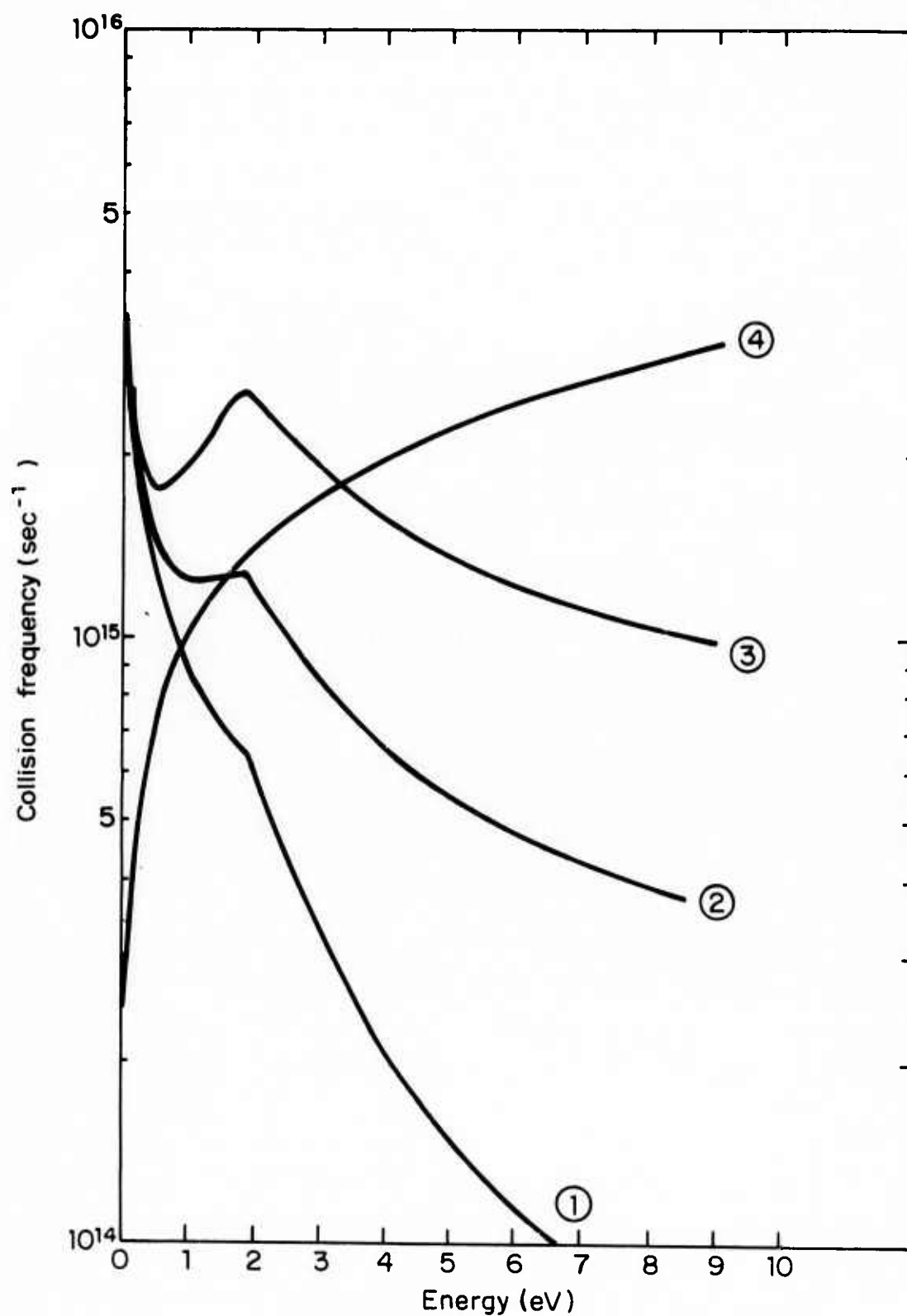


Fig. 34 Collision Frequency. Curve (1) is Fröhlich's model from Eq. (10); curve (2) includes nonpolar contributions of Eq. (14) with  $d u_0 = 0.65 \times 10^{15}$ ; curve (3) has  $d u_0 = 2 \times 10^{15}$ ; curve (4) is constant mean free path  $= 1 \times 10^{15} u_2^{1/2}$ .

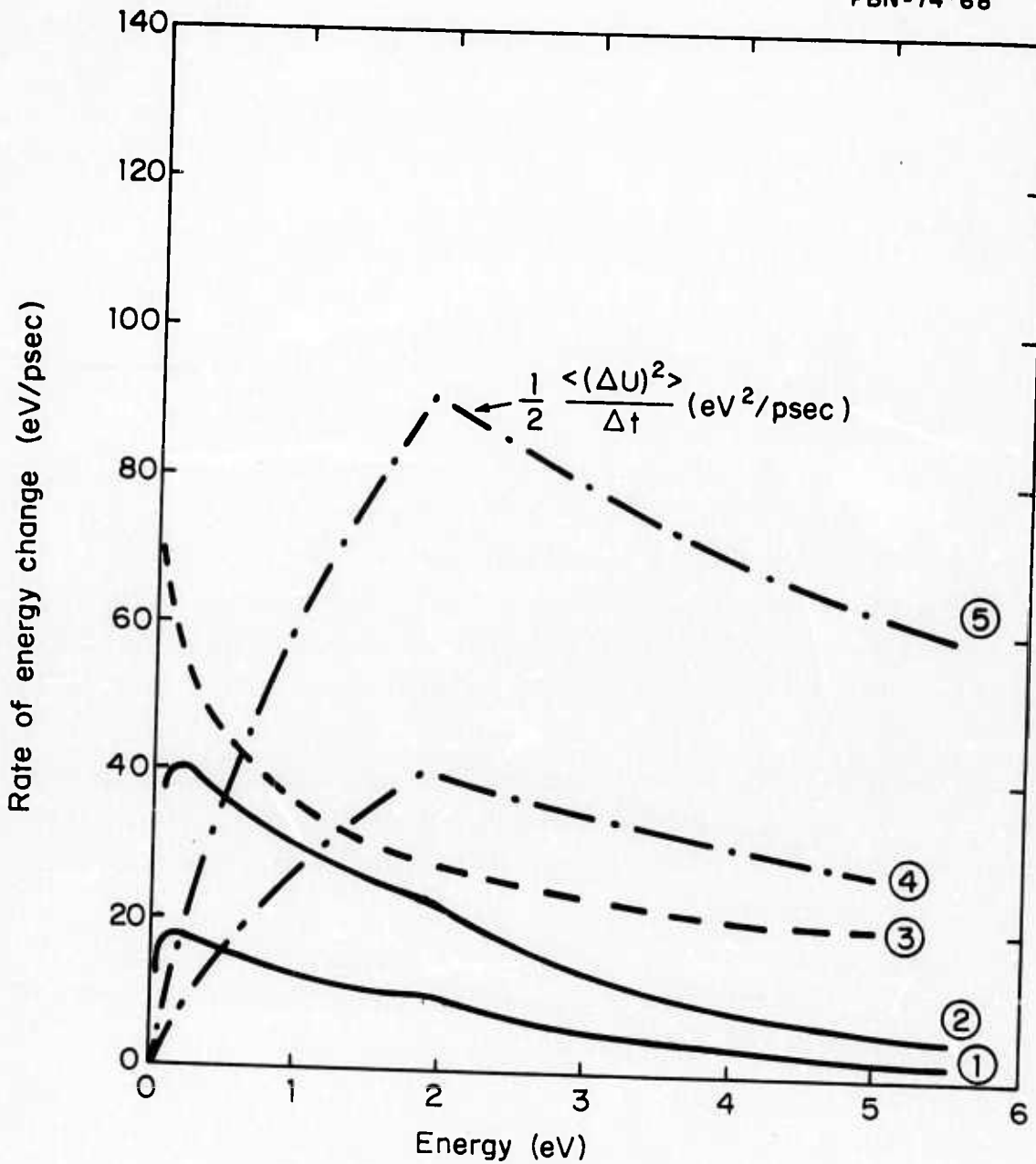


Fig. 35a Coefficients in the Fokker-Planck Equation for Collision Frequency (1) with  $\lambda = 1.06 \mu\text{m}$ . Curves (1) and (2) give  $A/3$  and (4) and (5) give  $D(u)$ . Curve 3 is the energy loss  $(d u/dt)_L$ . Curves (1) and (4) are for  $E = 10 \text{ MV/cm}$  while (2) and (5) are for  $15 \text{ MV/cm}$ .

ionization is going on,  $J$  must be greater than zero for  $u$  between a value  $u_1$  near zero and a value near the ionization energy  $I$ . Since  $D$  is positive, if  $G$  is negative, then  $\frac{\partial f}{\partial u}$  must also be negative with a magnitude

$$\left| \frac{\partial f}{\partial u} \right| > \frac{G}{D} f$$

which implies

$$f < \exp - \int_{u_1}^I \left| \frac{G}{D} \right| du' \quad . \quad (17)$$

Thus, if  $G$  is negative and  $-(G/D) I$  is much larger than one, the number of electrons reaching ionization energy will be exponentially small. Figs. 35a and b compare the coefficients for  $\lambda = 1.06$  and  $\lambda = 1.06 \mu\text{m}$ . For  $E = 10$   $\text{Mv/cm}$  in Fig. 35a, we see from Curves 1 and 3 that  $G$  is negative while  $D$  is less than  $-G$  below 1 eV and is only slightly larger above 1 eV.  $A$  has its maximum near 0.3 eV where  $\nu = \omega$ . On the other hand,  $A/3$  is much larger than  $(du/dt)_L$  in Fig. 35b except below 1 eV and has a maximum near 4.4 eV where  $\nu = \omega$ . In addition,  $D$  is extremely large except near the origin so we expect the ionization rate to be orders of magnitude larger. Note that it is difficult for these electrons below 0.5 eV to gain energy, so there is an effect like a low energy trap.

The energy loss term used in Fig. 35 was the form given by Fröhlich<sup>74, 75</sup>, neglecting deformation potentials, which is

$$\left( \frac{du}{dt} \right)_L = d_1 u^{-1/2} \ln \gamma \quad , \quad (18)$$

where

$$\gamma = (4/\hbar \omega_t) u \quad u < u_0$$

$$\gamma = (4 u_0^{1/2} / \hbar \omega_t) u^{1/2} \quad u > u_0$$

and

$$d_1 = \pi e^4 (2m)^{1/2} / M a^3 \quad .$$

The current  $J$  is positive so that electrons are carried up beyond  $I$  the ionization potential, given as 7.7 eV for NaCl.

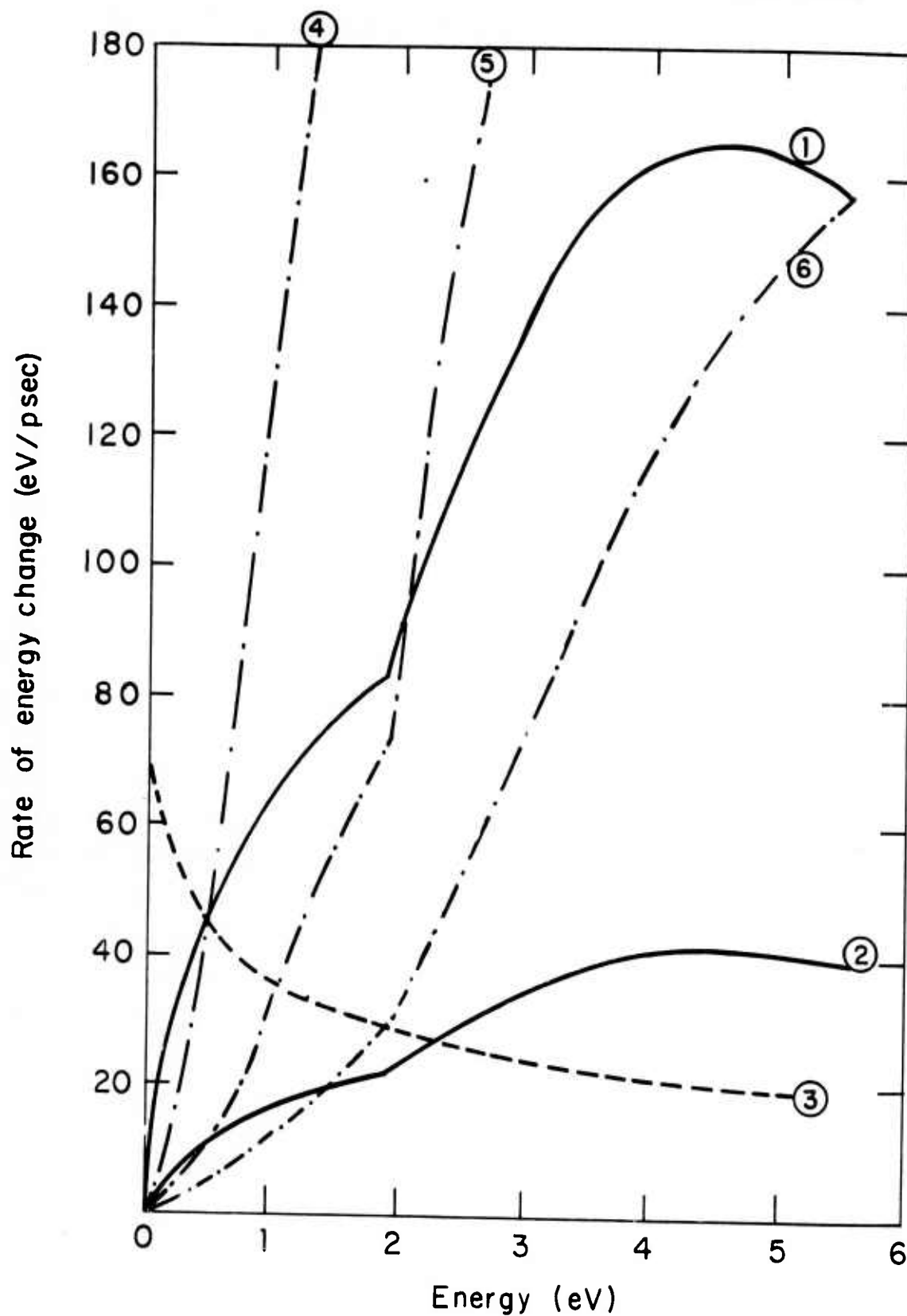


Fig. 35b Curves Similar to 35a for  $\lambda = 10.6 \mu\text{m}$ . Curves (1) and (4) are for 10 MW/cm as before but now (2) and (5) are for 5 MV/cm and curve (6) is for  $E = 3 \text{ MV/cm}$ .

An electron having an energy  $u$ , greater than  $I$  can use that energy to move a second electron from the valence band to the conduction band by impact ionization, leaving an energy  $u-I$  to be shared by two electrons in the conduction band. If the energy is shared equally, Eq. (15) becomes

$$\frac{\partial f}{\partial t} = - \frac{\partial J}{\partial u} - \nu_i(u) f(u) + 4 \nu_i(2u+I) f(2u+I) ; \quad (19)$$

Integrating Eq. (19) over  $u$ , the current term vanishes, yielding

$$\frac{\partial n}{\partial t} = \int_I^{\infty} \nu_i(u) f(u) du$$

where

$$n = \int_0^{\infty} f du .$$

For lack of information on  $\nu_i(u)$  we assume, not only that it is zero below  $I$ , but also that it increases linearly above  $I$  as

$$\nu_i(u) = a_1 (u - I) \quad u > I$$

where, in the numerical examples, we have taken  $a_1 = 4 \times 10^{14} \text{ sec}^{-1} \text{ eV}^{-1}$ . This value insures that most electrons will cause ionization within 1 or 2 eV of  $I$ , so that the results are only slightly different from those obtained previously<sup>13</sup> by assuming that all electrons reaching the ionization energy immediately cause ionization. In atmospheric breakdown Kroll and Watson<sup>70</sup> use  $\int G(u|u') f(u') du'$  in place of the last term in Eq. (19) which would reduce to our term if they took

$$G(u|u') = 4 \nu_i(u') \delta(u' - 2u - I) ,$$

as would be proper if the energy were shared equally.

The boundary conditions for Eq. (19) are  $J(0) = 0$  and  $f$  approaches zero as  $u \rightarrow \infty$ . We anticipate that the solution for  $f$  can be written as

$$f = \sum_m a_m \phi_m e^{\alpha_m t}$$

where  $\phi_m$  and  $\alpha_m$  are eigenfunctions and eigenvalues of Eq. (19), i.e.,

$$-\frac{\partial}{\partial u} J(\phi_m) - \nu_i(u) \phi_m(u) + 4 \nu_i(2u+1) \phi_m(2u+1) = \alpha_m \phi_m(u) \quad , \quad (20)$$

where  $E$  is assumed to remain constant.

The  $\alpha_m$  can be determined from the initial condition. If  $\alpha_0$  is the largest eigenvalue, at late times the distribution function assumes the asymptotic form

$$f = a_0 \phi_0(u) \exp(\alpha_0 t) \quad (21)$$

which means that the number density satisfies

$$\frac{\partial n}{\partial t} = \eta(E) n = \alpha_0 n \quad . \quad (22)$$

We have written a finite difference computer program in which we specify an initial distribution function and follow its evolution in time by means of Eq. (19). After increments  $\Delta t$  we calculate

$$\alpha = \frac{1}{\Delta t} \ln \left( \frac{n(t)}{n(t-\Delta t)} \right) \quad (23)$$

and find that  $\alpha$  converges to a constant value  $\alpha_0 = \eta(E) \text{ sec}^{-1}$  after times which are typically of the order of  $0.2 \eta^{-1}$ . Since this is very fast compared to the time in which the electric field changes, we can calculate  $\eta(E)$  for fixed  $E$  and then compute the electron density from

$$n = n_0 \exp \left[ \int_0^t \eta(E(t')) dt' \right]$$

as anticipated in Section 2. We may sometime refer to Eq. (21) as a "steady state" even though it is important to realize  $n$  is exponentially increasing and the current is not zero.

## 5. Numerical results

Numerical results for NaCl are given in this section. They differ from the results obtained previously for sapphire<sup>72</sup> because  $\nu$  is about an order of magnitude larger. Thus, for 0.69 radiation,  $\omega \gg \nu$  except for energies below 0.1 eV. On the other hand, Fröhlich's model for NaCl has  $\nu = \omega$  near 0.3 eV for 1.06  $\mu\text{m}$  lasers and  $\nu = \omega$  near 4.4 eV for 10.6  $\mu\text{m}$  lasers. Moreover, since  $u_0$  is 0.8 eV for sapphire, it was reasonable to use the collision frequency formula defined for  $u > u_0$ , but, for NaCl,  $u_0 = 1.89$  eV, so that we must also use the  $u < u_0$  formula. Another difference from the earlier calculation is that we now include an ionization frequency  $\nu_i$  as discussed in the last section, which gives slightly lower ionization rates than are obtained by assuming every electron whose energy reaches  $I$  causes impact ionization.

The finite difference program was advanced by an explicit Euler method in which  $\Delta u$  was taken typically as 0.1 eV and  $\Delta t$  was kept less than  $(\Delta u)^2 / 2D$  to maintain stability. For one test problem  $\Delta u$  was reduced by a factor of two and  $\Delta t$  by a factor of four, which resulted in 1.4 percent change in the calculated value of  $\eta$ . The program was written with a second order Runge-Kutta integration as an option, but this nearly doubled the running time with only a slight increase in accuracy.

Figure 36 shows a distribution function that was calculated for an electric field  $E = 15$  MW/cm and a 1.06  $\mu\text{m}$  wavelength, with an initial distribution assumed to be Maxwellian at 300°K, with an electron density of  $10^8$  per unit volume. After 0.03 psecs the distribution function has already spread considerably from its initial shape which was concentrated around .025 eV.

The evolution of the distribution function can be seen more clearly from the density contours displayed in Fig. 37a and b. Here a quantized representation has been used in which we print an integer "0" if  $f$  is below a base of  $10^6 \text{ eV}^{-1}$ ; if  $f$  exceeds the base by less than 1 dB, the entry is left blank. For 1-2 dB above the base a "1" is printed and for 2-3 dB above the base the entry is blank. The algorithm proceeds, leaving every other dB blank and printing an integer "N" when  $f$  exceeds the base by an amount

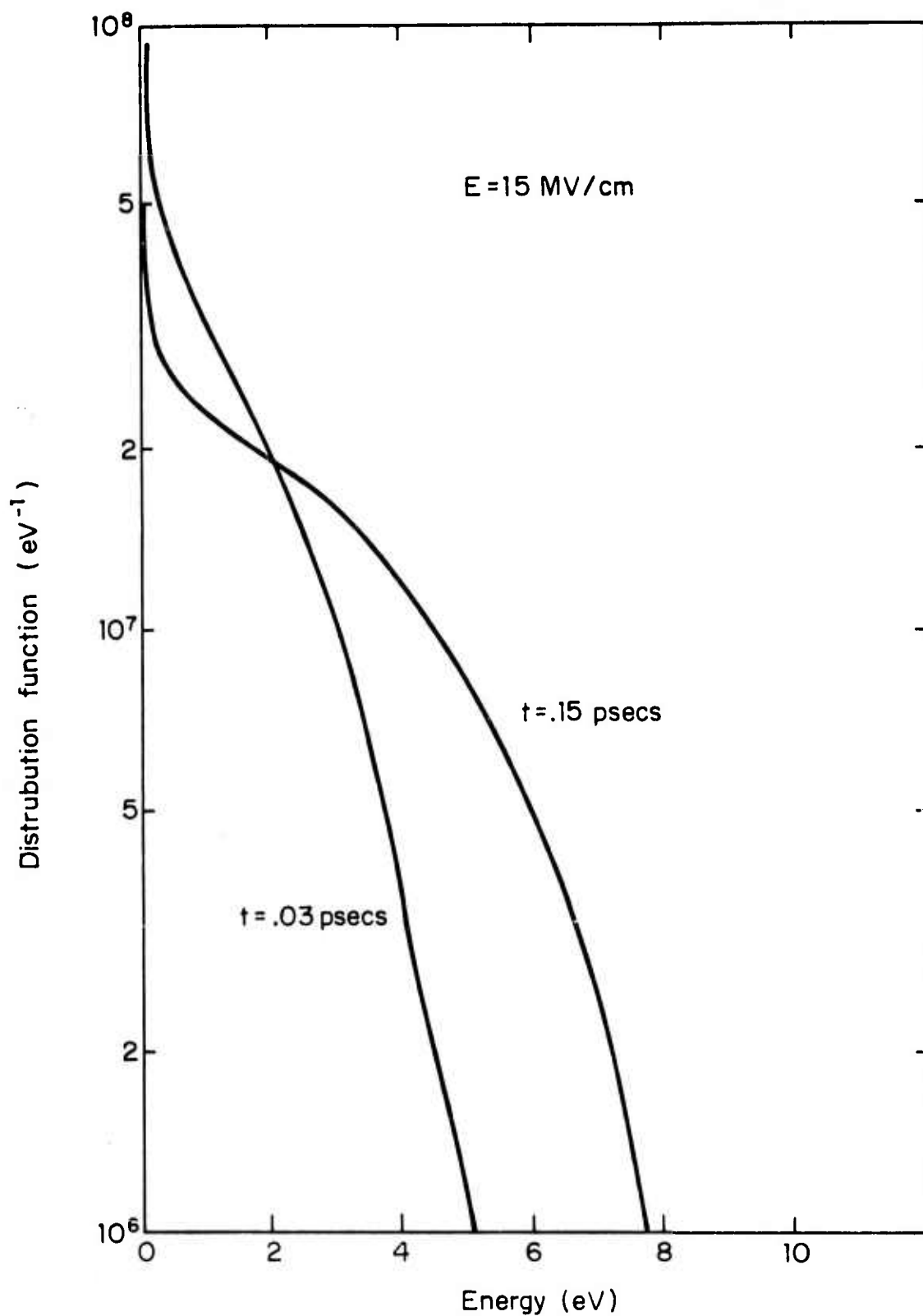


Fig. 36 Distribution Function which Evolves from an Original Maxwellian at 300°K and a Total Number Density of 10<sup>8</sup> per Unit Volume when NaCl is Irradiated by an RMS Field of 15 MV/cm with a 1.06  $\mu$ m Wavelength.

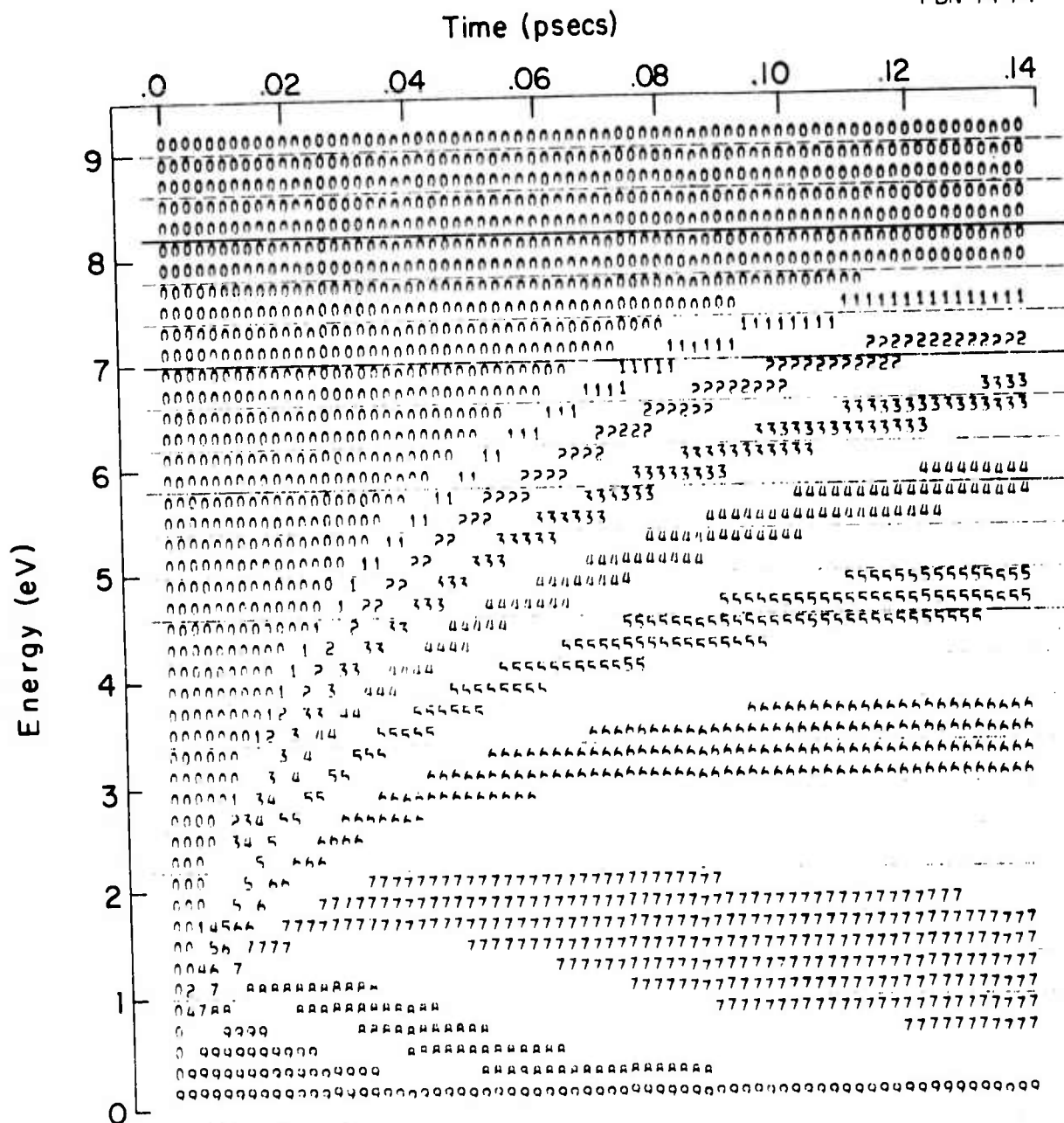


Fig. 37a Quantized Contours of a Distribution Function Which Evolving from an Initial Maxwellian at 300°, When NaCl is Irradiated by a 1.06  $\mu\text{m}$  Laser with  $E = 15$  MV/cm. The first column represents the initial condition when almost all the electrons are on the lowest energy bin and the distribution spreads to a asymptotic form after about .14 psecs. Collision frequency is curve (1) of Fig. 34.

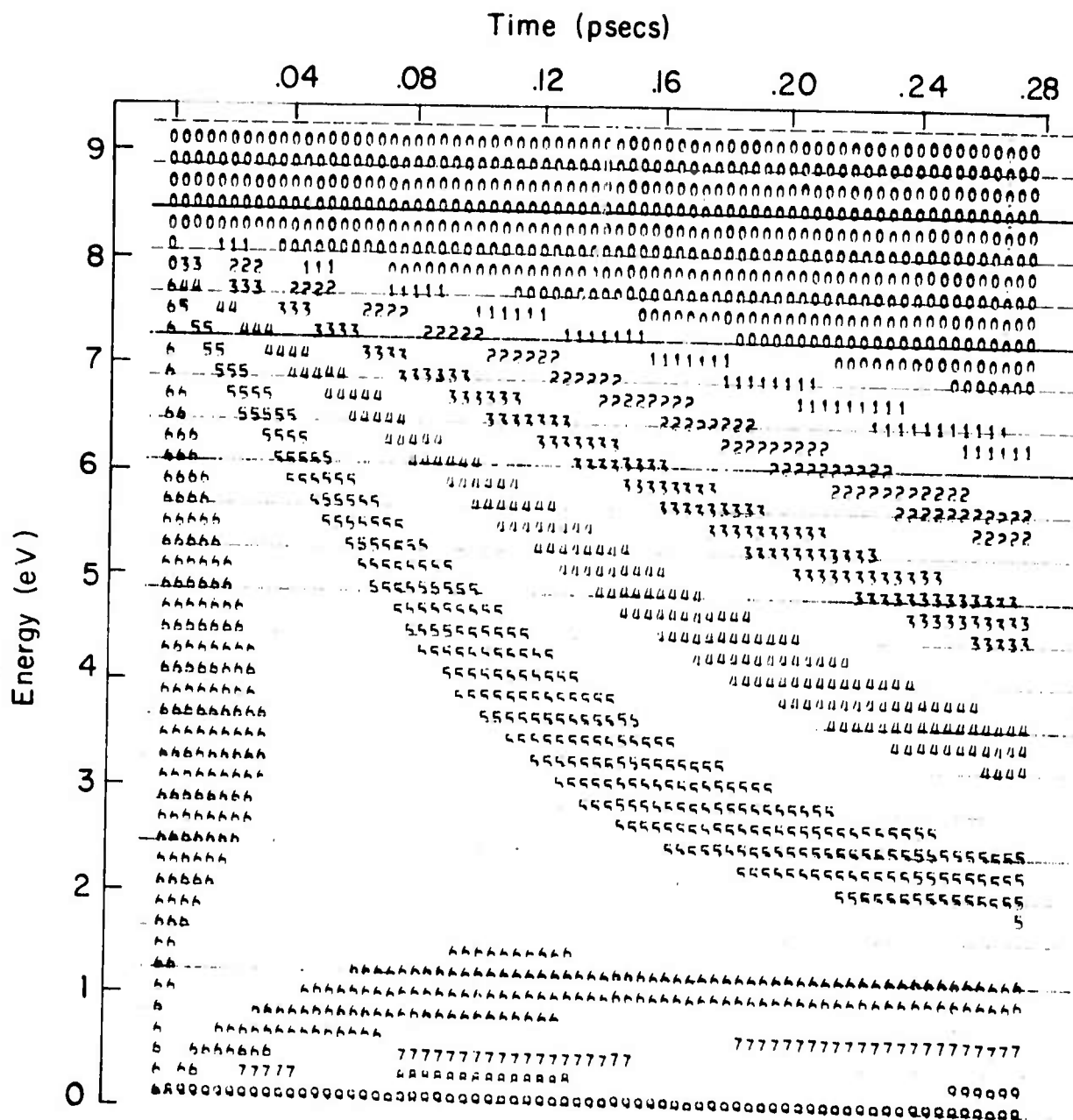


Fig. 37b Quantized Contours Evolving from a Uniform Distribution Function,  $E = 10 \text{ MV/cm}$ ,  $\lambda = 1.06 \mu\text{m}$ . With a lower field, the asymptotic distribution function is compressed in toward lower energy.

ranging from  $2N-1$  to  $2N$  dB. Finally, a "9" is printed when  $f$  exceeds the base by more than 17 dB. Each column represents the distribution function at a specific time. Thus, the 16th column in Fig. 37a gives the same information as the curve for .03 psecs in Fig. 36. Each horizontal line gives the density as a function of time at the center of an energy bin 0.1 eV in extent. Only every second bin has been printed so the bottom row corresponds to 0.05 eV, the next row to 0.25 eV, etc.

Figure 37a shows the evolution of an initially Maxwellian distribution function for the same conditions as Fig. 36. The electrons, irradiated by a field  $E = 15$  MV/cm which is switched on at  $t=0$ , spread in energy space until they have nearly reached an asymptotic form after 0.14 psecs. Figure 37b shows the compression of an initial distribution function  $f = 10^8/I$  for  $u < I$  when NaCl is irradiated by a 10 MW/cm field with 1.06  $\mu$ m wavelength. With the weaker field, the distribution function at late times collapses closer to the origin than the asymptotic distribution function in Fig. 37a.

The electron currents in energy space, normalized to one electron, are plotted in Figs. 38a and b for the same conditions as those contained in Figs. 37a and b. In Fig. 38a, the electrons initially flow towards higher energy, and finally reach the steady state form after 0.15 psecs.

The current  $J(I)$ , where  $I$  is the ionization energy, has a special significance which can be seen by integrating Eq. (19) from 0 to  $I$ , which produces

$$\frac{\partial n}{\partial t} - \int_I^\infty \frac{\partial f}{\partial t} du = -J(I) - \int_0^I \nu_i f du + 2 \int_I^{3I} \nu_i(u) f(u) du$$

where the boundary condition  $J(0) = 0$  has been used. The second term on the r.h.s. vanishes, and since

$$\int_I^{3I} \nu_i f du \cong \int_I^\infty \nu_i f du = \frac{\partial n}{\partial t}$$

we obtain

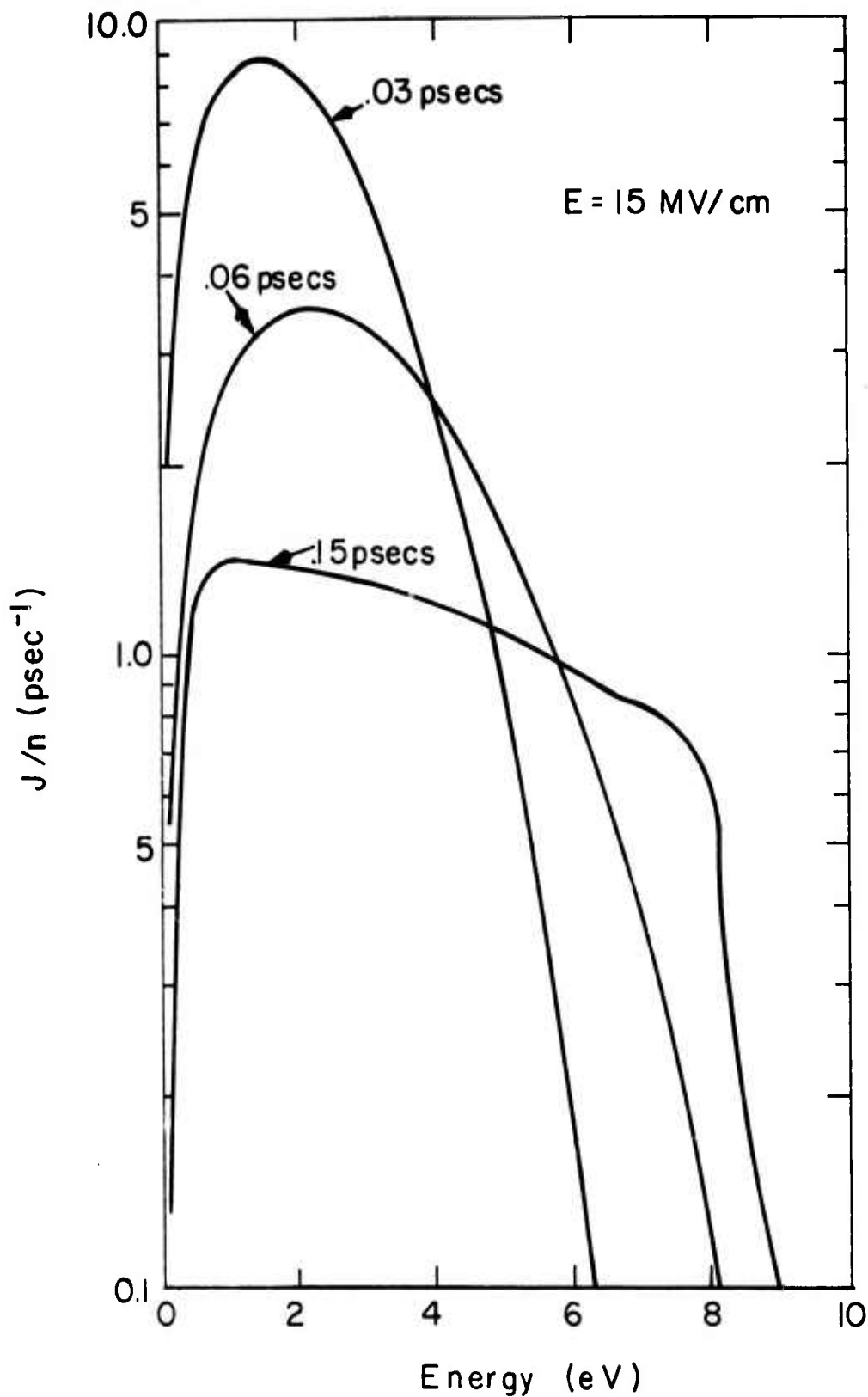


Fig. 38a Currents in Energy Space Normalized to One Electron for the same conditions as Fig. 37a. The electrons initially gain energy until they finally reach a steady state distribution.

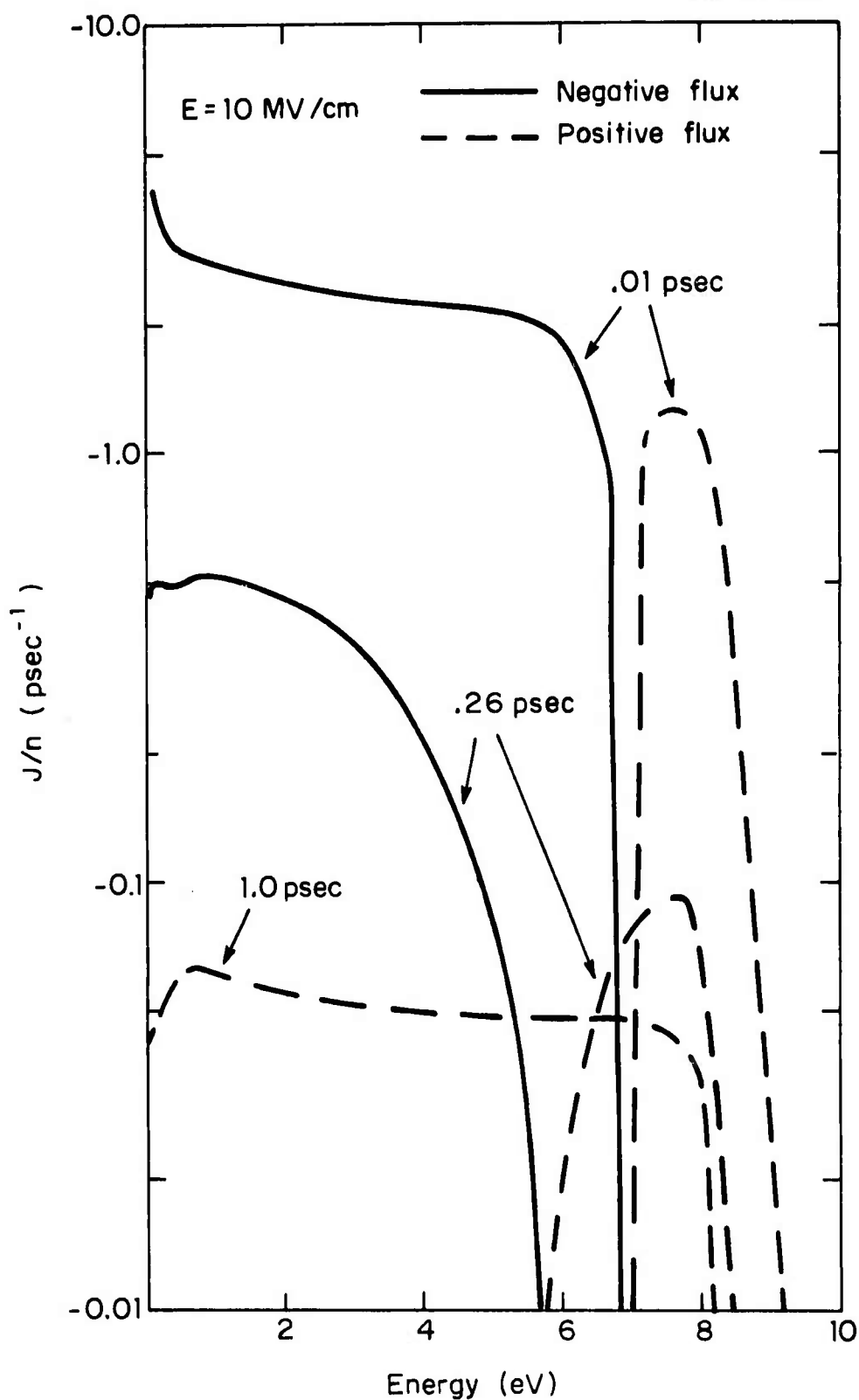


Fig. 38b Currents in Energy Space Normalized for Conditions in Fig. 37b. The current at 0.01 psecs is negative below 6.8 eV as electrons from the original distribution lose energy.

$$\frac{\partial n}{\partial t} = J(I) - \int_I^{\infty} \frac{\partial f}{\partial t} du \quad (24)$$

which states that every electron passing I either causes an ionization or else is used to increase the number of electrons in "storage" at energies greater than I. Since the last term is relatively small, we have approximately

$$\frac{J(I)}{n} \cong \frac{1}{n} \frac{\partial n}{\partial t} = \eta(t) \quad (25)$$

where  $\eta$  is the instantaneous ionization rate. For example, from Fig. (38a) the asymptotic value of  $J(I)/n$  at 7.7 eV is  $0.74 \text{ psec}^{-1}$  which compares with a numerical result for  $\eta$  of  $0.73 \text{ psec}^{-1}$  at 0.15 psec.

In Fig. 38b the current is negative at early times as the electrons rapidly lose energy, except for electrons in the tail of the distribution which diffuse upward and are eventually ionized. Finally after 1.0 psecs, the distribution reaches its asymptotic form and  $J(u)$  is everywhere positive. Note that the asymptotic form of  $J(u)$  does not monotonically decrease as it would do if all the electrons were born at zero energy. Instead, a considerable amount of electrons are created with energies as high as 1 eV which requires  $J(u)$  to increase at low energies, as shown by Eq. (19), suggesting that a considerable fraction of electrons avoid the low energy "trap".

The calculated ionization rates, based upon curve 1 of Fig. 34, for the collision rate frequency and Frohlich's model for the energy loss are shown in Fig. 39 where they are compared with experimental results<sup>17</sup> for 1.06  $\mu\text{m}$  pulses. The experimental ionization rates were taken equal to  $18/t_p$  where  $t_p$  was the measured pulse length for breakdown. (The factor "18" was obtained by assuming the ambient electron density must be increased by  $10^8$  to cause damage.<sup>17</sup> This factor would be increased to "27" if Seitz' "40 generation" model was used.)

If the time variable in Eq. (2) was changed to  $t' = tE^2$ , and  $(du/dt)_L$  were neglected, then the electron field would disappear from the equation. When the electric field becomes large enough, this

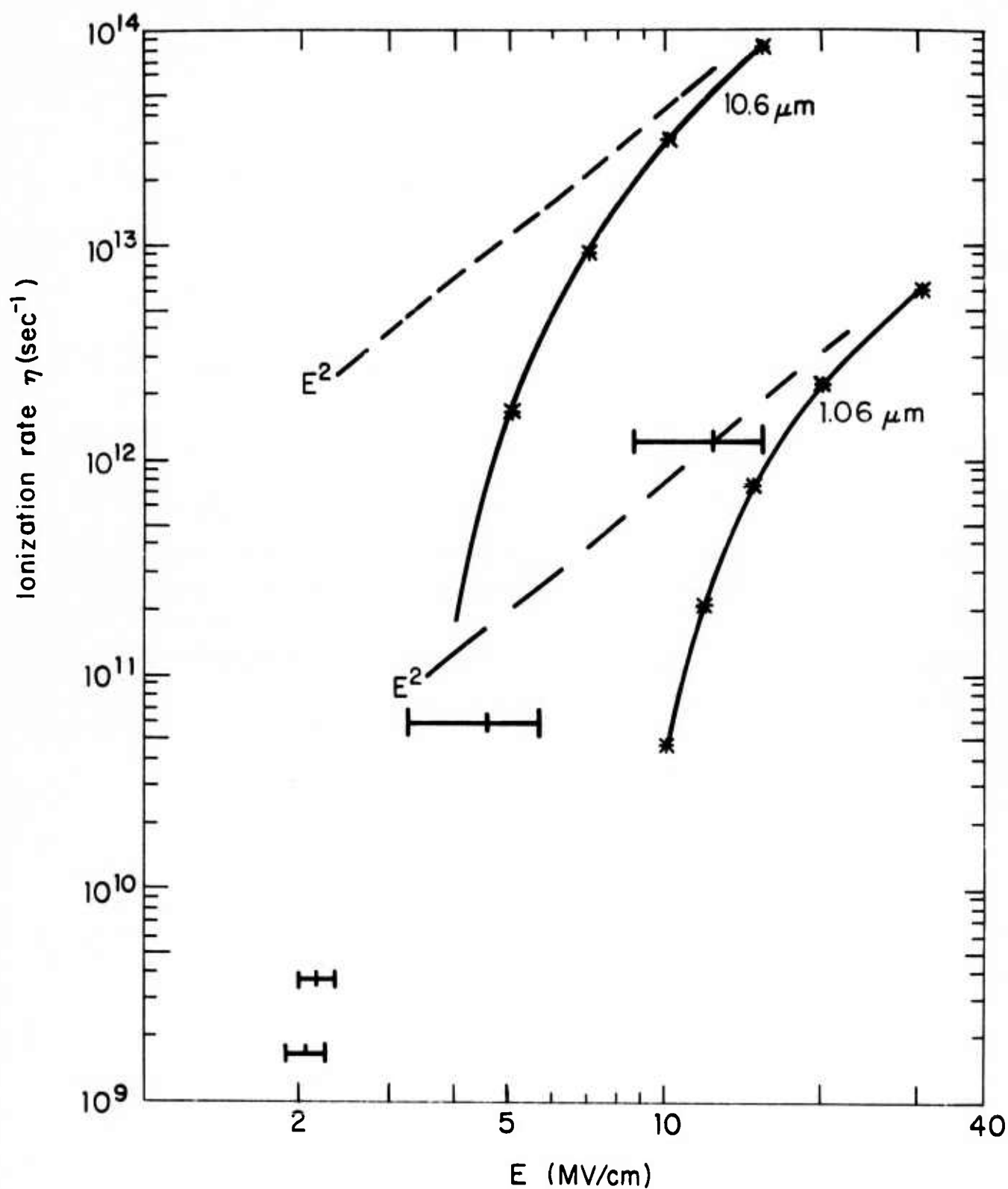


Fig. 39 Ionization Rate from Theory and Experiments for 1.06 and 10.6  $\mu\text{m}$  Radiation. The solid curves connect points calculated using curve (1) of Fig. 34 and Fröhlich's loss rate. The error bars indicate experimental points and the dashed straight lines are loci for ionization rates proportional to  $E^2$ . Here  $E$  is the rms field.

neglect will be valid, thus  $\eta$  will become proportional to  $E^2$ . This expectation is born out by Fig. 39, where the dotted straight lines were drawn as loci  $\eta/E^2 = \text{constant}$  and correspond to high field asymptotes to the theoretical curves.

Considering that there were no adjustable constants in calculating the curves in Fig. 39, the agreement may be considered quite good. However, our other experiments<sup>67</sup> indicated little difference between 1.06  $\mu\text{m}$  and 10.6  $\mu\text{m}$  radiation, which could only be exactly true if  $\nu \gg \omega$  at all energies. Since Seitz<sup>59</sup> suggested the deformation potential will be important for hot electrons, we have made further calculations using curve 3 of Fig. 34.

To be consistent, deformation potential effects should be included in  $(du/dt)_L$ , so we have taken

$$\left(\frac{du}{dt}\right)_L = \left(\frac{du}{dt}\right)_1 + \left(\frac{du}{dt}\right)_2 \quad (26)$$

where  $(du/dt)_1$  is the polar crystal effect given by Eq. (18) and

$$\begin{aligned} \left(\frac{du}{dt}\right)_2 &= \left(\frac{3}{2}\right)c \sqrt{2mu} \nu_s, \quad u < u_0, \\ &= \left(\frac{3}{2}\right)c \sqrt{2mu_0} \nu_s, \quad u > u_0, \end{aligned} \quad (27)$$

where  $\nu_s$  is the deformation potential collision frequency from Eq. (13) and  $c$  = velocity of the longitudinal optical phonon =  $4.58 \times 10^5$  cm/sec for NaCl.<sup>82</sup> Equation (27) follows from requiring Eqs. (10) and (11) of Seitz<sup>59</sup> paper to be consistent with Eq. (13).

The energy loss from Eq. (26) is plotted as curve 3 of Fig. 40 (which is similar to a sketch<sup>59</sup> given as Seitz' Fig. 34b). The other curves are plots of  $A/3$  and  $D(u)$  which are based on curve 3 of Fig. 34 (which is similar to a sketch<sup>59</sup> given as Seitz' Fig. 33b).

This plot is for  $\lambda = 1.06$  but, since  $\nu$  exceeds  $\omega$  over most of the energy range, the coefficient do not change drastically for  $\lambda = 10.6$ . The coefficient  $G$  (and the rate of energy change) is negative, so the breakdown occurs due to the diffusion term,  $D(u)$ .

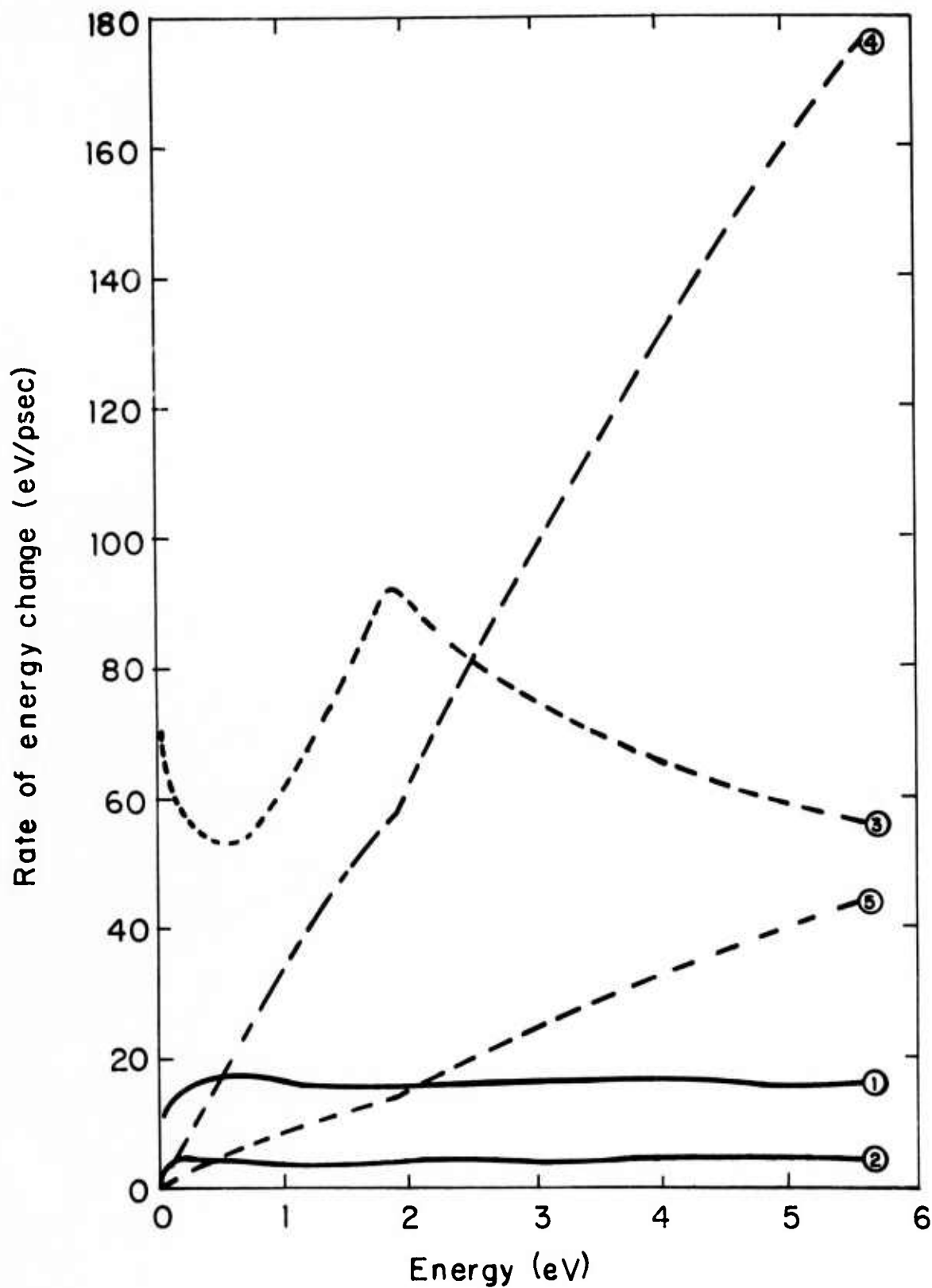


Fig. 40 Coefficients in the Fokker-Planck Equation for  $\lambda = 1.06 \mu\text{m}$  Including the Effects of the Deformation Potential.

The results in Fig. 41 include deformation potential effects and were computed with curve 3 of Fig. 34 for the collision frequency and Eq. (26) for the energy loss to the lattice. The RMS field is 8 MW/cm and the wavelength is 1.06  $\mu\text{m}$ . Figure 41a shows quantized density contours for an initially uniform electron density collapsing towards its asymptotic form. Figure 41b shows the energy flux  $J(u)$  at different points in time. The flux at .01 psecs is negative below 6.2 eV since most of the hot electrons lose energy initially. At 0.68 psecs, the distribution appears to be at its asymptotic limit, judging from the convergence of successive values of  $\eta$ . It is possible that a steady state could exist in which many electrons are born near 0.5 eV and lose energy in order to populate the energy range below 0.5 eV, with  $f$  increasing as  $\phi_0(u)e^{\alpha_0 t}$ . This may explain the negative flux below 0.4 eV in the 0.68 curve in Fig. 41b. However, because we have not carried this calculation to later times, we cannot be sure whether  $J$  becomes positive at later times.

Figure 42 plots the ionization rate including the deformation potential effect in the collision frequency with the solid curves showing results using the energy loss rate given to Eq. (26) while the dashed curve uses only the Fröhlich energy loss from Eq. (18). The figure shows clearly that when  $E$  becomes large enough so that the loss rates are inconsequential, the curves approach their asymptotic forms proportional to  $E^2$ . Compared to Fig. 39, the 10.6  $\mu\text{m}$  curve has moved downward while the 1.06  $\mu\text{m}$  curve has moved upward so that the two curves are close enough together so that the breakdown at 1.06  $\mu\text{m}$  would appear to be dc within the experimental error. The agreement is good except for the experimental points near the bottom of the figure, which have larger ionization rates than would be expected from the calculations. The calculated points would move upward if  $(du/dt)_L$  were decreased, or if the loss processes responsible for  $(du/dt)_L$  cause a dispersion which is an important contribution to the diffusion coefficient  $D$  for fields less than about 5 MW/cm.

Once again the ionization frequency for an electron with energy  $u$  was taken as  $a_1(u-I)$  where  $a_1$  was  $4 \times 10^{14} \text{ sec}^{-1} \text{ eV}^{-1}$ . This was large enough

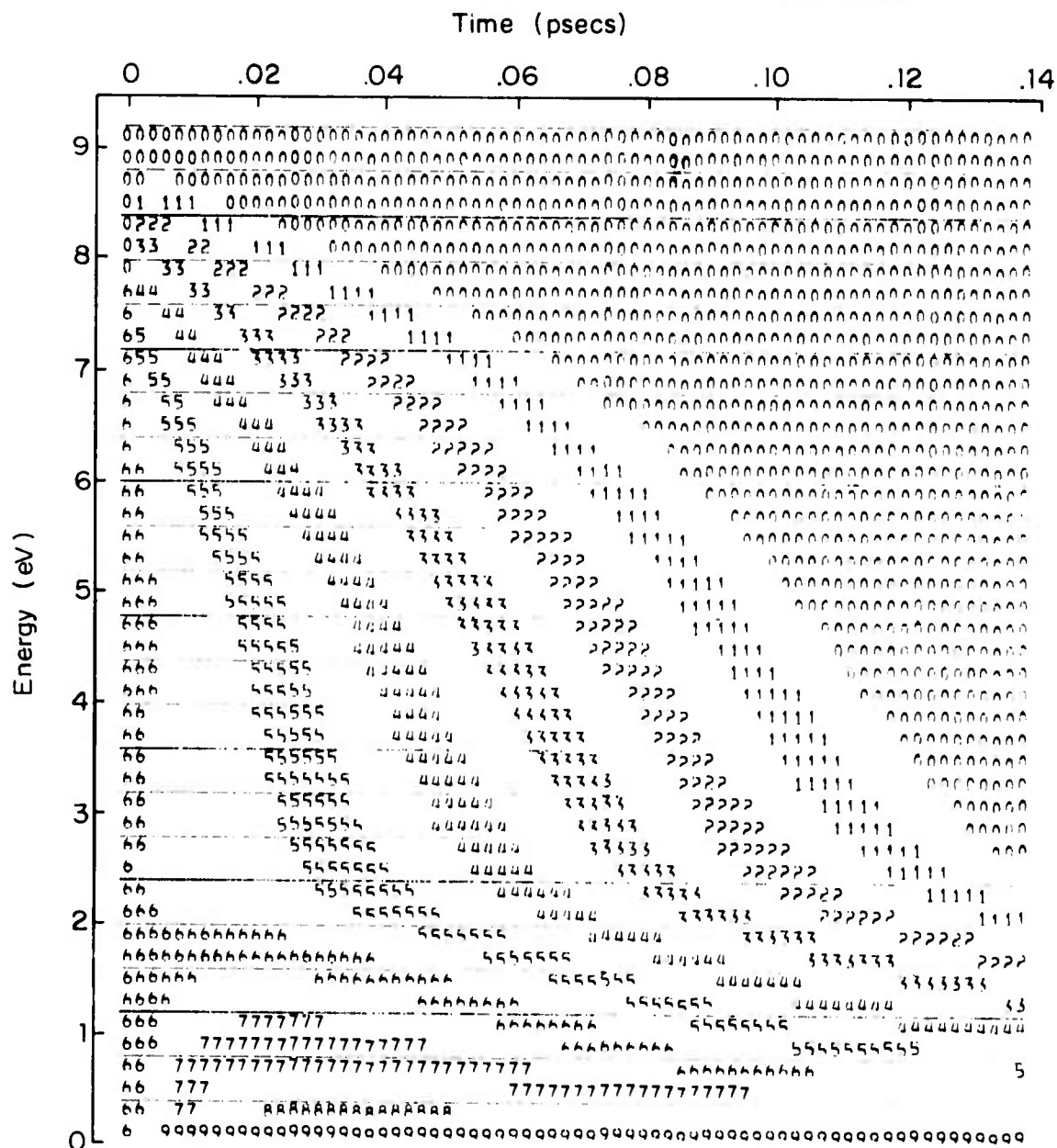


Fig. 41a Quantized Contours of a Distribution Function  
Calculated Using the Coefficients of Fig. 40  
with  $E = 8 \text{ MW/cm}$  and  $\lambda = 1.06 \mu\text{m}$ . An  
initially constant distribution function collapses  
in energy space for 0.14 psecs.

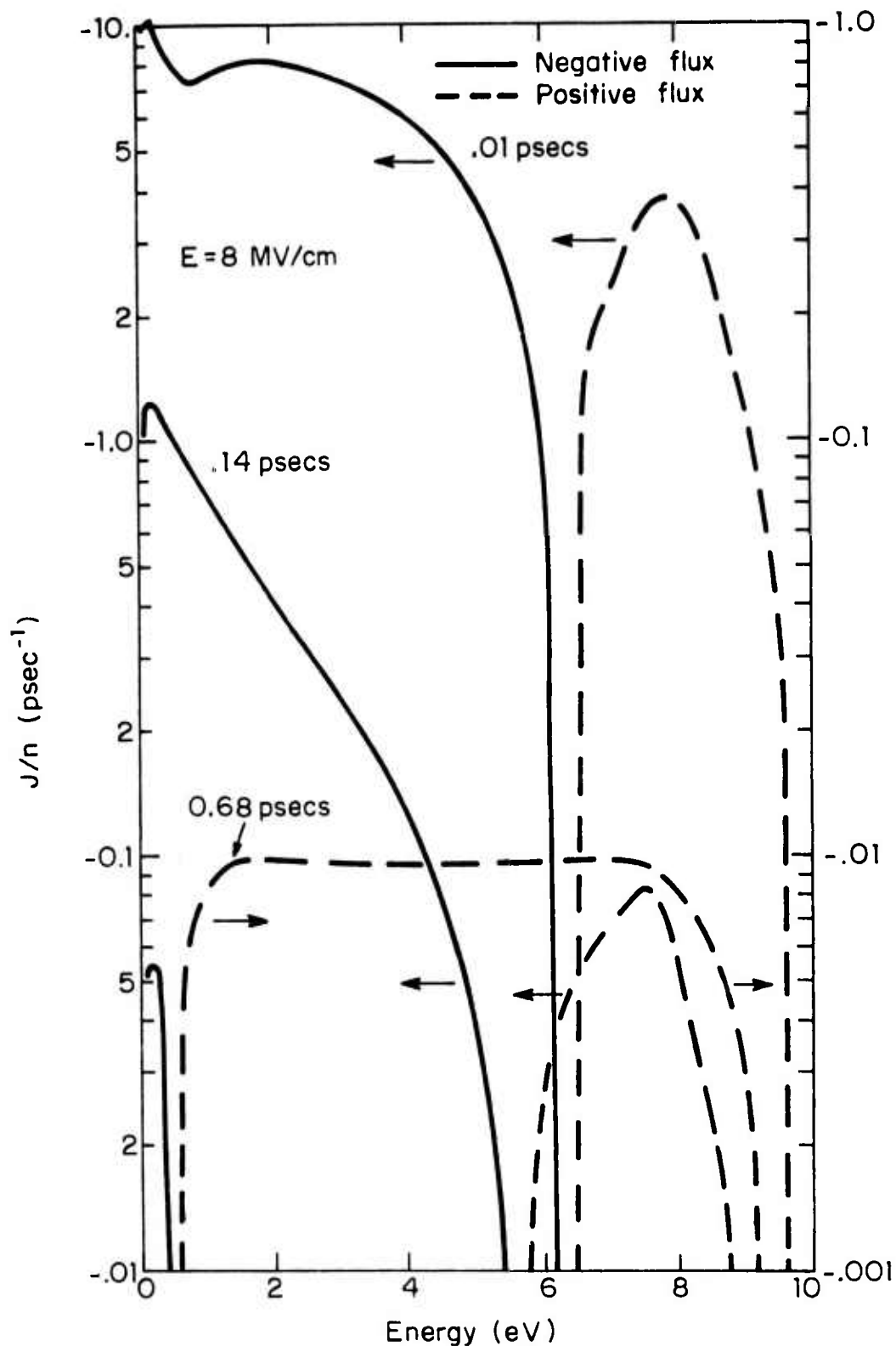


Fig. 41b Currents in Energy Space for the Problem in Fig. 41a. Note that the right hand scale applies only to the bottom curve. Initially the flux is only positive for energies close to 1 but after 0.68 psecs the flux is close to its asymptotic form.

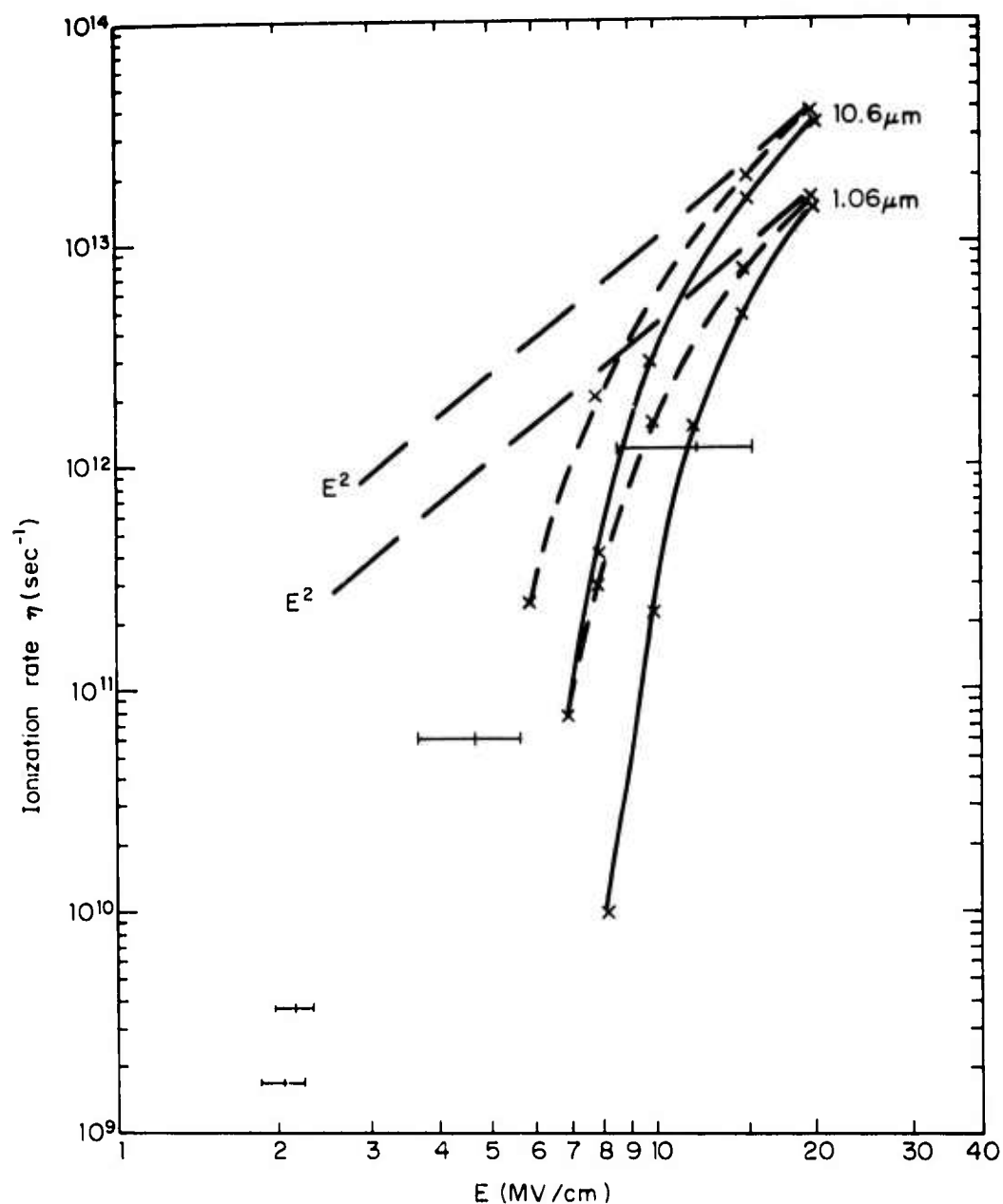


Fig. 42 Ionization Rate From Experiment and Calculated by Including the Deformation Potential. The solid curves include the full energy loss for deformation potentials while the dotted curve includes deformation potential effects in the collision frequency but not in the energy loss. The curves are again asymptotic to the dotted lines drawn so that  $\eta/E^2 = \text{constant}$ . The computed curves are for  $\lambda = 1.06$  and  $10.6 \mu\text{m}$ ; the experiment used  $1.06 \mu\text{m}$  radiation.

so that most electrons caused ionization near I and that the results were relatively insensitive to changes in this cross section.

The difficulty of increasing the energy of thermal electrons constitutes a low energy trap which may affect the statistics<sup>20</sup> of the starting process for avalanche breakdown, but these starting statistics were not studied.

## 6. Conclusions

In answer to the questions posed in the Introduction, we conclude that the experimental results are in agreement with calculations based upon the hypothesis that the process causing optical damage to NaCl can be described by a classical diffusion equation. This agreement may be considered very good considering the incomplete state of the theory for calculating the collision frequency for hot electrons, and the fact that our treatment ignores effects due to the finite energy quanta in 1.06  $\mu\text{m}$  laser radiation and the uncertainty in the electron energy due to collision frequencies of  $10^{15} \text{ sec}^{-1}$ .

The experimental results suggest that the deformation potential interaction suggested by Seitz is the most important source of momentum transfer for electrons with energy greater than 1 eV in NaCl. It is not sufficient to include only the polar interaction described by Fröhlich because this implies collision frequencies below  $10^{15} \text{ sec}^{-1}$  above 1 eV and, if this were the case, the 1.06  $\mu\text{m}$  laser would require much larger rms breakdown fields than the 10.6  $\mu\text{m}$  laser.

As usual, the Fokker-Planck equation is derived under the assumption that the distribution function can be expanded in a Taylor series. As discussed more thoroughly in Appendix A; this assumption is valid for fields up to about 20 MV/cm which is sufficient to describe the breakdown process even for psec pulses. In addition, we assumed that the dispersion due to energy losses to the lattice could be neglected in computing the diffusion coefficient  $D$ ; in Appendix A we show that this approximation is no longer negligible when the field drops below about 5 MV/cm. Consequently, the

ionization rates computed in Fig. 42 are in good agreement with the experiments involving 15 and 300 psec pulse durations,<sup>17</sup> but the calculated rates fall below the measurements for 4.7 and 10.3 ns pulses.

The computations also indicated that electrons often diffuse from the low energies to the high energies when the "average" electron is actually losing energy over a large part of the energy range.

## REFERENCES

1. P.R. Pearson and H.M. Lamberton, IEEE J. Quant. Elec. QE-8, 145 (1972).
2. T.Y. Chang and O.R. Wood, IEEE J. Quant. Elec. QE-8, 721 (1972).
3. A.J. Bealieu, Appl. Phys. Lett. 16, 504 (1970).
4. A.J. Bealieu, Proc. IEEE 59, 667 (1971).
5. R. Dumanchin, Post deadline paper 13 A-6, IEEE, Laser Eng. and Appl. Conf. Washington (1971).
6. A.K. Laplamme, Rev. Sci. Instr. 41, 1578 (1970).
7. J.D. Cobine, Gaseous Conductors (McGraw-Hill, New York, 1941), p. 177.
8. D. Bua and D. Wilson, unpublished.
9. E. Yablonovitch, Appl. Phys. Lett. 19, 495 (1971).
10. D.W. Fradin, E. Yablonovitch and M. Bass, Appl. Optics 12, 700 (1973).
11. R.W. Hopper and D.R. Uhlman, J. Appl. Phys. 41, 4023 (1970).
12. D.R. Whitehouse, C.F. Luck, C.P. VonMertons, F.A. Horrigan, and M. Bass, Paper A-7, IEEE, Laser Eng. and Appl. Conf., Washington (1973).
13. A.E. Siegman and R. Arrathoon, IEEE J. Quant. Elec. QE-3, 156, (1967).
14. D. Bua, D. Fradin and M. Bass, IEEE J. Quant. Elec. QE-8, 916, (1972).
15. J.A. Weiss and L.S. Goldberg, IEEE J. Quant. Elec. QE-8, 758, (1972).
16. A. von Hippel and R.J. Mauer, Phys. Rev. 59, 820 (1941).
17. D. Fradin, N. Bloembergen and J.P. Letellier, Appl. Phys. Lett. 22, 635 (1973).
18. M. Bass and D. Fradin, IEEE J. Quant. Elec., QE-9, 890 (1973).
19. J.J. O'Dwyer, The Theory of Dielectric Breakdown of Solids, (Oxford University Press, London, 1964).

20. M. Bass and H.H. Barrett, IEEE J. Quant. Elect. QE-8, 338(1972).
21. M. Munasinghe and A. Linz, Phys. Rev. B4, 3833 (1971).
22. J. VanderSande, MIT, private communication (1973).
23. J.H. Fertel and C.H. Perry, Phys. Rev. 184, 874 (1969).
24. D.W. Fradin and M. Bass, Appl. Phys. Lett. 22, 157 (1973).
25. E. Yablonovitch and N. Bloembergen, Phys. Rev. Lett. 29, 907 (1972).
26. A.A. Vorob'ev, G.A. Vorob'ev, and L.T. Musashko, Fiz. Tverd. Tela 4, 1967 (1962) [Sov. Phys. Solid State 4, 1441 (1963)].
27. D.B. Watson, W. Heyes, K.C. Kao, and J.H. Calderwood, IEEE Trans. Elec. Insul. 1, 30 (1965).
28. G.A. Vorob'ev, N.I. Lebedeva, and G.S. Nadorova, Fiz. Tverd. Tela 13, 890 (1971) [Sov. Phys. Solid State 13, 736 (1971)].
29. J.P. Letellier, Naval Research Laboratory Report 7463 (1972).
30. D.W. Fradin and M. Bass, Appl. Phys. Lett. 22, 206 (1973).
31. H. Raether, Electron Avalanches and Breakdown in Gases (Butterworths, London, 1964).
32. J.R. Hanscomb, J. Appl. Phys. 41, 3597 (1970).
33. N. Bloembergen, Appl. Optics 12, 661 (1973).
34. Bliss, E.S., "Opto-Electronics 3, 99-108 (1971).
35. Bliss, E.S. and Milam, D., "Laser Induced Damage to Mirrors at Two Pulse Durations," Proc. 4th ASTM Symp. Damage in Laser Materials, NBS Spec. Pub. No. 372 (1972).
36. Bliss, E.S. and Milam, D., "Laser Damage Study with Subnanosecond Pulses," AFCRL Report No. 72-0233 (1972). Available from Defense Documentation Center, the National Technical Information Center, or the authors.
37. Milam, D., Bradbury, R.A., and Gallagher, C.C., "Evaluation of Three Techniques for Producing Laser Pulses of Nanosecond Duration," AFCRL Report No. 73-0007. Available from Defense Documentation Center, the National Technical Information Center, or the authors.

38. Bliss, E.S., Milam, D., and Bradbury, R.A., *Applied Optics* 12, 602 (1973).
39. Bass, Michael, *IEEE J. Quant. Elect.* QE-7, 350 (1971).
40. DeShazer, L.G., "Role of Coating Defects in Laser Induced Damage to Thin Films," *Proc. 5th ASTM/NBS Boulder Damage Symp.*, to be published.
41. Schwartz, H., "Thin Films of Metals and Inorganic Compounds Vacuum Deposited by High Energy Laser" in "Laser Interactions and Related Plasma Phenomena," Vol. I, Ed. by Helmut J. Schwarz and Heinrich Hora (Plenum Press, New York, N.Y. 1972) p. 71.
42. Kelley, P.L., *Phys. Rev. Lett.*, 26, 1005 (1965).
43. Duguay, M.A., Hansen, J.W. and Shapiro, S.L., *IEEE J. Quant. Elect.* QE-6, 725 (1970).
44. Giuliano, C.R. and Marburger, J.H., *Phys. Rev. Lett.* 27, 905 (1970).
45. McMahon, J.M., "Damage Measurements with Subnanosecond Pulses," *NBS Spec. Publ.* 372, 100 (1972).
46. Newnam, B.E. and DeShazer, L.G., "Direct Measurement of Self-Focusing in Glass," *NBS Spec. Publ.* 356, 113 (1971).
47. Bloembergen, N., *Amer. J. Phys.* 35, 989 (1967).
48. Dawson, E.L. and Marburger, J.H., *Phys. Rev.* 179, 862 (1968); Wang, C.S., *Phys. Rev.* 173, 908 (1968).
49. Wagner, W.G., Haus, H.A. and Marburger, J.H., *Phys. Rev.* 175, 256 (1968).
50. Zverev, G.M. and Pashkov, G.M., *Sov. Phys. - JETP* 30, 616 (1970); *Zh. Eksp. Teor. Fiz.*, 57, 1128 (1969).
51. Akhmanov, S.A., Sukhorukov, A.P., and Khokhlov, R.V., *Sov. Phys. Usp.* 10, 609 (1968); *Usp. Fiz. Nauk.* 93, 19 (1967).
52. Kerr, E.L., *IEEE J. Quant. Elect.* QE-6, 616 (1970); Smith, W.J. *Modern Optical Engineering* (New York: McGraw-Hill) (1966).
53. Giuliano, C.R., Marburger, J.H. and Yariv, A., *Appl. Phys. Lett.* 20, 58 (1972).
54. Yablonovitch, E., Bloembergen, N., *Phys. Rev. Lett.* 26, 907 (1972).
55. Wang, C.C. and Baardson, E.L., *Phys. Rev.* 185, 1079 (1969); *Phys. Rev. B1*, 2827 (1970).

56. Fradin, D.W., "Laser Induced Damage in Solids," Final Report No. 643 for Office of Naval Research under Contract No. N00014-67-A-0298-0006, Harvard University (May 1973).
57. Feldman, A., NBS, private communications (1973).
58. Pappis, J., "Window Development for Low Power IR Laser Systems," Contract F33615-73-C-5019; and "Exploratory Development for the Chemical Vapor Deposition of Polycrystalline ZnSe for High Power IR Windows," Contract No. F33615-71-C-1779, Raytheon Company.
59. Seitz, F. Phys. Rev. 76, 1376 (1949).
60. DeShazer, L.G., Neuman, B.E. and Leung, K.M., Appl. Phys. Lett 23, 607 (1973).
61. Canavan, G.H. and Nielson, P.E., Appl. Phys. Lett. 22, 409 (1973).
62. See; for example, Dwight, H.B. "Tables of Integrals and Other Mathematical Data, The MacMillan Co., New York (Integrals 623 and 623.2) (1963).
63. The authors are grateful to Dr. T.F. Deutsch for having made this observation. The measured value of  $\alpha$  was supplied by Dr. A. Swanson of Raytheon.
64. Bloembergen, N., Appl. Optics 12, 660 (1973).
65. Miles, P. and Willingham, C., Raytheon Research Division, unpublished results.
66. Fradin, D.W. Laser Focus 10, 39 (1974).
67. Fradin, D.W. and Bass, M., 5th NBS-ASTM Laser Damage Symp., Boulder, Colorado (May 1973).
68. Bloembergen, N., "Laser-Induced Electric Breakdown in Solids", to be published.
69. Akhmanov, S.A., Sukhorvov, A.P. and Khoklov, R.V., Soviet Physics JETP 23, 1025 (1966).
70. Kroll, N.A. and Watson, K.M., Phys. Rev. A5, 1883 (1972); Brown, S.C., Introduction to Electrical Discharges in Gases (Wiley, N.Y., 1966) p. 177; Zel'dovich, Ya, B. and Raizer, Ya, P., Soviet Physics JETP 20, 772 (1965).
71. Thornber, K.K. and Feynman, R.P., Phys. Rev. B1, 4099 (1970).
72. Holway, L.H., J. Appl. Phys. 45, 677 (1974); Phys. Rev. Lett. 28, 280 (1972).
73. For example, Uhlenback, G.E. and Ornstein, L.S., Phys. Rev. 36, 823 (1930).

74. Fröhlich, H., Proc. Roy Soc. A160, 230 (1937).
75. For example, O'Dwyer, J.J., The Theory of Dielectric Breakdown Of Solids, Oxford University Press (1964).
76. Eaton, C.F. and Holway, L.H., Phys. Rev.
77. Wolff, P.A., Phys. Rev. 95, 1415 (1954).
78. Baraff, G.A., Phys. Rev. 128, 2507 (1962).
79. Shkarofsky, I.P., Proc. IRE 49, 1857 (1961); Sen, H.K. and Wyller, A.A., J. Geophys. Res. 65, 3931 (1960).
80. Keldysh, L.V., Sov. Physics JETP 21, 1135 (1965).
81. Zverev, G.M., Mikhailova, T.N. and Soloveva, N.M., Sov. Phys-JETP 26, 1053 (1968).
82. Physical Acoustic, Vol. III, Ed., Warren Weaver (Academic Press, N.Y.) (1965).
83. Shockley, W., Czech. J. Phys. B11, 81 (1961).
84. Chapman, S. and Cowling, T.G., "The Mathematical Theory of Non-Uniform Gases", p. 350 (Cambridge University Press, 1952).
85. G.H. Wannier, Bell System Tech. J. 32, 170 (1953).

## APPENDIX A

### RANGE OF VALIDITY OF THE FOKKER-PLANCK EQUATION

The Shockley theory of ionization<sup>78,80,83</sup> suggests ionization rates should be proportional to  $\exp - (I/eE\ell)$  where  $\ell$  is the mean free path. Such an expression can be conveniently plotted on semilog paper since  $\log \eta$  is a linear function of  $1/E$ . In fact, the experimental results fit this form reasonably well,<sup>67</sup> although the Shockley slope is sensitive to  $\ell$ . Our calculated values for  $\eta$ , which agree well with the high field measurements in Fig. 42, are more conveniently plotted on log-log plots to show that  $\eta$  is asymptotically proportional to  $E^2$ .

The Shockley argument emphasizes the exceptional electrons which gain energies equal to  $I$  without undergoing collision. Actually these exceptional electrons also contribute to the calculation<sup>72</sup> of the Fokker-Planck coefficients, although they are inaccurately treated by this approach. The contribution to the ionization rate due to the exceptional electrons alone will be of the order of  $\nu \exp - (I/eE\ell)$  since each electron undergoes  $\nu$  collisions per unit time. This contribution will be negligible compared with the rates in Fig. 42 if

$$I/eE\ell \gg 1 \quad . \quad (28)$$

Although  $\ell$  is a function of energy, we can approximate it by its value at  $u = I/2$  using the relation  $\ell = (2u/m)^{1/2}/\nu$ . Then the criterion of Eq. (28) is

$$I^2/e^2E^2\ell^2 \gg 1$$

or

$$\frac{e^2 E^2}{m v^2} \ll 1 \quad . \quad (29)$$

This last expression is exactly the condition we have already given for applying the Fokker-Planck equation (when  $\omega = 0$ ). Thus the Shockley effect becomes important for fields greater than the breakdown fields measured in NaCl. Even in other materials, breakdown will often occur before Eq. (29) is violated because ionization will be caused at lower fields by electrons which suffer many collisions but, by chance, they rebound with their velocity oriented so that they continue to gain energy from the field. The diffusion equation (whether obtained from the Legendre expansion or the Fokker-Planck approach) can be expected to describe these electrons accurately, when Eq. (29) is obeyed.

The diffusion coefficient used in this paper has ignored the dispersion in  $(du/dt)_L$ , an approximation which is valid for a cold background gas,<sup>72,76</sup> i.e.,  $kT \ll u$ . For finite  $kT$  and weak fields, the diffusion coefficient  $D = \frac{2}{3} uA$  must become

$$D = \frac{2}{3} uA + P \quad , \quad (30)$$

where  $P$  is independent of the field. When  $P$  is not zero,  $G$  is given by

$$G = \frac{1}{3} A - \left(\frac{du}{dt}\right)_L - \frac{\partial P}{\partial u} \quad . \quad (31)$$

If an equilibrium function,  $f_0$ , is known for zero field, and the ionization rate is negligible so that the current is zero, then  $P$  must satisfy

$$J = G f_0 - D \frac{\partial f_0}{\partial u} = 0 \quad (32)$$

where, taking  $f_0$  to be the Maxwellian,  $\sqrt{u} \exp(-u/kT)$ , Eq. (32) becomes a differential equation for  $P$ ,  $\frac{dP}{du} = \left(\frac{1}{kT} - \frac{1}{2u}\right) P - \left(\frac{du}{dt}\right)_L$ , which has the solution

$$P = -u^{-1/2} \exp(u/kT) Q \quad (33)$$

where

$$Q = \int_0^u u'^{1/2} \exp - (u' / kT) \left( \frac{du}{dt} \right)_L du' .$$

The integral  $Q$  is proportional to the average of the energy loss over a Maxwellian distribution and thus must equal zero if the upper limit is taken to be infinity.

As an example of the use of Eq. (33), it is instructive to consider an electron of energy  $u$  colliding elastically with a collision frequency  $\nu$  with gas molecules of mass  $M$  in a Maxwellian distribution at temperature  $T$ . Then the rate of energy loss from the electron to the molecules can be shown to be

$$\left( \frac{du}{dt} \right)_L = \epsilon \nu (u - 3kT/2) - \epsilon u k T \frac{\partial \nu}{\partial u} , \quad (34)$$

where the physical reason for the last term is that, if  $\frac{\partial \nu}{\partial u}$  is positive, molecules moving antiparallel to the electron are more likely to cause a collision and these molecules have a higher energy in a center of mass coordinate system than molecules moving parallel to the electron. Here  $\epsilon = 2mM/(m+M)^2$ . Substituting Eq. (34) into Eq. (33),  $Q$  is seen to be a perfect integral such that

$$P = \epsilon \nu k T u , \quad (35)$$

as can be verified independently. If we take  $J = 0$  and a nonzero field, substituting Eqs.(30) and (31) into (16) yields<sup>84</sup>

$$f = f(0) \exp \left[ \int_0^u \frac{A + 3\epsilon \nu \left( \frac{kT}{2} - u \right)}{(2A + 3\epsilon \nu kT)} \frac{du}{u} \right] . \quad (36)$$

If much more energy is gained from the field in a collision time than is lost by a thermal electron so that

$$\frac{e^2 E^2}{m(\nu^2 + \omega^2)} \gg \frac{3}{2} \epsilon kT , \quad (37)$$

i. e., so that  $A \gg P/u$ , Eq. (36) becomes

$$f = f(0) \sqrt{u} \exp \left( - \int_0^u \frac{3}{2} \frac{\epsilon_v}{A} du \right) \quad (38)$$

which has the form  $\sqrt{u} \exp (-g(u)/E^2)$  corresponding to Wolff's diffusion form.<sup>77,78</sup> If Eq. (37) is satisfied, it is permissible to assume that the Maxwellian describing the background gas has a zero temperature, i. e., it becomes a delta function as was assumed by Wannier,<sup>85</sup> in his version of the diffusion equation which was intended for sufficiently high fields.

When ionization is occurring it is no longer strictly correct to set  $J = 0$  since the ionization rate is proportional to  $J(I)$ , and Eq. (36) must be considered an upper bound as in Eq. (17). However, it is probably true that Eq. (38) is an approximation to the distribution function so that the ionization rate is proportional to  $Gf - D \frac{\partial f}{\partial u}$ , i. e., proportional to  $E^2$  as the numerical solutions show. Of course, the exact values for the ionization rate cannot be obtained from a solution which assumes that  $J = 0$ , which prevents us from using the elegant formalism of Keldysh<sup>80</sup> to obtain accurate results.

If we take  $T = 300^\circ\text{K}$ ,  $\epsilon = 10^{-4}$  and  $v^2 + \omega^2 = 10^{30}$ , the inequality in Eq. (37) becomes an equality at .05 MV/cm.

It is tempting to find  $Q$  for NaCl by substituting  $(du/dt)_L$  into Eq. (33). However, if we substitute  $(du/dt)_L = d_1 u^{-1/2} \ln d_2 u$  into Eq. (33), we obtain

$$Q = d_1 kT \left[ \ln d_2 kT [1 - \exp(-u/kt)] + \int_0^{u/kT} e^{-x} \ln x dx \right] \quad (39)$$

which does not go to zero for large  $u$  if we use the value of  $d_2$  in Eq. (18). The reason is that the derivation of Eq. (18) is only accurate for energies greater than thermal energies, and  $(du/dt)_L$  is negative below thermal energy

in order to balance energy gains and losses in the equilibrium distribution. We make an arbitrary fixup by choosing  $d_2$  so that

$$\ln d_2 kT = - \int_0^{\infty} e^{-x} \ln x dx ,$$

when we calculate  $P$ . Then

$$P = d_1 kT u^{-1/2} \left[ e^y \int_y^{\infty} e^{-x} \ln x dx - \int_0^{\infty} e^{-x} \ln x dx \right]$$

where  $y = u/kT$ , which can be numerically integrated to obtain the values in Table II. The inequality  $A \gg 3P/2u$  requires  $E$  to be greater than 0.15 MV/cm assuming  $\nu/(\nu^2 + \omega^2) = 10^{-15}$ ,  $u = I/2$  and  $P = 0.1 \text{ eV}^2/\text{sec}$ .

We have added  $P$  to the diffusion term in the Fokker-Planck equation, with the same value for  $(du/dt)_L$  that we used previously. The result for  $\lambda = 10.6 \mu\text{m}$  and  $E = 7 \text{ MV/cm}$  in Fig. 42 which had been  $8.8 \times 10^{10} \text{ sec}^{-1}$  was increased by 8.2 percent. The increase in  $\eta$  is correspondingly greater for fields below 7 MV/cm.

TABLE II

$u(\text{eV})$	.1	.5	1.1	2.1	3.1	4.1	6.1	8.1
$P(\frac{\text{eV}^2}{\text{psec}})$	.192	.144	.118	.097	.086	.079	.069	.063

The values of  $P$  given here are only a rough approximation since they depend on a model of the energy loss to the lattice which we know to be inexact near thermal energies.

Our arguments are not intended to deny that the low field data for  $\eta$  may be approximately described by a curve proportional to  $\exp(-\text{constant}/E)$  since our experimental results lie close to such a curve, but only that the low field behaviour may be explored by means of the Fokker-Planck equation without undertaking a special treatment for those exceptional electrons which do not suffer any collisions before they reach the ionization energy.

## APPENDIX B

### PUBLICATIONS AND PRESENTATIONS ON VISIBLE AND INFRARED LASER-INDUCED DAMAGE TO TRANSPARENT MATERIALS

1. D. W. Fradin and M. Bass, "Electron Avalanche Breakdown at Optical Frequencies," Winter Meeting of the American Physical Society, paper GE3, New York, February 1973.
2. D. W. Fradin and M. Bass, "A Comparison of Laser-Induced Surface and Bulk Damage," Appl. Phys. Lett. 22, 157 (1973).
3. D. W. Fradin and M. Bass, "Electron Avalanche Breakdown Induced by Ruby Laser Light," Appl. Phys. Lett. 22, 206 (1973).
4. D. W. Fradin, E. Yablonovitch, and M. Bass, "Confirmation of an Electron Avalanche Causing Laser-Induced Bulk Damage at 1.06 Microns," Appl. Optics 12, 700 (1973).
5. D. W. Fradin, "The Relationship Between Self-Focusing and Optical Bulk Damage and the Measurement of Self-Focusing Parameters," Twelfth Symposium on Electron, Ion, and Laser Beam Technology, MIT, Cambridge, Mass. (1973).
6. D. W. Fradin and M. Bass, "Studies of Intrinsic Optical Breakdown," Proc. 5th ASTM-NBS Symposium on Laser Damage, Boulder, Colorado, May 15-16, 1973 (NBS Spec. Publ. 387).
7. M. Bass and D. W. Fradin, "Statistics in Surface and Bulk Breakdown and Identification of Intrinsic Mechanisms," IEEE J. Quant. Elect. QE-4, 890 (1973).
8. M. Bass, "Laser Damage to Transparent Media," Invited Paper 19.6, 1973 Conference on Laser Engineering and Applications, Digest of Technical Papers, Washington, D. C., May 30 - June 1, 1973.
9. D. W. Fradin, "The Measurement of Self-Focusing Parameters Using Intrinsic Optical Damage," IEEE J. Quant. Elect. QE-9, 954 (1973).
10. D. W. Fradin, M. Bass, D. P. Bua, and C. A. Christian, "Optical Damage in Laser Materials," Proc. of Air Force Conference on High-Power IR Laser Window Materials, Hyannis, Mass., November 12-14, 1973.
11. D. W. Fradin, N. Bloembergen, and J. P. Letellier, "Dependence of Laser-Induced Breakdown Field Strength on Pulse Duration," Appl. Phys. Lett. 22, 635 (1973).
12. D. W. Fradin and M. Bass, "Effects of Lattice Disorder on the Intrinsic Optical Damage Fields of Solids," Appl. Phys. Lett. 23, 604 (1973).

13. David Milam, R. A. Bradbury, and M. Bass, "Laser Damage Threshold for Dielectric Coatings as Determined by Inclusions," Appl. Phys. Lett. 23, 654 (1973).
14. D. W. Fradin and D. P. Bua, "Laser-Induced Damage in ZnSe," submitted for publication (Feb. 1974).